

A Dynamic Approach to Evaluating the Effect of Slamming on a Jacket Foundation Template Lowered Through the Wave Zone

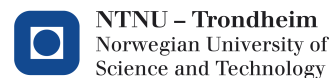
R.J.M. Nours

Master of Science Thesis

October 6, 2015



Delft University of Technology



A Dynamic Approach to Evaluating the Effect of Slamming on a Jacket Foundation Template Lowered Through the Wave Zone

Master of Science Thesis

October 6, 2015

European Wind Energy Master - EWEM
Delft University of Technology
Norwegian University of Science and Technology
Royal Boskalis Westminster

Author:

R.J.M. Nous

Committee:

Prof. dr. ir. A. Metrikine (Chairman) - TU Delft

ir. J.S. Hoving - TU Delft

Prof. dr. ir. T. Moan - NTNU

Assoc. Prof. dr. ir. Z. Gao - NTNU

ir. J.G.L. Janssen - Boskalis

Summary

The joint venture between Boskalis and VolkerWessels is responsible for installing 70 jacket foundations for the Wikinger offshore wind farm. The critical phase in this installation procedure is lowering a jacket foundation template through the wave zone. This installation phase will induce large dynamic loads on the hoisting wire. Lowering through the wave zone is a difficult process due to the occurrence of a wave slamming forces on the template. This slam force is highly uncertain and rather difficult to estimate. The aim of this thesis is to investigate the effect of the wave slamming force on the dynamic behavior of the template and the dynamic tension in the hoisting wire.

The wave slamming force on the template and the dynamic tension in the hoisting wire was analyzed using the OrcaFlex software. In order to determine the wave slamming force a range of characteristic slam coefficients were used. The range of the slam coefficients were investigated for different wave periods. A total of 4 test were performed. The first test focused on the behavior of the wave slamming force. The second test was dedicated to the influence of the vessel motion. In the third test the effect of the buoyancy, inertia and drag forces was analyzed. Finally, the effect of irregular waves was evaluated.

The performed tests showed a large influence of the wave slamming force on the dynamic tension of the hoisting wire. The influence decreased when the vessel motions and the other wave forces were taken into consideration. The influence of the slam coefficient decreased as well. In regular waves a scatter of 25 % was found in the prediction of the dynamic amplification factor (DAF) for all considered slam coefficients. A Comparing was made between the minimum C_s value according to guidelines. A possible maximum error of 18 % was found. Due to the extreme environmental conditions input, this was considered to be within commonly used safety margins. It was concluded that the wave slamming force will not limit the operational condition in the Wikinger project. Furthermore, it was concluded that thorough local flow analysis like CFD will not improve the prediction of the tension in the hoisting wire.

Acknowledgements

Performing this thesis project was not possible without the help and support of several people. Therefore I would like to thank them for helping me throughout the process.

First of all I would like to thank my supervisors. Zhen Gao, thank you for your supervision in the beginning phase of my project in Norway. Despite the great distance between Delft and Trondheim you kept engaged in the project. Something which I am very grateful for. Jeroen Hoving, all the talking sessions really helped me on finding a direction and focusing on what was important. This has helped me a lot. Professor Metrikine, despite the limited time for discussions all comments were always spot on and have really helped me to improve the level of this thesis. Lastly, I would like to thank Jasper Janssen for all the discussion sessions and helping me to find a way at Boskalis.

Furthermore, I would like to thank the people of EWEM and Boskalis for making his thesis possible. The EWEM program allowed me to live in Copenhagen and Trondheim. This has been such a great experience. Thanks to the elite cohort for sharing this journey with me. At Boskalis I was part of the offshore engineering department. This has been a joy. Thank you for your support.

Last but not least I would like to thank my friends and family. Thanks guys for sharing the struggle and for helping me out. Mom and Dad, thank you for your love and support.

Rotterdam, Oktober 2015

Roel Nous

Contents

Summary	iii
Acknowledgements	v
List of Figures	xi
List of Tables	xiii
Nomenclature	xv
1 Introduction	1
1.1 The Wikinger project	1
1.2 Thesis outline	4
2 Lowering Through the Wave Zone and Slamming	7
2.1 Installation of a sub-sea template	7
2.2 Slamming	9
2.3 Thesis objective	11
3 Modeling of the Template Lowered Through the Wave Zone	13
3.1 Modeling techniques	13
3.2 Environmental forces	15
3.2.1 Wave forces	15
3.2.2 Current and wind force	26
3.3 Components	26
3.3.1 Vessel: Giant 5	27
3.3.2 Template	28
3.3.3 Rigging	29
3.4 Model	31
3.4.1 Modeling considerations in OrcaFlex	31
3.4.2 Simulation considerations	35
3.4.3 Model and simulation overview	38

4	Effect of Slamming on the Hoisting Wire	43
4.1	Simulation set-up I	43
4.2	Results and discussions on the effect of slamming on the hoisting wire . .	44
4.2.1	Time domain simulation	45
4.2.2	Comparison for different slam coefficients and wave periods	51
5	Influence of the Vessel Motions	57
5.1	Simulation set-up II	57
5.2	Results and discussions on the influence of the vessel motions	58
5.2.1	Time domain simulation	59
5.2.2	Comparison for different slam coefficients and wave periods	63
6	Other Wave Forces and Irregular Waves	67
6.1	Simulation set-up III	67
6.2	Results and discussions on the influence of F_i, F_d and F_b	69
6.2.1	Time domain simulation	69
6.2.2	Comparison for different Cs and wave periods	73
6.3	Results and discussion on the influence of irregular waves	75
6.3.1	Time domain simulation	75
6.3.2	Comparison for different Cs	76
7	Conclusions and Recommendations	79
	References	83
A	Linear Wave Kinematics	87
B	Verification Vessel RAOs	89
C	Summary Theoretical Background	93
D	Slam Results for each Mud Mat	98
E	Template Motions Maxima	102
F	Summary Slam Results Template Test 1-3	105

List of Figures

1.1	Wikingen wind farm location	1
1.2	Schematic side view of the jacket structure	2
1.3	Installation steps foundation piles	3
1.4	Side view jacket installation using a sheerleg	3
1.5	Top view jacket foundation template	4
2.1	Subsea template lowered through the wave zone, K. Aarset [2]	8
2.2	Flow visualization from impact studies of a circular cylinder, M. Greenhow [5]	10
2.3	Frame taken by high speed camera after initial water entry capturing trapped air, F.J. Huera-Huarte [8]	11
3.1	Modeling Approaches, ANSYS [9]	14
3.2	C_d versus Reynolds number for various values of KC, Sarpkaya [11]	16
3.3	Drag coefficient for a fixed circular cylinder for steady flow in critical flow regime, for various roughnesses, DNV [12]	17
3.4	C_m versus Reynolds number for various values of KC, Sarpkaya [11]	19
3.5	Vertical added mass coefficient for circular cylinder at different distances from free surface; r is the cylinder radius, DNV [12]	20
3.6	Added Mass Coefficient of an oscillating disc. $h=2 r_d$, Garrido-Mendoza [18]	21
3.7	Slam coefficient as function of non-dimensional time, C.O. Ng [27]	22
3.8	Plots of the parameters A and B against wave steepness H/L: Δ =parameter A, \square = parameter B, N.J. Smith [7]	23
3.9	Plots of slam coefficient C_s against flight path angle for various wave steepness H/L: \diamond = <i>flatwater</i> , \blacklozenge = 0.035, * = 0.06, + = 0.07, <i>o</i> = 0.09, Δ = 0.1, \square = 0.11, N.J. Smith [7]	24
3.10	Relation between the slamming coefficient and the duration of impact, F.J. Huera-Huarte [8]	24

3.11	Giant 5 geometry and proposed deck equipment, lif [35]	27
3.12	Template geometry, lif [35]	28
3.13	Schematic view Mud mat, rev [38]	29
3.14	Line configuration: (a) side view (b) Top view, lif [35]	30
3.15	Top view ship and template configuration, lif [35]	30
3.16	Discretized mud mats top view	32
3.17	Coupled/Uncoupled RAOs: Pitch 0deg	33
3.18	Coupled/Uncoupled RAOs: Sway 90deg	34
3.19	Coupled/Uncoupled RAOs: Roll 0deg	34
3.20	Slam force compare to wave period for different wave heights	36
3.21	Simulation set-up overview	39
3.22	OrcaFlex model geometric view	41
3.23	OrcaFlex model top view	41
3.24	OrcaFlex model side view	41
4.1	Simulation set-up I	44
4.2	Wave elevation $T = 7.1$ s	45
4.3	Slam force over time for each mud mat at $T=7.1$ s	46
4.4	Slam force on each Mud mat at $T=7.1$ s	48
4.5	Roll and Pitch motion for 2 wave periods $T=7.1$ s	50
4.6	Wire tension heave motion comparison	50
4.7	Total slam force and contributing Mud Mat fractions for Wave periods T , $C_s=13.04$	52
4.8	Total slam force versus Wave periods for different C_s values	52
4.9	Schematic representation of δt for the wave impact on the template.	53
4.10	Pitch (a) & Heave motion (b) over Wave periods T for different C_s values	54
4.11	Dynamic tension and DAF of the hoisting wire	55
5.1	Simulation set-up II	58
5.2	Slam force over time for each Mud mat [$C_s=11.5$, $T_w=7.1$ s]	59
5.3	Slam force on each Mud mat $T_w=7.1$ s	60
5.4	Roll and Pitch motion for 2 wave periods $T=7.1$ s	61
5.5	Wire tension heave motion comparison	62
5.6	Slam force over wave period for different C_s values	63
5.7	Dynamic tension and DAF of the hoisting wire	64
6.1	Simulation set-up III	68
6.2	Wave force comparison	70
6.3	Roll and Pitch motion for 2 wave periods $T=7.1$ s	71
6.4	Wire tension heave motion comparison	72

6.5	Slam force over wave period for different C_s values	73
6.6	Dynamic Tensions and DAF of the hoisting wire	74
6.7	Jonswap spectrum [Hs=3, Tp=7]	75
6.8	Total slam force over time in irregular waves	76
6.9	Slam force Histogram	76
6.10	Histogram trend lines for different values of C_s	77
A.1	Linear theory relations for regular sinusoidal propagating waves on finite and infinite water depth. Faltinsen [4]	87
B.1	Coupled/Uncoupled RAOs: 0deg	90
B.2	Coupled/Uncoupled RAOs: 45deg	91
B.3	Coupled/Uncoupled RAOs: 90deg	92

List of Tables

1.1	Jacket foundation properties	2
3.1	Summary literature review C_d values cylinder	17
3.2	Summary literature review C_d values disc	18
3.3	Summary literature review C_m values cylinder	20
3.4	Summary literature review C_a values 3D discs	21
3.5	Summary literature review C_s values Cylinder	25
3.6	Summary literature review C_s values Disc & Plates	25
3.7	Main parameters Giant 5	27
3.8	Template component properties	29
3.9	Rigging properties	30
3.10	Model Overview	40
4.1	Slam parameter summary for each mud mat	47
4.2	Total slam force parameters	48
4.3	Maximum template motions	49
4.4	Tension and corresponding DAF	51
5.1	Total slam force parameters	60
5.2	Maximum template motions	61
5.3	Tension and corresponding DAF	63
6.1	Maximum wave forces	69
6.2	Total slam force parameters	70
6.3	Maximum template motions	71
6.4	Tension and corresponding DAF	72

Nomenclature

Latin Symbols

A_p	Projected area	$[m^2]$
C_a	Added mass coefficient	[-]
C_d	Drag coefficient	[-]
C_m	Inertia coefficient	[-]
C_s	Slam coefficient	[-]
F_b	Buoyancy force	[N]
F_d	Drag force	[N]
F_i	Inertia force	[N]
F_s	Slam force	[N]
P_D	Undisturbed pressure over a object	[Pa]
V_s	Submerged volume	[s]
E	Young's modulus	[Mpa]
I	Mass moment of inertia	$[kg \cdot m^2]$
V	Velocity vector	[m/s]
A	Added mass	[kg]
g	Gravitational acceleration	$[m/s^2]$
H	Wave height	[m]
h	Water depth	[m]
I	Turbulence intensity factor	[-]
k	Wave number	[-]
L	Wave length	[m]

m	Mass	[kg]
p	Pressure	[Pa]
T	Wave period	[s]
t	Time	[s]
v	Velocity	[m/s]

Greek Symbols

β	Flight path angle	[rad]
λ	Wave length	[m]
ν	Viscosity	[kg/(s · m)]
ω	Radial frequency	[rad/s]
ρ	Density	[kg/m ³]

Other Symbols

∇	Vector differential operator
----------	------------------------------

Chapter 1

Introduction

In this introduction an explanation will be given on the Wikinger project. Furthermore, the thesis outline will be given.

1.1 The Wikinger project

Wikinger is a new offshore wind park which will be installed near the German coast by the Iberdrola Energy Company. The wind park is placed in the Baltic sea 35 km from the island of Rugen at coordinates of N54.834, E14.068. The location for the Offshore wind park is given in Figure 1.1. The total area of the park is 34 km^2 . The Wikinger wind park will consist of 70 wind turbines with a rated power of 5 MW for each turbine. The total capacity of the wind farm is 350 MW. The turbine's foundation type is a jacket structure. The joint venture between Boskalis and VolkerWessels have been awarded the contract for the installation of the foundations of the wind park.



Figure 1.1: Wikinger wind farm location

Jackets

A jacket type will be used for foundation of the turbines. An illustration of this jacket is given in Figure 1.2. Different types of jackets are used dependent on the the water depth. All jackets can be categorized in type A and type B jackets. The footprint of both jacket types is the same. An overview on the specification of the jacket can be found in Table 1.1. Foundation piles are used to connect the jacket with the soil.

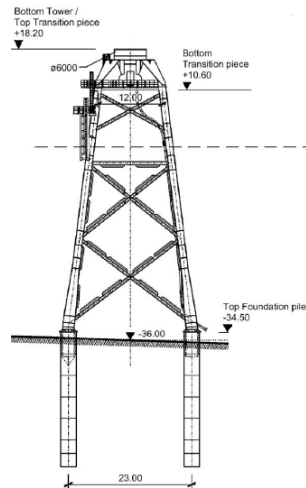


Figure 1.2: Schematic side view of the jacket structure

Table 1.1: Jacket foundation properties

	Foundation type A	Foundation Type B
No. of Jackets	41	29
Water depth	39-42m	36-39m
Total jacket weight (excl. Piles)	619t	602t
Weight foundation piles	Max 200 mt	Max 200 mt
Jacket height	62.2m	59.2m
Jacket width	23.0m	23.0m
Pile length	18-62m	18-62m

Installation procedure

The installation procedure can be split up into 2 parts. The installation of the foundation piles and the installation of the jacket. In the installation of the foundation piles a pre-piling method will be used in which 4 piles are installed using a sub-sea template. Afterwards, the jacket will be installed.

First a jacket foundation template is installed on the sea bed. The template will be used to guide and to accurately place the foundation piles. When the sub-sea template is installed a foundation pile is lifted and positioned in one of the sleeves of the template. Next a hammer is placed on top of the foundation pile which will pile the foundation piles vertically into the soil. This process will be repeated 4 times. The foundation piles will

be installed by using a crane vessel. An illustration of this process is given in Figure 1.3.

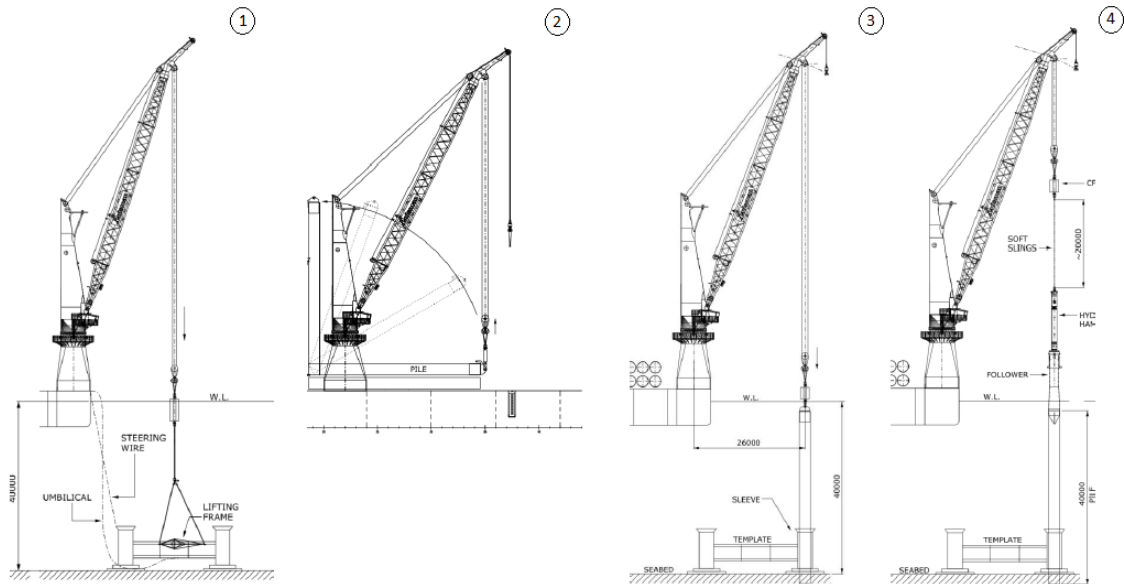


Figure 1.3: Installation steps foundation piles

Once the piles are installed, the template will be removed. Next the jacket will be placed. The jacket structure will be transported to the Wikinger site on a barge. For the installation of the jacket structures a floating sheerleg will be used. A drawing of the sheerleg and jacket during installation phase is given in Figure 1.4. The jacket is equipped with sleeves which need to be positioned into the piles. When the jacket is placed over the piles grouting is used to connect the piles to the jacket.

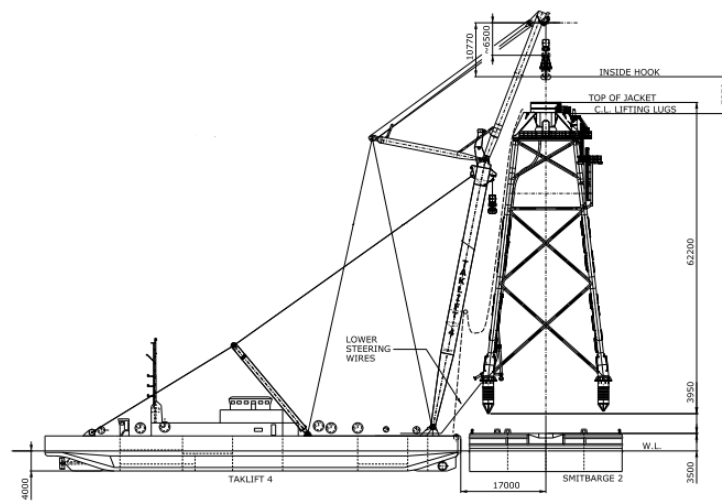


Figure 1.4: Side view jacket installation using a sheerleg

A critical phase in this installation procedure is the installation of the jacket foundation template. This will be elaborated further.

Installation of a jacket foundation template

The point of interest in the thesis is the installation of the jacket foundation template. This is due to the uncertain loads and dynamics during this operation. The installation of the template is illustrated in phase 1 of Figure 1.3.

The installation of the sub-sea template can be described in 4 phases. DNV characterizes these phases in their guidelines. The 4 lifting phases are as follows. DNV [1]

- 1) Lift off from deck and manoeuvring object clear of transportation vessel
- 2) Lowering through the wave zone
- 3) Further lowering down the sea bed
- 4) Positioning and landing

An important factor in the uncertainties during this installation phase is the geometry of the jacket foundation template. An illustration of the sub-sea template is given in Figure 1.5. The template ensures the correct placement of the foundation piles. It can be observed that the template contains large mud mats at each sleeve.

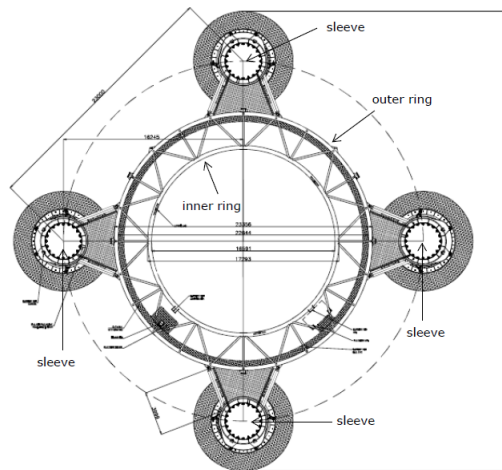


Figure 1.5: Top view jacket foundation template

1.2 Thesis outline

Critical points need to be investigated during the lowering operation of the template. The critical phase of the template lowered through the wave zone will be investigated in this thesis. As the template has a large surface area compared to its weight, the effect of the wave slamming force is deemed significant. The effect of slamming will be investigated

extensively. In order to obtain solutions a structured analysis need to be performed. The thesis will define the problems and will investigate this by creating simulation models. The outline of the report is as follows.

- Chapter 2 describes the problems concerning the lowering operation. From this a problem definition and thesis objective is formulated.
- Chapter 3 discusses the created model for analyzing the problem. Description are given on the involved components together with simplifications and assumptions.
- Chapter 4 will focus on the behavior of the wave slamming force.
- Chapter 5 is dedicated to the influence of the vessel motion.
- Chapter 6 will analyze the effect of the buoyancy, inertia and drag force. Next to this it will evaluate the effect of irregular waves.
- Chapter 7 will give conclusions and recommendations on the thesis project.

Lowering Through the Wave Zone and Slamming

The Wikinger project and installation procedures have been discussed in the introduction. Chapter 2 will elaborate on the challenges in the procedures for installing the foundations of the offshore wind turbines. First, the critical installation phase is discussed. Next, a discussion is given on the difficulties concerning slamming during installation. The Chapter will conclude with elaborating the thesis objective.

2.1 Installation of a sub-sea template

As mentioned in Chapter 1, 4 installation phases are identified for installing the sub-sea template. An important parameter in the installation phase is the hoisting wire tension. The hoisting wire tension and corresponding dynamic amplification factor (DAF) determine the operational limits of the installation.

Phase 1 is the lift-off from deck. In this phase the loading in the hoisting wire is governed by the weight of the template. Phase 2 is governed by the weight and wave forces. This phase endures the highest loads on the system during installation. In phase 3 and 4 the loading in the hoisting wire is governed by the submerged weight.

The critical phase in the installation procedure is phase 2. This lowering phase endures the highest loads and tension in the hoisting wire. It is critical to understand the behavior and forces on the system in this procedure. An example of a sub-sea template lowered through the wave zone is given in Figure 2.1. The main concerns are explained in this section.



Figure 2.1: Subsea template lowered through the wave zone, K. Aarset [2]

Waiting on Weather

The first issue to be considered is the waiting on weather time. Lowering the template through the wave zone causes template motions and dynamic tension in the wire. The maximum allowable loads on the system are restricted by regulations and crane capacity.

The limiting parameters of the crane are the maximum load, off lead and side lead angles. Since the static load is mostly known, a maximum dynamic load is allowed. This results in a restriction in the motion of the structure in the hook. These motions are caused by the incoming waves. From this a maximum allowable wave can be found. This will determine the operability and will result in a waiting on weather time.

Understanding the forces and behavior of the template for all possible environmental conditions can result in a more accurate estimation of the operational limits. This will improve the waiting on weather estimation and will reduce the cost of the operations.

Suitable Installation Vessel

For the installation of the sub-sea template a suitable installation vessel is chosen. The critical parameters in choosing a suitable vessel are the crane capacity and responses of the vessel due to waves. This is of main concern during the lowering operation. Thorough research in understanding the wave zone dynamics results in a less conservative vessel choice. This means a smaller vessel can be chosen which is more cost efficient.

Safety

The most important issue in the offshore industry is safety. This also applies for the Wiking project. Crew on deck can be seen in Figure 2.1. Their safety needs to be guaranteed. During phase 2 of the installation phase possible hazards are present. The phenomenon of slacking can occur in the hoisting wire. Motions of the template cannot be controlled when the hoisting wire is slacking. The template can hit the side of the vessel or hit the deck. This endangers the crew. Furthermore, snap loading can occur. This may break the rigging or hoisting wire or overload the crane. The snapped cable can possibly damage the vessel or injure crew members.

Understanding the phenomena during lowering through the wave zone will help in knowing the operation limits better. This also gives more insight in when to stop the operation. This reduces the risk of dangerous situations from happening. This will help in ensuring the safety of the crew members and equipment.

2.2 Slamming

The previous section illustrated the importance of investigating the behavior of the template as it is lowered through the wave zone. In the splash zone, slamming is present. The wave slamming force is a highly uncertain wave force which is hard to model. Analyzing the slam force is critical for understanding the behavior of the template lowered through the wave zone. This section will discuss the difficulties concerning this slam force.

Literature has been written on the wave slamming force. The definition of slamming is however different. Bertram characterizes 4 types of slamming for ship hulls: bottom slamming, bow-flare slamming, breaking wave impact and wet-deck slamming. Similar behaviors but different definitions are found for jacket structures. Bertram [3]

The Installation of the Wiking project will be governed by a vertical slam force. The definition used throughout this thesis is given by Faltisen and is as follows :

'Impulse loads with high pressure peaks during impact between a body and water'. Faltisen [4]

As mentioned slamming is a uncertain phenomena. This makes it difficult to analyze. The difficulties in the slam force can be characterized as listed below. These difficulties in determining the slam force will be discussed and elaborated further in this section. Bertram [3]

- Slamming is a highly non-linear phenomenon, which is sensitive to relative motion and the contact angle between body and free surface
- Predictions in natural seaways are inherently stochastic; slamming is a random process in reality
- Since the duration of wave impact loads is very short, hydro-elastic effects are large.
- Air trapping may lead to compressible, partially supersonic flows were the flow in the water interacts with the flow in air.

Non-linear

The first difficulty to be considered is the non-linearity of the slam force. Small differences in flow properties and orientation have a large impact on the slam behavior due to the impulse and non linear behavior of the slam force. This makes slamming difficult to estimate. A representation of the slam force for a circular cylinder is given Figure 2.2. The non-linear behavior can be observed at the edges of the cylinder. For a circular disc

like the mud mat it is more difficult for the flow to go around the shape causing higher turbulence and uncertainty in the flow response.

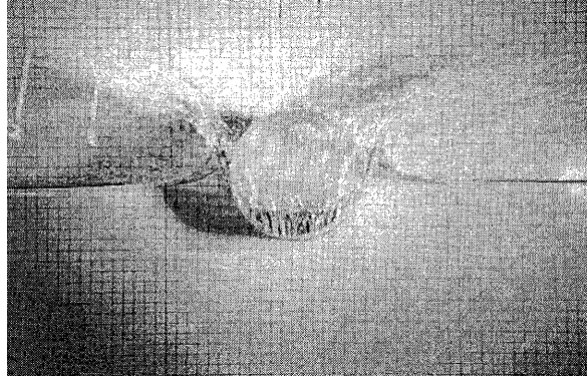


Figure 2.2: Flow visualization from impact studies of a circular cylinder, M. Greenhow [5]

Hu, states the following about slamming behavior: 'Wave impact is a strong nonlinear phenomenon and a random process which is very sensitive to relative motion between body and free surface'. The hydrodynamic pressure acting on the body due to slamming and the distribution on the contact area are very sensitive. The slam force is the resulting integrated force. Hu [6]

Smith investigated sensitivities for different parameters considering the behavior of the slam force. Smith states that the non-linear slam force behavior depends on the flight-path angle, Froude number, wave steepness and wave height over longitudinal length scale. N.J. Smith [7]

Wave stochasticity

What was found from investigating the wave slamming force is that multiple parameters are of influence. Controlling the parameters is however difficult. This causes a random response. This stochastic effect of slamming will be elaborated further.

The stochastic effect of slamming can be split up into 2 segments. The first effect is the local flow phenomena. At the point of interaction between wave and body small and large eddies can occur. This effects the interaction between the body and the water. The occurrence of these flow phenomena are stochastic for real waves. This means that the local flow properties are different for each slam event. The second effect is the wave interaction. Waves in real sea conditions are random. This means a stochastic range of wave shapes and sizes of the wave train. The wave influences the response of the body and effects the local interaction. This means parameters like incidence angle, slam area and relative velocity are influenced by the incoming wave. These parameters are effectively random due to the stochastic nature of the incoming wave. This results in a random behavior of the slam force. This makes it very difficult to predict the actual slam force at the moment of installation.

Hydro-elastic effects

Slamming can induce large hydro-elastic effects. Hydro-elastic effect refers to the fact that elastic deformation of the body surface will influence the hydrodynamic loads. This is primarily important for the template structure. From reference it was found that these hydro-elastic effects can influence the vibrations on the template. This can damage the template. Hydro-elastic effects have however no influence on the dynamic response in the hoisting wire in the case of the Wiking project.



Figure 2.3: Frame taken by high speed camera after initial water entry capturing trapped air, F.J. Huera-Huarte [8]

Air trapping

The last uncertainty in determining the slam force is the occurrence of air trapping. Air trapping can occur for high relative velocities between body and water when the deadrise angle is close to zero. Due to the high impact speed, air cannot escape quickly from the point of impact. The air will get trapped in the water. This will result in a mixed area with air and water. A visualization of trapped air from a flat plate at an deadrise angle of 0 degrees is given in Figure 2.3. The air is compressible and will cause a variation in pressure on the body. The air trapping effect is non linear and stochastic. This gives an added uncertainty in the slam behavior. Air trapping will have a positive cushioning effect on the slam force.

2.3 Thesis objective

The previous sections of this Chapter discussed the difficulties for investigating the effect of slamming on the hoisting wire for the Wiking project. This will be used to determine the thesis objective. First a problem definition will be discussed. From this a thesis objective will be formulated.

Problem Definition

During installation of the sub-sea template the critical phase is when the template is lowered through the wave zone (phase 2). The highest loads occur during this point of installation. This effects the waiting on weather, crane operability and costs of the oper-

ation. The high loads also cause safety risks. The loads are however complex. In order to optimize the operation this needs to be investigated.

The governing wave force on the system at the wave crest is the wave slamming force. It was concluded that the slam force is hard to predict. Understanding the slamming behavior on the installation can help in increasing the safety and reducing the costs.

Thesis objective

The problems found in lowering the template through the wave zone are the wave slamming force, the template motions and the hoisting wire dynamics. From this a thesis objective can be formulated. The thesis objective can be written as:

Determine the effect of the slam force on the total motion and loading in the hoisting wire during lowering of the template through the wave zone.

The behavior of the slam force will be investigated. Next, the response of the motions will be discussed. The reaction of these motions on the rigging will be evaluated. This will result in the analysis of the dynamic amplification factor (DAF) of the hoisting wire. The goal of the thesis is to give a recommendation on how slamming will effect the installation of the template. Furthermore, a recommendation will be given on modeling the slam force. The main questions of this thesis can be written as follows.

- What is the local behavior of slamming on the mud mats?
- What is the total behavior of slamming on the template?
- How does slamming effect the motion of the template?
- How does slamming effect the tension in the hoisting wire?
- What is the influence of the Vessel motions on the behavior of the slam force?
- What is the effect of the other wave forces on the behavior of the slam force?
- Does slamming affect the limits of the operation?

The thesis will focus on establishing answers by performing dynamic time domain simulations. Four tests will be performed in order to investigate the operation. The tests are used to answers the listed questions and give recommendations to the Wiking project. In order to perform the simulation a model must be created. This will be discussed in the next Chapter.

Modeling of the Template Lowered Through the Wave Zone

In order to solve the defined problem a model has been created. This Chapter will elaborate and discuss the created model. First the decision on the type of modeling technique is made. After this all present forces during the lowering operation are discussed. The model components are discussed next. The last section of this Chapter will give an overview on the simplifications and the input of the created model.

3.1 Modeling techniques

This section will discuss the possible modeling techniques which can be used to model the lifting analysis. The main goal of the model is to determine the slam force and investigate the interaction with the motions of the system and tension in the hosting wire. Figure 3.1 gives an overview on the possible paths to take for doing a lifting analysis. Different main options can be observed: A analytically methodology, mixed methodology and full CFD methodology. The 3 illustrated options will be discussed in this section.

Analytical Methodology

The analytical methodology will be discussed first. The analytical method calculates simplified equations from reference "by hand". Software like Excel, Python and Matlab may be used to solve the equations. It can be chosen to perform a static or dynamic analysis. A dynamic analysis is however complex. Specialized software may be needed to solve the dynamic solution. therefore it is often chosen to solve the problem statically in the analytical method. DNV suggests a static solution.

The advantage of this method is that it is simple and can be performed fast. Furthermore the input and equations used can be controlled completely. This is beneficial for validation. The main disadvantage is the accuracy of the results. Estimation of the dynamic

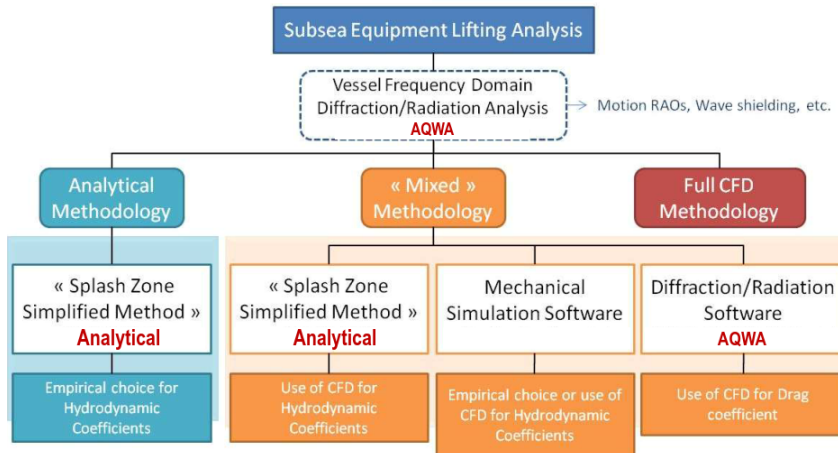


Figure 3.1: Modeling Approaches, ANSYS [9]

forces is poor. This makes this model often conservative.

Mixed Methodology

The mixed methodology is split up into 3 segments. The segments are arranged by complexity. First, an analytical approach is combined with the determination of the hydrodynamic coefficients with CFD. The other given options in the mixed methodology are time domain simulations. CFD or empirical values are used for the hydrodynamic coefficients. Software packages like Ansys AQWA, Orcaflex, Moses and SIMO can be used to solve the dynamic solution of the system. The methodology solves the dynamic forces and motions of the system. This increases the accuracy. However, assumptions are made on how to include the forces in the system. The calculation time is longer compared to the analytical solution, but much faster than the CFD solution.

Full CFD Methodology

The last method to consider is a full CFD analysis. CFD is a method to calculate the complete flow behavior of the water. Different CFD methods can be considered. A choice is made depending on computer capacity and simulation time. Examples of CFD methods are the vorticity confinement method (VC method), large eddy simulation (LES), Direct numerical simulation (DNS), Reynolds-averaged Navier-Stokes (RANS). Software packages as Ansys, PyFR and OpenFoam provide tools to perform CFD calculations.

CFD is a powerful tool and can calculate the flow behavior accurately. The accuracy is dependent on the chosen method. The simulation time is however very long compared to the other 2 methods. For the installation of the Wiking project it is important to investigate the response of the system. This is difficult when using CFD methods. CFD is good in modeling local effects and not in global motion behavior. Furthermore, the result is dependent on the set boundary conditions and mesh size. Experience and thorough understanding is needed for a good result.

Three methodologies have been discussed in this section. From discussion about the

methodologies it can be concluded that a static analysis is too simplified for the Wiking project. The CFD method can give high accuracy. However to obtain accurate results, high computer capacity, time and experience is needed. Furthermore it is difficult to obtain a dynamic response from pure CFD simulations. From this it was concluded that a mixed methodology is the best fit for understanding the slam force and dynamic behavior of the template lowered through the wave zone. The chosen mixed methodology for the model is a time domain simulation. Hydrodynamic coefficients will be obtained from experiments and guidelines given in references.

3.2 Environmental forces

This section will discuss the environmental forces acting on the system. The primary force of influence are the wave forces. The wave forces will be elaborated on extensively in this section. Furthermore wind and current forces will be discussed. The determination of the forces is dependent on the type of modeling technique which was chosen in section 3.1.

The forces can be characterized by force coefficients. This is dependent on the overall shape of the structure. The template can be split up into simple shapes segments. The cylindrical tubes can be simplified by slender elements. The mud mats can be defined as a disc shape. Both cylinder and disc shape will be discussed for all wave forces.

3.2.1 Wave forces

The wave forces are considered as the main source of influence on the system. The forces are caused by disturbances in the flow field and by accelerations exerted on the body. Both forces are related to the fluid motion and therefore to nonlinear processes. In order to determine the force, models can be applied which represent the behavior of the forces. This section will discuss the listed force contributions due to waves. The wave forces can be described as the sum of 4 contribution forces listed as follows.

- Buoyancy force
- Drag force
- Inertia force
- Slam force

Buoyancy Force

When an object is submerged in water an upward force is created due to the buoyancy of the object. The total buoyancy force is dependent on the level of submergence of the object. The Buoyancy force can be written as Equation 3.1. Where ρ , g and V_s are the density, gravity acceleration and submerged volume respectively. The direction of the buoyancy is opposite to the gravity force.

$$F_b = \rho g V_s \quad (3.1)$$

Drag Force

The drag force on a 3D body can be described by Equation 3.2. The characteristic of the drag is determined by the drag coefficient. For slender bodies the drag force can be expressed as given in Equation 3.3.

$$F_D = 0.5\rho C_D A_p v|v| \quad (3.2)$$

$$\delta F_d = 0.5\rho C_D A_p v|v|\delta t \quad (3.3)$$

Drag coefficient for cylinders

Extensive studies have been performed to determine the slam and drag coefficient of a cylinder. As previously mentioned the coefficients are dependent on the Reynolds number and the Keulegan Carpenter number. Clauss [10] (1992) suggests drag coefficients for different Reynolds regions and KC values. The drag coefficient varies from 0.6 to 1.2.

Sarpkaya (2010) presents results of the drag coefficient as function of the Reynolds number for various values of KC. This is given in Figure 3.2. The figure shows Reynolds numbers in the unstable phase of C_d . What can be seen from the figure is that C_d increases from $Re = 3 \cdot 10^{-5}$ to $0.1 \cdot 10^{-5}$. It can also be concluded that the drag coefficient stabilizes for Reynolds number higher than 15.

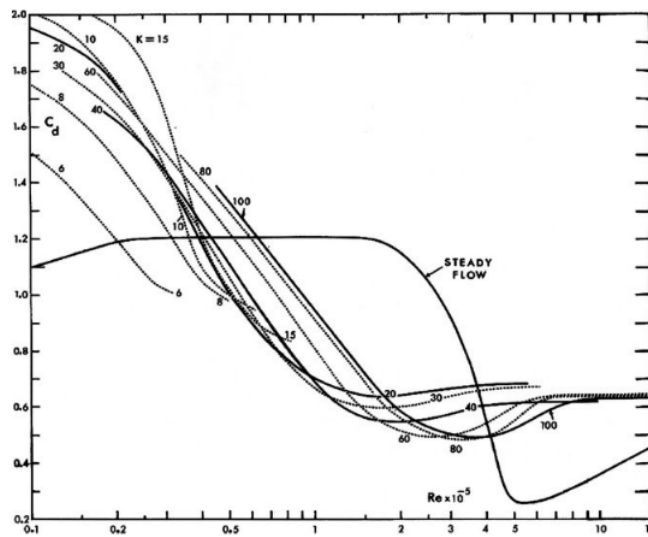


Figure 3.2: C_d versus Reynolds number for various values of KC, Sarpkaya [11]

Sarpkaya [11] (2010) performed a literature review in conjunction with experiments. It states that from reference and design codes a drag and slam coefficient of $C_D = 0.6$ to 1.0 can be assumed. DNV suggests C_D values as function of the roughness. The drag coefficient as function of Reynolds number for different roughnesses is given in Figure 3.3. Again the region for Reynolds numbers is given where C_D is unstable. What can be seen from the figure is that for Reynolds number lower than 10^4 C_d converges to a constant value of 1.2.

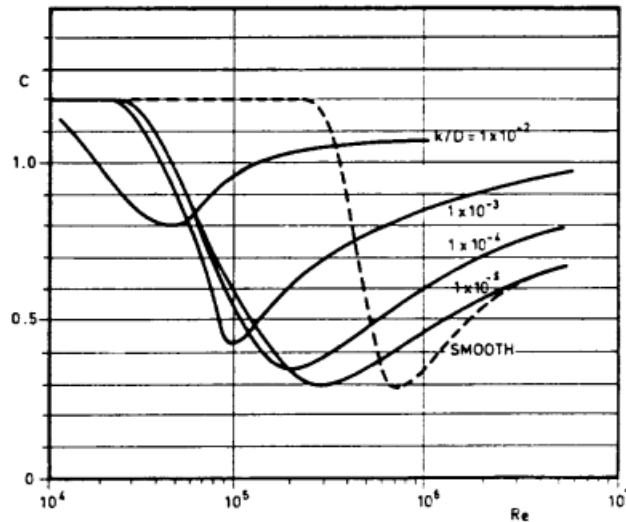


Figure 3.3: Drag coefficient for a fixed circular cylinder for steady flow in critical flow regime, for various roughnesses, DNV [12]

J.M.J. Journee [13] states suggestion from design codes of the American Petroleum Institute (API) and the Society of Naval Architects and Marine Engineers (SNAME). Both guidelines provide drag coefficient for different roughnesses. The given C_D values from API and SNAME are given as 0.65-1.05, 0.65-1 respectively. An overview of the presented drag coefficients is given in Table 3.1.

Table 3.1: Summary literature review C_d values cylinder

No	Author	Model	Focus	Drag
1	Claus (1992)	Cylinder	KC, Rn	$C_D = 0.6 - 1.2$
2	Sarpkaya (2010)	Cylinder	Reference study	$C_D = 0.6 - 1$
3	Sarpkaya (2010)	Cylinder	KC, Rn	$C_D = 0.5$
4	DNV-RP-C205	Cylinder	Smooth/Rough	$C_D = 1.2$
5	API	Cylinder	Smooth/Rough	$C_D = 0.65 - 1.05$
6	SNAME	Cylinder	Smooth/Rough	$C_D = 0.65 - 1$

Drag coefficient for discs

Research has been done on drag coefficient for disc shapes. Compared to C_d values for cylinders limited literature is available. R. Clift [14] (1978) presents C_d values for different Reynolds numbers for a disc. It states that for Reynolds number higher than 10^4 , C_d can be taken as 1.17. NASA conducted experiments for different shapes and suggests a drag coefficient of 1.28. For AQWA software a default value of 1.14 is used for a disc shape. it must be noted that this value only holds for a disc with hydrodynamic interaction on 1 side. If both sides are interacting with water this value should be doubled. An overview on the given drag coefficients for a disc shape is given in Table 3.2. R. Clift [14] (1978), NASA and Administration [15], aqw [16]

Table 3.2: Summary literature review C_d values disc

No	Author	Model	Focus	Drag
1	Clift (1978)	Disc	Re	$C_D=1.17$
2	AQWA (2011)	Disc		$C_D=1.14$
3	NASA (2014)	Disc	Shape	$C_D=1.28$
4	DNV-RP-H103	Disc	$Re > 10^4$	$C_D=1.9$

From the literature study on the drag force it can be concluded that the drag coefficient for a cylinder and disc is well known. The deviation between values of different references is small. In the model the maximum C_d value for a cylinder of 1.2 was chosen. A value of 1.9 was chosen for a disc.

Inertia Force

The inertia force is related to the added mass of the object in water. It can be noted that the inertia force is in phase with the wave acceleration. The inertia force can be split up into 2 components. the Froude-Krylov force and the disturbance force. The Froude-Krylov force describes the undisturbed pressure field and can be described as Equation 3.4 given by Faltinsen [17]. P_D describes the undisturbed pressure over the area of the located object.

$$F_{FK} = \iint_S P_D ds \quad (3.4)$$

DNV suggests a relation for the dynamic wave pressure. From this the Froude-Krylov force can be simplified to Equation 3.5. Where V_s is the submerged volume and \dot{v} the vertical fluid acceleration.

$$F_{FK} = V_s \rho \dot{v} \quad (3.5)$$

The Froude-Krylov force describes the forces for an undisturbed flow. The second force describes, as the name suggests, the disturbance force of the flow. It describes the forces which will affect the flow due the occurrence of the body. These disturbance forces are drag, inertia and slam forces. The inertia and drag loads can be described by Morison's theory. For an object located in the splash zone this can be described as given in Equation 3.6.

$$F_{Morison} = V_s \rho \dot{v} + A \dot{v} + \frac{\rho}{2} C_D A_p |v|v \quad (3.6)$$

Comparing The Morison equation with Equation 3.5 it can be seen that the first term in the equation is the Froude-Krylov force. The second term is denoted as the added mass term. The last term in the equation is the drag force component. In conclusion the total inertia force on the system can be written as Equation 3.7.

$$F_I = V_s \rho \dot{v} + A \dot{v} = C_m V_s \rho \dot{v} \quad (3.7)$$

Inertia coefficient cylinders

Research is done in order to obtain the inertia coefficient for a cylinder. Clauss [10] (1992) states a inertia coefficient for different roughness and Reynolds number. It suggest C_m values from 1.5-2.

Since the inertia coefficient is dependent on the added mass, a difference is made between the level of submergence of the cylinder. Sarpkaya [11] presents a relation for the added mass coefficient C_a for partly submerged cylinders. The added mass coefficient is related to the inertia coefficient by $C_m = 1 + C_a$. The relation for the added mass coefficient for a partly submerged cylinder is given by Equation 3.8.

$$C_a = \frac{0.5}{\pi} \left[\frac{2\pi^3 (1 - \cos \alpha)}{3 (2\pi - \alpha)^2} + \frac{\pi}{3} (1 - \cos \alpha) + \sin(\alpha - 1) \right] \quad (3.8)$$

For fully submerged cylinders the inertia coefficient can be represented as a function of the Reynolds number and the Keulegan-Carpenter number. The inertia coefficient as function of the Reynolds number for different KC values is given in Figure 3.4. For increasing Reynolds number, C_m converges to 1 value for all values of KC. It was found that the value for which C_m converges is equal to 1.85.

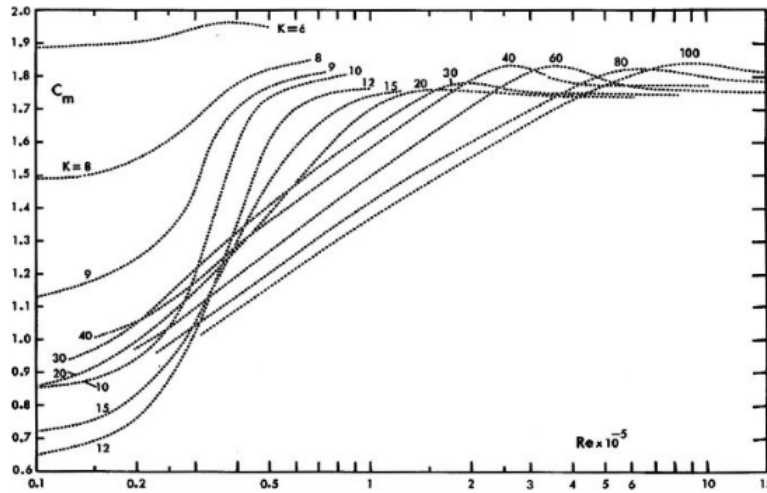


Figure 3.4: C_m versus Reynolds number for various values of KC , Sarpkaya [11]

Far from the seabed and free surface DNV suggests Equation 3.9 as an estimation of C_m for a submerged cylinder.

$$C_m = \max \begin{cases} 2.0 - 0.44(KC - 3) \\ 1.6 - (C_d - 0.65) \end{cases} \quad (3.9)$$

DNV [12] presents the effect of the free surface on the added mass coefficient. It states that the vicinity effect of the free surface depends on the frequency of oscillation ω and the distance h to the free surface. This relation is represented in Figure 3.5. For a cylinder going through the free surface Equation 3.10 is suggested.

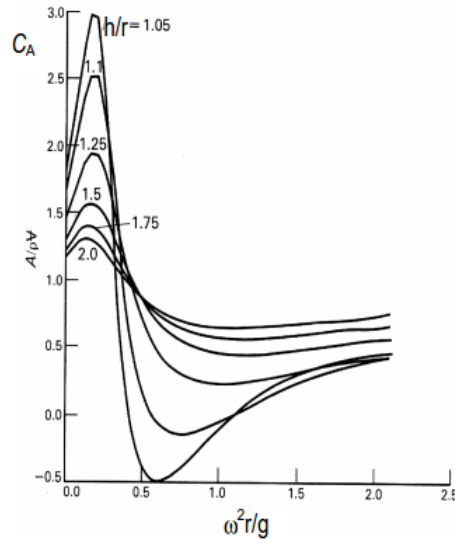


Figure 3.5: Vertical added mass coefficient for circular cylinder at different distances from free surface; r is the cylinder radius, DNV [12]

$$C_m = \frac{4}{\pi(kR)^2 \sqrt{A(kR)}} \quad (3.10)$$

Suggestions are made in API and SNAME guidelines. An overview of the obtained inertia coefficients is given in Table 3.3.

Table 3.3: Summary literature review C_m values cylinder

No	Author	Model	Focus	Drag
1	Claus (1992)	Cylinder	KC, Rn	$C_m = 1.5 - 2$
2	Sarpkaya (2010)	Cylinder	Reference study	$C_m = 0.5 - 2$
3	Sarpkaya (2010)	Cylinder	KC, Rn	$C_m = 1.85$
4	DNV-RP-C205	Cylinder	submergence	See Equation 3.9, 3.10
5	API	Cylinder	Smooth/Rough	$C_m = 1.2 - 1.6$
6	SNAME	Cylinder	Smooth/Rough	$C_m = 1.8 - 2$

Inertia coefficient discs

Similar to C_d values limited literature is available on inertia coefficients for discs compared to cylinders. Garrido-Mendoza [18] conducted experiments on added mass coefficient for discs in relation to different KC values. Results were compared with similar experiments from H. Wadhwa, B Krishnamoorthy [19], K. Vu [20] and L. Tao [21]. The added mass as a function of Keulegan-Carpenter values is given in Figure 3.6. What can be notified from the figure is that the added mass coefficient increases for higher KC values. Furthermore it must be notified that only small KC values were considered in the experiments.

H. Wadhwa, B Krishnamoorthy [19] conducted experiments in order to investigate the effect of the elevation of the disc from the sea bed on the added mass. Suggestions are made by AQWA and DNV on inertia coefficients for disc shapes. An overview on the

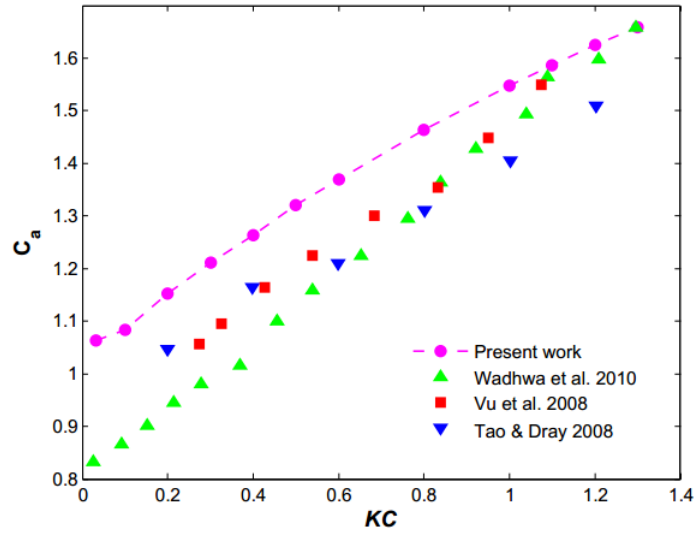


Figure 3.6: Added Mass Coefficient of an oscillating disc. $h=2 r_d$, Garrido-Mendoza [18]

added mass coefficient from literature is given in Table 3.4. Again the inertia coefficient is related to the added mass coefficient by $C_m = 1 + C_A$.

Table 3.4: Summary literature review C_a values 3D discs

No	Author	Model	Focus	Drag
1	Vu (2008)	Disc	KC	$C_a=1-1.7$
2	TAO (2008)	Disc	KC	$C_a=1-1.5$
3	Wadhwa (2010)	Disc	Elevation	$C_a=1.1-1.4$
4	Wadhwa (2010)	Disc	KC	$C_a= 0.8-1.7$
5	AQWA (2011)	Disc		$C_a=1$
6	Mendoza (2013)	Disc	KC	$C_a=1.1-1.7$
7	DNV-RP-C205	Disc	Shape	$C_a = \frac{2}{\pi} \approx 1.57$

Similar to the drag coefficient it can be concluded that the inertia coefficient for cylinders and discs are well known. The scatter is small between the references. A maximum C_a value of 2 and 1.7 is chosen for the cylinder and disc respectively.

Slam Force

The slam force is characterized by the slam coefficient C_s . Numerous experiments have been performed to determine the slam coefficient for different geometries. The literature study for the slam coefficient will focus on tests made by cylinders and plates. From the literature study a conclusion will be made for the determination of the slam load for the template.

The slam load was studied by Von Karman [22] (1929). He considered a circular cylinder representing its immersion as an expanding flat plate for a flat water surface. Von Karman provides a general asymptotic theory for the pressure distribution during the slamming

event. Wagner [23] (1932), extended this approach for a wedge entry by incorporation of a local jet analysis.

S.Chuang [24] (1966), performed experiments on slamming for a ship with a flat bottom. The test consisted of a drop test with a structural scale model. Chaung found a linear relationship between the maximum pressures at the center of pressure and the impact speed on the panel. Verhagen [25] (1967), introduced the effect of the compressible layer of air between the flat plate and the water surface.

Sarpkaya [11] (1978,) conducted numerical and experimental tests on wave slam loads for horizontal cylinders with different diameters. The conclusion of his research was that the force was dependent on the dynamic response of the model. Greenhow [26] (1987), applied these theories to the cylinder slamming problem showing reasonable agreements with the experiment models. Faltinsen [17], contributed in numerous articles for slam loads in vessel and deck slamming during his lifetime. An article of him considered the slam loads on a high-speed vessel. The conclusion of this article was that the vertical velocity of the wave is of high important for slam forces.

C.O. Ng [27] (1992), carried out numerical computations using a volume-of-fluid method (VOF). From this slam coefficients were obtained as function of time. The model used in the calculation was a rectangular section of 0.3m width and 0.5 height. The result of the computation is given in Figure 3.7.

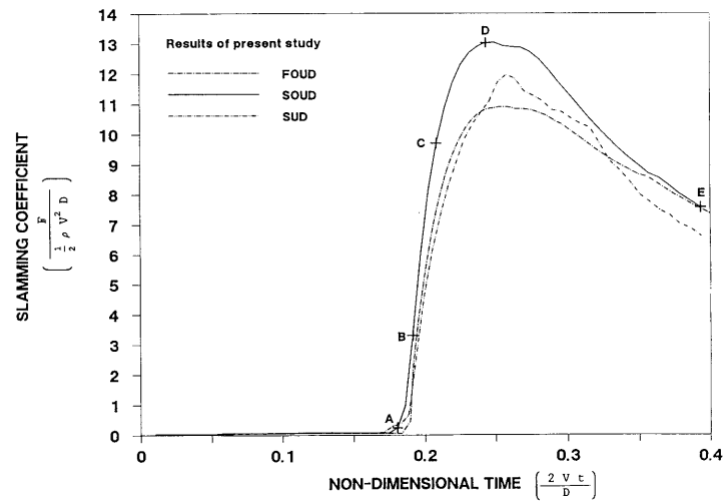


Figure 3.7: Slam coefficient as function of non-dimensional time, C.O. Ng [27]

The figure shows the slam coefficient over time for 3 advection schemes. The 3 schemes approximate the Navier-Stokes equations by different advection terms. A maximum slam coefficient of 13.04 was found. Results were compared with B. R. Koehler [28], which showed similarities.

A laboratory study was carried out to investigate the slamming effect on horizontal slabs using regular waves by N. Suchithra [29](1994). The purpose of the experiment was to check if freak waves could cause potential danger for deck loading. Regular waves with different frequencies were used. Comparison was made between the wave frequency and C_s . Another comparison which was made was the relation between the Keulegan-Carpenter number and the slam coefficient. Suchithra concluded that the slam coefficient for a horizontal slab in regular waves ranged from 2.5 to 10.2.

N.J. Smith [7] (1997), conducted an experimental investigation on the maximum vertical force on a flat plate due to impact of the water waves. A thin plate was used in the model. The mass, impact velocity, flight path angle and wave steepness were varied. A relation was found for the slam coefficient using a best fit method for the obtained data points. N.J. Smith [7], states that the slam coefficient is dependent on flight path angle, Froude number, wave steepness and wave height over longitudinal length scale. This is given in Equation 3.11.

$$C_s = C_s \left(\beta, \frac{U}{\sqrt{gl}}, \frac{H}{L}, \frac{H}{l} \right) \quad (3.11)$$

The experiment showed that the dependence on $\frac{U}{\sqrt{gl}}$ and $\frac{H}{l}$ is very small. From this the slam coefficient can be determined by Equation 3.12. The parameters A and B as function of the wave steepness are given in Figure 3.8. Figure 3.9 illustrates the dependence of the flight path angle for different $\frac{H}{L}$ values.

$$C_s = A\beta^B \quad (3.12)$$

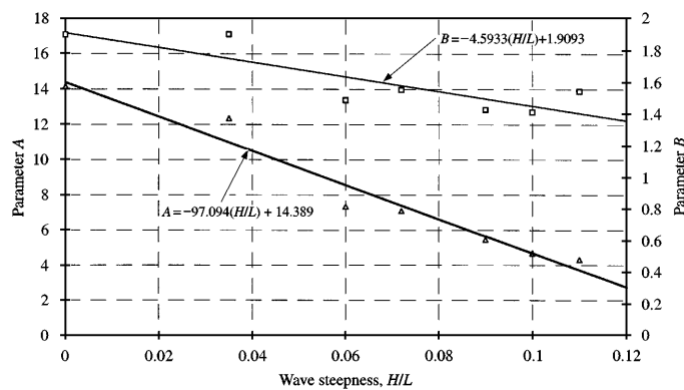


Figure 3.8: Plots of the parameters A and B against wave steepness H/L : Δ =parameter A, \square =parameter B, N.J. Smith [7]

Lin [30] (1997), continued on investigation the air pocket created under a flat plate. Experiments led to the development of an equation which relates the pressure to the thickness of the air cushion. G. Bea [31](1999), performed a case study on a platform in the gulf of Mexico. The aim of the analysis was to verify guidelines given by the American Petroleum Institute (API). Suggestions were made to improve this guideline. Main

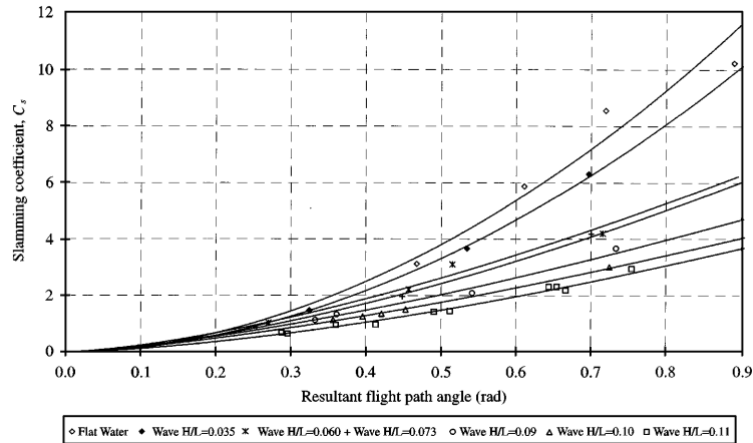


Figure 3.9: Plots of slam coefficient C_s against flight path angle for various wave steepness H/L : \diamond = flatwater, \blacklozenge = 0.035, $*$ = 0.06, $+$ = 0.07, o = 0.09, \triangle = 0.1, \square = 0.11, N.J. Smith [7]

improvement considered the procedure on tackling the slam load.

E.V. Ermanyuk [32] (2004), investigated the slamming of a circular disc on shallow water. It was shown that the presence of an air cushion has a large influence on the time-scale of impact and the splash-jet shape. F.J. Huera-Huarte [8] (2010), performed tests on water slamming on a flat panel. A plate was dropped by a sling shot on calm water. The plate was set at different incident angles and compared with each other. The impact time was also measured. From the experiments a relation was obtained for the slam coefficient as function of the impact time. This relation is given in Equation 3.13.

$$C_s = 0.79\delta t^{-1.4} \quad (3.13)$$

Figure 3.10, illustrates the obtained data points together with the suggested relation given in Equation 3.13.

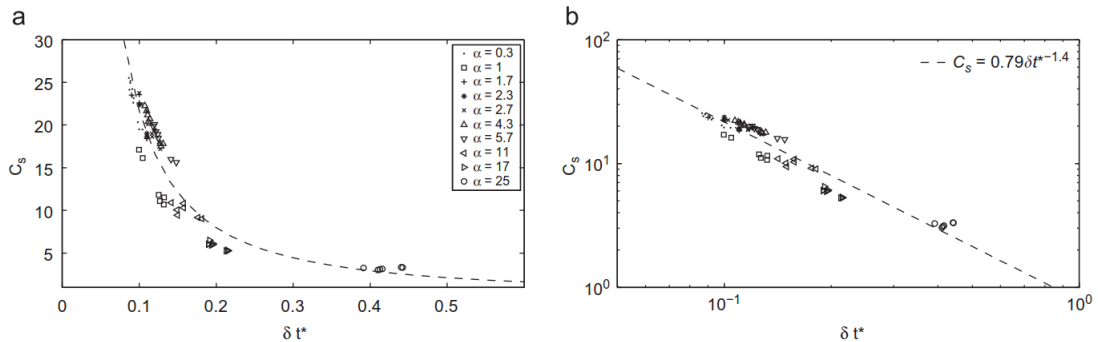


Figure 3.10: Relation between the slamming coefficient and the duration of impact, F.J. Huera-Huarte [8]

G. Sekhar [33] (2011), investigated the effect on horizontal slamming for different shapes with the use of particle image velocimetry (PIV). Sekhar concluded that the horizontal

slam force is highly dependent on wave steepness. Furthermore it was noted that the slam load decreases with increasing period. For the case of the template the horizontal slamming will be considered negligible compared to the vertical slamming.

DNV [1] suggests Equation 3.14 as a determination of the slam coefficient for a circular cylinder. Where s is the submergence of the cylinder and D the diameter of the cylinder. No suggestion are made for the slam coefficient of plates.

$$C_s(s) = 5.15 \left[\frac{D}{D + 19s} + \frac{0.107s}{D} \right] \quad (3.14)$$

An overview of the literature on the slam coefficient is given in Table 3.5 and Table 3.6. The type of model and focus of each article can differ and is therefore included in the summary. A list is given on the obtained ranges of the slam coefficient from the different authors.

Table 3.5: Summary literature review C_s values Cylinder

No	Author	Model	Focus	Slam
1	Faltinsen (1977)	Cylinder	impact	$C_s=3.1$ (num.), $C_s=5.3$ (exp.)
2	Sarpkaya (1978)	Cylinder	impact	$C_s = \pi$
3	DNV (2014)	Cylinder	guideline	see Equation 3.14

Table 3.6: Summary literature review C_s values Disc & Plates

No	Author	Model	Focus	Slam
1	Ng & Kot (1992)	Panel	time	$C_{s(max)} = 13.04$
2	Suchithra (1995)	Disc	waves	$C_s = 2.5-10.2$ (regular)
	Suchithra (1995)	Disc	waves	$C_s = 8.7-10.2$ (random)
3	Smith (1997)	Disc	$\frac{H}{L}, \beta$	$C_s = A\beta^B$
4	Bea (1999)	Platform	guidelines	changes to API guide
5	Huarte (2010)	Panel	duration	$C_s = 0.79\delta t^{-1.4}$
6	DNV (2014)	Disc	guideline	$C_s \geq 5$

What can be concluded from the literature study on the slam coefficient is that C_s is dependent on multiple parameters. Important parameters found in the reference are size of the specimen, geometry, incident angle, speed, Keulegan-Karpenter number, Froude number and wave steepness $\frac{H}{L}$. From this it can be concluded that it is very complex to determine the correct slam coefficient for the template. From the study it was found that the slam coefficient ranges from 2.5-13.04.

The thesis will investigate the effect of the slam load by performing a sensitivity study on the slam load by altering C_s for the range found from the literature study being 2.5-13.04.

3.2.2 Current and wind force

Next to wave conditions other environmental conditions need to be considered. Two significant factors elaborated in this section are the wave current and wind speed.

Current

The current in a offshore site can be found due to measurements and reference. The current has a large influence on the station keeping conditions. The tension in the mooring lines are influenced by this. The current can be modeled by using a constant value. In this way the drift properties can be evaluated. The current will have a contribution in the total wave loading. Dependent on the structure the current will induce viscous effects on the structure. The forces and moments exerted on a floating objects by a current can be split up in 2 different parts. The first part is a viscous part. Friction between the structure and fluid together with pressure drag cause a force on the structure. The second part is a potential part which is the component due to a circulation around the object together with free water wave resistance. The contribution to the current is however small. The current force can be written as Equation 3.15 and Equation 3.16. Here A_{TS} and A_{LS} are the submerged transverse and lateral projected area respectively. α_c is the current direction.

$$X_c = \frac{1}{2}\rho \cdot V_c^2 \cdot C_{x_C}(\alpha_c) \cdot A_{TS} \quad (3.15)$$

$$Y_c = \frac{1}{2}\rho \cdot V_c^2 \cdot C_{Y_C}(\alpha_c) \cdot A_{LS} \quad (3.16)$$

Wind simulation

The wind at a certain location can be obtained using site specific observation. The wind can be modeled by a constant wind speed together with a turbulence intensity factor. The turbulence intensity factor can be found by Equation 3.17. Were I_{ref} is the reference turbulence intensity factor. V_w is the constant wind speed. From this the loads from the wind can be obtained. This is primarily important for the rotor of the wind turbine. The wind can have an effect on the weather window of the installation procedure. The wind force on the structure will mainly influence the lateral loading needed on the foundation piles. For operations it is sufficient to consider a constant wind speed. iec [34]

$$TI = I_{ref} \frac{0.75V_w + 5.6}{V_w} \quad (3.17)$$

3.3 Components

The environmental forces on the system have been discussed. This section will focus on the elaboration of the components which are affected by these forces. The system is split up into 3 segments. The vessel, template and rigging. They will be elaborated in this section.

3.3.1 Vessel: Giant 5

The barge used for the installation of the foundations is the Giant 5. The technical drawing of the side view of the Giant 5 is given in Figure 3.11. The Giant 5 has a length of 137m, a width of 36m and a draft of 5.5m. The chosen coordinate system is given in the figure. The origin of the coordinate system is aft of the ship at the water line. The coordinates created for modeling the ship are with respect to this origin. The shape of the hull is of primary importance since it influences the interaction with the waves. The deck equipment will be modeled by point masses and corresponding moments of inertia.

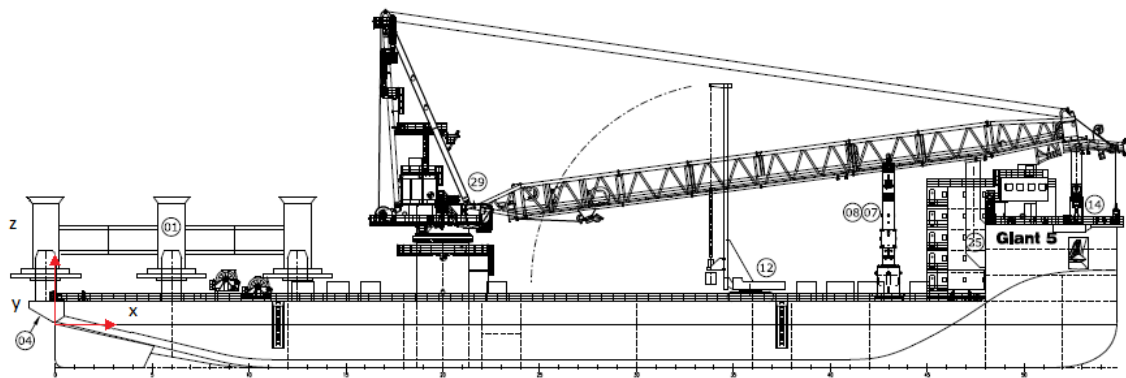


Figure 3.11: Giant 5 geometry and proposed deck equipment, lif [35]

For this installation the equipment on the barge will be as such that the draft of the ship is 5.5m. The main parameters of the ship are given in Table 3.7. The vessel motion will be included via force RAOs calculated in the pre-thesis. Ansys AQWA was used to obtain the RAOs of the vessel. Interaction between the vessel and the template will be discussed in the last section of this Chapter. Nous [36]

Table 3.7: Main parameters Giant 5

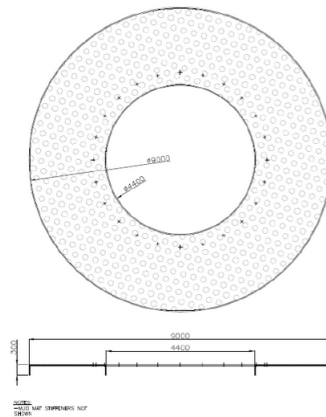
Principle length:	137	[m]
Principle breadth:	36	[m]
Draft:	5.5	[m]
Dead weight	$21 \cdot 10^3$	[mt]
Submerged volume:	$2.3 \cdot 10^4$	[m^3]
Crane capacity	1000	mt

An important feature of the deck equipment is the crane. The crane will hoist the template and foundation piles. The capacity of the crane is 1000 mt. The crane tip point can be found in figure Figure 3.14.

Table 3.8: Template component properties

Member/item	Flooding	OD		ID [mm]	A [m ²]	Length [m]
		[mm]	t[mm]			
Diagonals	NO	193.7	10	N/A	0.03	259.44
Sleeve support members	NO	457.2	25	N/A	16	94.16
Inner ring	NO	508	16	N/A	0.2	53.76
Outer ring	NO	508	25	N/A	0.2	145.92
Verticals	NO	244.5	16	N/A	0.05	75.6
Sleeve upper	YES	3280	20	3240	0.2	22.8
Sleeve lower	YES	3300	30	3240	0.31	9.52
Mud mats, 13% of the steel weight						

mud-mat is a large plate or mat which main task is to provide stability for the structure. The mud-mats have a large surface area to provide for stability on the sea bed. The mud mats are placed around each sleeve of the template. A schematic view of one mud-mat is given in Figure 3.13.

**Figure 3.13:** Schematic view Mud mat, rev [38]

3.3.3 Rigging

The template will be installed using a crane on the vessel. The crane will hoist the template using steel wires. The property and geometry of the wires together with the orientation of the crane are of importance for the interaction and dynamic behavior of the complete system. A side and top view of the lines and the lift configuration is given in Figure 3.14. The minimal angle of the lines is in accordance with DNV specifications.

$$x = \frac{WL}{AE} \quad (3.18)$$

The properties of the wires are obtained from the Balmoral marine handbook. The elastic stretch of the wire is calculated using Equation 3.18. From this the stiffness could

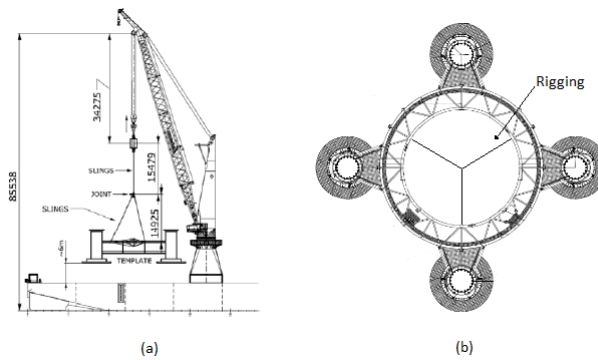


Figure 3.14: Line configuration: (a) side view (b) Top view, lif [35]

be determined. Here W is the applied load, L the length of the rope, A the area of the rope diameter and E the elasticity modulus. An overview of the obtained wire properties is given in Table 3.9. bal [39]

Table 3.9: Rigging properties

	Crane Wire	Short rigging
n [-]	1	3
Length [m]	50.965	17.5
EA [kN]	1.56E+06	1.01E+05
k [Nm]	3.06E+07	5.77E+06

The template will be connected with the wires through a handling system. The handling system is designed to facilitate the sub sea disconnection and re-connection. Figure 3.15 illustrates the orientation between ship and template during installation. This configuration will be used in the model. What can be seen from the figure is that the yaw motion of the template will be restricted by 2 steering lines connected to the ship.

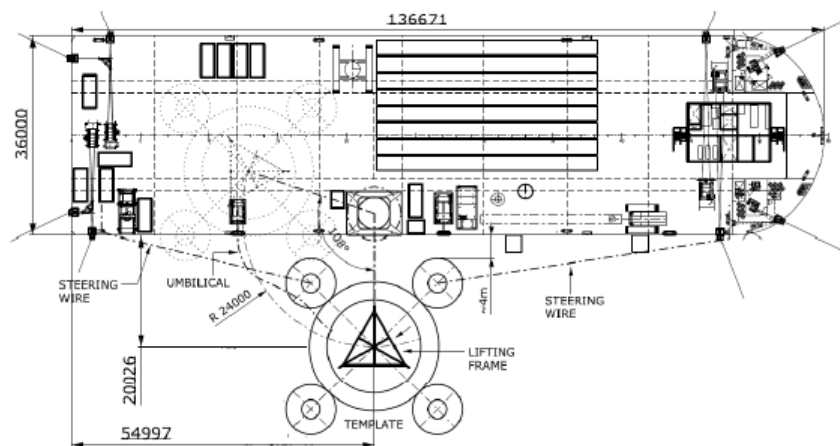


Figure 3.15: Top view ship and template configuration, lif [35]

3.4 Model

The modeling techniques, forces and system components have been discussed. This has to be combined in one model. This section will discuss the complete model made in OrcaFlex. The made assumptions are discussed as well as the modeled interaction between the forces and the components.

First, the modeling considerations in OrcaFlex are discussed. Secondly, the consideration for the performed simulations are discussed. Lastly, an overview on the complete model and simulations will be given.

3.4.1 Modeling considerations in OrcaFlex

This section will discuss the model consideration in OrcaFlex. First, the general modeling method in OrcaFlex is discussed. Secondly, the force interaction between the components are elaborated. Thirdly, the mud mat discretisation will be explained. Lastly, a validation will be given on the de-coupling of the vessel motions.

Modeling in OrcaFlex

First the general modeling method in OrcaFlex is discussed. OrcaFlex is a software package for the dynamic analysis of offshore marine systems. OrcaFlex can perform both static and dynamic calculations. OrcaFlex is the leading software package for performing dynamic calculation in the offshore industry. Main strong capabilities of the software is the breadth of the technical capabilities and the user friendliness. Furthermore, the software was chosen because Boskalis has a lot of experience with this software.

The steps to be taken in OrcaFlex can be set up in 3 segments. The input of simulation parameters, environment and model components. The simulation parameters can be given in the 'general' tab. the simulation time, time step and sample time can be given here. In the environment section the type of wave, wind and current parameters can be given. After this a model for the geometry of the system can be created. This can be done using the following modeling options.

The system can be created using the following options: Vessel, 6D buoy, line type, winch, link and shape. The vessel option can be used to create the Giant in the model. For this model force RAOs are used. A length and depth can be given for the vessel. 6D buoys are used to model the bodies like the template and the main hook. Several types of 6D buoys are available. It was chosen to use a lumped buoy. Reason for this is the wide range of input parameters. It was also chosen to model the templates mud mats as 6D buoys. In order to capture the slam force multiple buoys were used. This will be explained further in this section. The rigging of the system can be modeled using line types. coordinates and properties can be given to the lines. Links are used to model the mooring lines of the vessel and to balance the yaw motion of the template. The winch and shape type are not used in this model.

Force interaction between waves and components

The model will interact with the given environmental input. The main interaction with the environment are the waves. In order to calculate the response of the system due to this waves, simplifications are made to calculate the forces on the system.

Bernoulli

6D buoys are used to model the interaction between waves and template. For 6D buoys the wave forces are calculated using the Bernoulli equation as given in Equation 3.2 and Equation 3.3. The force is dependent on the contact area, relative velocity and force coefficients. They are discussed in Chapter 3. The contact area and force coefficients are given as input in the 6D buoy. The relative velocity is dependent on the velocity of the buoy and incoming wave. For this a Froude-Krylov assumption is made.

Froude-Krylov

Viscous phenomena occur when the waves interact with the template. The wave particles cannot go through the template which results in viscous effects under the template. This influences the relative velocity between the body and the water. The viscous response is difficult to determine. In the model no viscous responses are taken into account. The Froude-Krylov method is used. The forces are determined for a undisturbed wave. Only non-viscous forces are included.

Mud mat discretization

As discussed in this section 6D buoys are used to model the forces on the mud mats. A 6D buoy calculates the forces in 1 single point. This creates a problem when determining the slam force. Slamming is a impulse force with a small time step. This means that the behavior on the total mud mat cannot be modeled by 1 6D buoy. In order to capture the full behavior of the slam force multiple 6D buoys must be used.

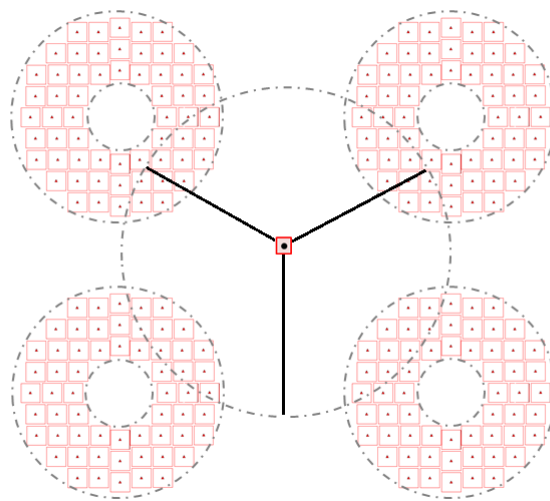


Figure 3.16: Discretized mud mats top view

The mesh of the 6D bouys on the mud mats is given in Figure 3.16. The mud mats are modeled by 240 6D bouys. This means 60 bouys for each mud mat. The chosen number of bouys depends on the accuracy of the results, time step and the overall simulation time. Multiple combinations of bouys and time steps were investigated. From this the optimal number of bouys was found. It was found that a finer mesh than the chosen mesh would not improve the accuracy of the result. Choosing a smaller time step could improve the results to some extent but would increase the simulation time drastically. A time step of 0.1 seconds was chosen. This will be elaborated further in section 3.4.2.

Validation coupled vessel motions

A decision has to be made whether the motion of the vessel and template can be decoupled. RAOs are checked for 0 deg, 45 deg and 90 deg to see in what manner the template affects the motion of the Giant 5. RAOs are compared for the Giant 5 with no connection elements and the Giant 5 with a template hanging on the hoisting wire of the crane. Both RAOs are checked with reference values from Boskalis. This section will discuss the main points of interest from the RAO comparison. An illustration of the complete set of RAOs for the 3 wave direction is given in Appendix B.

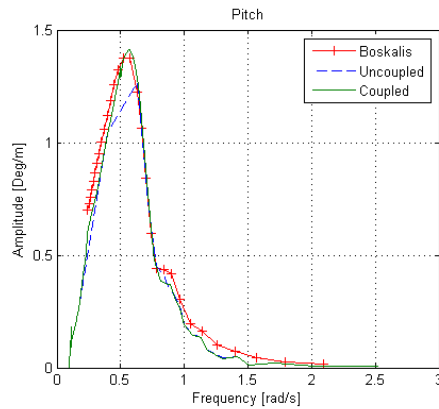


Figure 3.17: Coupled/Uncoupled RAOs: Pitch 0deg

Figure 3.17 illustrates the pitch RAOs for a wave direction of 0 deg. It shows that the Giant is not influenced by the template for this wave direction and degree of freedom. The reference values from Boskalis correspond to the calculated RAOs from AQWA.

Similarities as illustrated in Figure 3.17 are present for most degrees of freedom for this wave direction. For the wave directions in 45 en 90 degrees this is also the case. However there is one significant difference between the coupled and uncoupled RAOs. This is the presence of the eigenfrequencies. An illustration of this is given in Figure 3.18.

Figure 3.18 presents the sway RAOs for an incoming at 90 degrees. Again the coupled and uncoupled system show little differences. The only significant difference is a peak response at 0.11 rad/s. This corresponds to the eigenfrequency of the template for the sway and surge motion. The presence of the eigenfrequencies of the system can be found

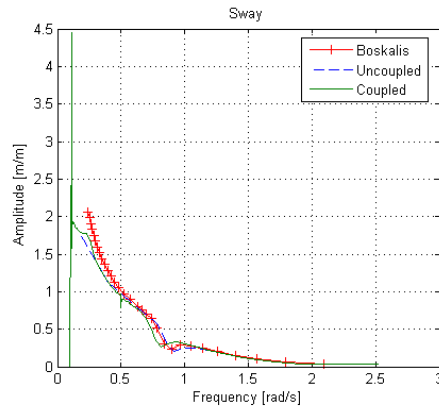


Figure 3.18: Coupled/Uncoupled RAOs: Sway 90deg

for several motions in multiple wave directions.

Small peaks were also observed at 0.5 rad/s. This height of this peak is dependent on the wave direction. The peak is explained by the phase of the template and the Giant. For this wave frequency the template is out of phase with the Giant 5 which causes induced motion in the RAO spectrum. A similar peak is present in the RAO given in Figure 3.19.

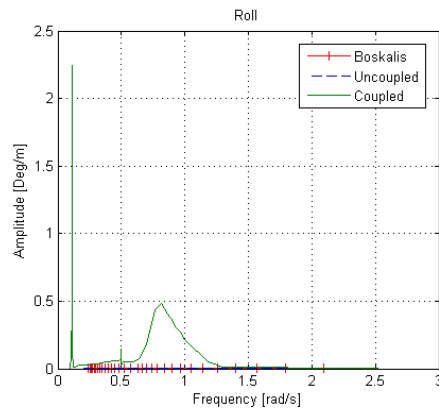


Figure 3.19: Coupled/Uncoupled RAOs: Roll 0deg

The most significant difference between the coupled and uncoupled system is given in Figure 3.19. For the roll motion in a wave direction of 0 degrees a peak can be observed at 0.74. This is the eigenfrequency for roll of the vessel. The peak can be explained by the coupling of the template and the Giant. For the incoming wave of 0 degrees the roll motion of the ship is small and therefore the template can have a possible influence. The template generally will follow the wave elevation in heave direction. For an incoming

wave of 0.74 rad/s this means that the template oscillates in the roll eigenfrequency of the Giant. Therefore the Giant will react on this motion. This is only the case for an incoming wave of 0 degrees. For incoming waves in other angles this effect is not important since the roll motion of the Giant itself is the dominant factor. The template will have negligible influence on the roll motion.

What can be concluded from the analysis is that the template has a small influence on the RAOs of the vessel. The effect is mainly present in the eigenfrequencies of the system and degrees of freedom for non-governing wave directions. In order to include this coupling, force RAOs will be used in the OrcaFlex model.

3.4.2 Simulation considerations

The modeling consideration haven been discussed. Next, a discussion will be given on the issues concerning all simulations. The Wave heading, simulation time, time step, wave period, wave height, slam coefficient and horizontal wave force components are discussed. The section is wrapped up by discussing the data processing of the results from the simulation.

Wave heading

In all simulation the assumptions is made that the installation will be performed for bow waves. The wave heading of 0 degrees is often chosen for the small roll motion on the vessel.

Horizontal wave forces

The incoming waves induce wave forces in the horizontal and vertical direction. The horizontal wave forces for a template with large mud mats is relatively small and can be neglected. The space frame is not affected by the waves since it is hanging above the maximum wave elevation. The sleeves induce horizontal drag and inertia forces. These horizontal forces induce side lead angles causing a higher tension in the wire. This effect is not of interest in this test. In order to understand the slam force, this phenomena is not considered. Therefore it is chosen to exclude the horizontal wave forces.

Wave height

A wave height of 3m was chosen for all time simulations. This is the extreme wave height found at the Wiking site. The wave height was found by weather data given by Iberdrola.

A check is done to investigate the influence of the wave height on the wave slamming force. 108 time simulations are performed for 27 wave periods and 4 wave heights. The slam force as function of wave period for 4 wave heights is given in Figure 3.20.

Two peaks are observed. This is common for the slam behavior. This will be elaborated in Chapter 5. A clear influence of the wave height is observed from comparing the 4 wave heights. The slam force for a wave height of 0.5 m is a factor 10 smaller compared to a

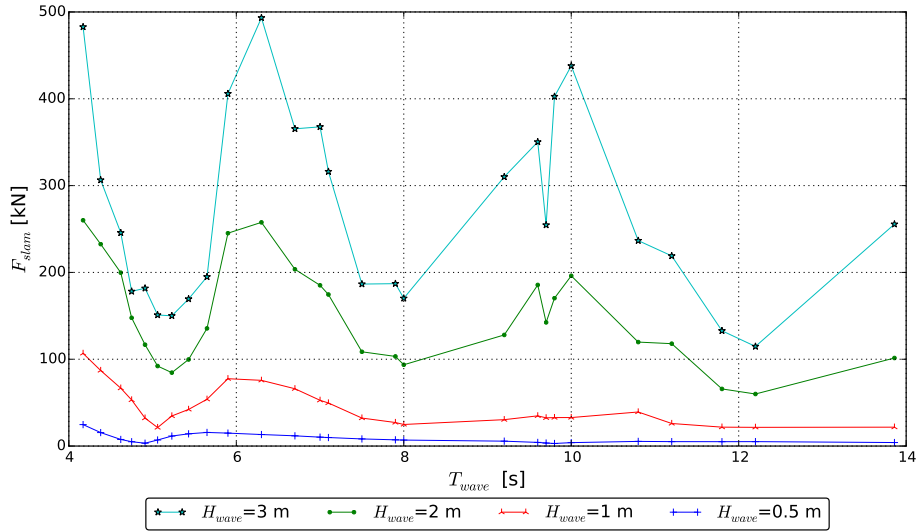


Figure 3.20: Slam force compare to wave period for different wave heights

wave height of 3 m. It is concluded that the slam force significantly decreases for smaller wave heights.

Wave period

In order to check the slamming behavior, a range of wave periods was chosen. The wave periods are limited for short and long waves. The long waves are limited by the size of the Baltic sea. The maximum fetch length for a wave at the wind farm location is 100 km. From this a maximum wave length is assumed for a wave height of 3 meter. A wave length of 300 m is chosen. Main reason for choosing a long wave period is to analyze the effect of slamming for an incoming wave which affects all mud-mats at the same time instant. The wave length of 300 meter corresponds to a wave period of 13.86 seconds.

Short waves are limited by the breaking limit. The wave will start to break for a certain wave height and wave length. The breaking limit given by Journee is given in Equation 3.19. It states that the fraction of the wave height and wave length cannot exceed $1/7$. Using the breaking limit a minimum wave period of 4.17 seconds was found. In the simulations wave periods are investigated in the range of $T_{wave} = 4.17 - 13.86$. J.M.J. Journee [13]

$$\frac{H}{\lambda} < \frac{1}{7} \quad \text{With} \quad \lambda = 1.56 \cdot T^2 \quad (3.19)$$

Simulation time and time step

The simulation time is significant for the accuracy and calculation time of the test. The simulation time for all simulations was chosen to be 15 minutes. The simulation time was chosen according to 2 main considerations. The first consideration is the limit in calculation time. The calculation time is approximately the same as the simulation time. Long

simulation times for multiple tests would mean a large calculation time. Furthermore, extra time is needed to process the data. This time was not available in the thesis. The second consideration is the operation time. The template is lowered to the sea bed with a hoist speed of 1 meter per minute. This would mean that the template is effected by the wave crest for approximately 15 minutes.

A time step of 0.1 s was chosen. Since the slam force is a impulse load the time step must be small. A time step of 0.1 seconds was chosen from a optimization between the accuracy and calculation time.

Slam coefficients

A range of the slam coefficients was found from reference. The variation in C_s represents the range of possible local slam behaviors. The values found cover the non-linear behavior of the force. The main question of the simulations is to investigate how this C_s variation effects the behavior on the system. The effect is measured by checking the dynamic tension of the hoisting wire. A maximum slam force of 13.04 was found. DNV suggest a minimum slam force of 5. From tests it was observed that slam coefficients of 2.5 are possible. It was chosen to analyze a C_s -range of 2.5-13.04. Five C_s values are chosen spread evenly over the range found from reference.

Data processing

The time domain simulations will produce results. The interface in OrcaFlex is able to analyze the data. However, for more advanced processing, other software can be used as Excel and Python. OrcaFlex provides Excel sheets and Python scripts to help in processing the data. For the investigation done in this thesis, Python is used. The capabilities of Python exceeds the Excel capabilities. The data obtained from the simulation in OrcaFlex can be imported as vectors in Python. Parameters of interested listed in the results section in OrcaFlex can be chosen to be transferred to Python. The motions of the vessel, motions of the template, wave elevation and effective tension in the wire were extracted from the OrcaFlex files.

In order to determine the slam force, the 240 elements representing the mud mats need to be processed. The results from each element are extracted to Python. After this the slam force of the elements are summed. For investigation of the separate mud mats a summation was done for the 60 elements from each mud mat. A total summation of the 240 elements was done to investigate the complete slam force on the mud mats.

$$\frac{Tension_{dyn,max} + Tension_{mean}}{Tension_{mean}} \quad (3.20)$$

Once the slam forces are calculated and parameters of interest are imported, the maxima and mean values are obtained. The effect of the initial starting conditions are canceled out by deleting the first 7,5 minutes of the simulation. From the remainder part the maximum values and mean value are determined. In this way the maximum slam force and tension were found. The DAF is found by dividing the mean value of the tension by

the maximum tension. The equation for calculating the DAF is given in Equation 3.20. From this the graphs can be constructed which are used to analyze the slam force and behavior of the system.

3.4.3 Model and simulation overview

A total overview of the modeled system in OrcaFlex is given in this section. The equation of motions are discussed. Next, a overview of the model and simulations will be given.

Equation of Motion

The complete system can be determined by 15 equations of motions. This consist of the 6 vessel motions, 6 template motions and 3 main hook motions. The main hook is modeled as 1 points, therefore it cannot move in the roll, pitch and yaw direction. The complete set of equations can be written as given in Equation 3.21. Where \mathbf{M} , \mathbf{C} and \mathbf{K} are the mass, damping and stiffness matrix respectively. The vector \mathbf{X} is the response vector in all directions.

$$\mathbf{M}\ddot{\mathbf{X}} + \mathbf{C}\dot{\mathbf{X}} + \mathbf{K}\mathbf{X} = F(t) \quad (3.21)$$

The determination of the values in the matrix is dependent on the type of structure. The values for the equation of motions of the vessel are determined by a diffraction analysis in Ansys AQWA. The values are dependent on the wave frequency and direction. From the diffraction analysis a set values for the added mass and damping was found for a range of direction and frequencies. The values for the template motions are found by using force coefficients as elaborated in section 3.2. The main hook motions are only effected by the mass of the hook and the stiffness of the rigging.

The motions of interest in the thesis are the heave motion and pitch motion of the template. These equations of motions are given in Equation 3.22 and Equation 3.24. The heave motion of the template is dependent on the heave motion of the main hook. The equation of motion for the heave motion of the main hook is given in Equation 3.23. What can be seen is that the added mass and damping forces are characterized by the force coefficients. The main challenge in the equations of motions is the determination of the slam force. It was found that OrcaFlex is the suitable tool to solve the described equation of motion.

$$(1 + C_a(t))m_1\ddot{X}_1 + \frac{1}{2}\rho C_d(t)A(t)V_{rel}|V_{rel}| + k_2(X_1 - X_2) - m_1g + \rho g \nabla(t) = F_s(V_{rel}, A(t), C_s) \quad (3.22)$$

$$m_2\ddot{X}_2 + k_2(X_2 - X_1) + k_1(u - X_2) = 0 \quad (3.23)$$

$$I_{yy}\ddot{\theta} + \frac{1}{2}\rho C_d(t)A(t)V_{rel}|V_{rel}| \cdot \frac{1}{2}L_{templ} = F_s(V_{rel}, A(t), C_s) \cdot \frac{1}{2}L_{templ} \quad (3.24)$$

Model overview

The complete overview of the input in OrcaFlex is given in Table 3.10. A visualisation of the OrcaFlex model is given in Figure 3.22, Figure 3.23 and Figure 3.24. A geometric view, top view and side view is given.

It can be observed that the vessel is modeled by the calculated RAOs in Ansys AQWA. The template is modeled as 1 6D buoy. The properties of the reference buoys are given in the table. The mud mats are discretized into 240 elements. The force coefficients used in the elements are chosen as the maximum values found in section 3.2. The properties of these elements are given in the mud mats row in the table. It can be noted that the slam coefficient is not 1 fixed value. From experiments and guidelines in reference a range of slam coefficients was found. The effect of this range will be investigated in this thesis.

Simulation overview

In order to investigate the effect of the slam force different simulations are created. Figure 3.21 gives an overview on the 3 model set-ups. The model set-ups are build up with an increase in complexity. Each model set-up aims on analyzing a specific part in the behavior of the slam force. They are discussed in Chapter 4,5 and 6.

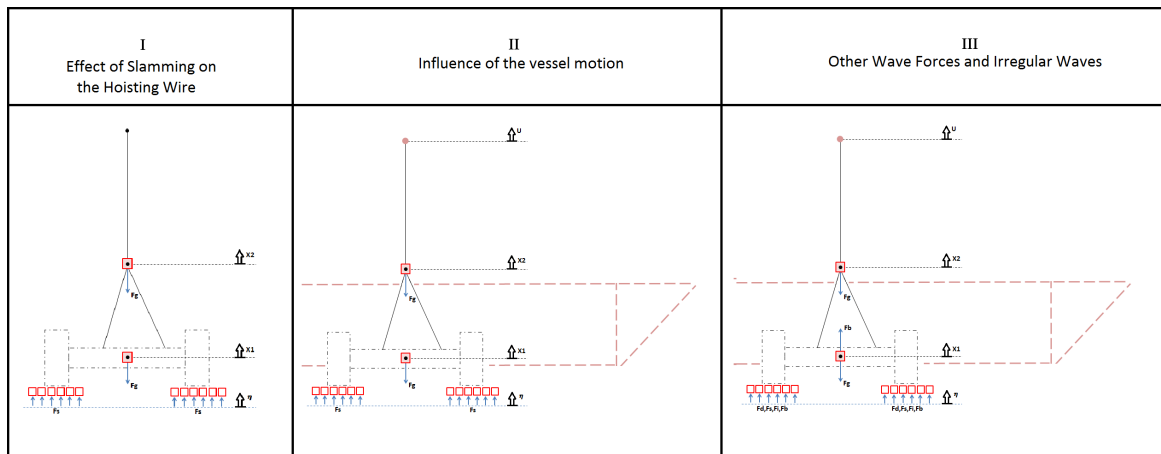


Figure 3.21: Simulation set-up overview

Table 3.10: Model Overview

Components Input				
Software	Orcaflex			
Vessel	Force RAOs			
Template				
Reference Buoy	Mass [te]	240		
	Inertia (I_{xx}, I_{yy}, I_{zz}) [$te \cdot M^2$]	1.89E+04	1.89E+04	3.03E+04
Mud mats	Elements [-]	240	Height [m]	0.3
	V_{el} [m^3]	0.021	C_s [-]	2.5-13.04
	$A_{Drag,el}$ [m^2]	0.807	C_a [-]	1.7
	$A_{Slam,el}$ [m^2]	0.807	C_d [-]	1.9
	$M_{Hydr,el}$ [te]	0.212		
Rigging				
Main Hook	Mass [te]	10		
Crane wire	Length [m]	59.065		
	EA [kN]	1.56E+06		
Short Rigging	Length [m]	17.5		
	EA [kN]	1.01E+05		
Schematic drawing complete model, Side View				
<p>The schematic drawing illustrates the side view of the complete model. It shows a vertical crane wire extending from a main hook. Below the main hook is a rigging structure supported by two sets of mud mats. Forces are indicated: F_g (gravity) acting downwards on the main hook and rigging, and F_b (buoyancy) acting upwards on the rigging. The mud mats are supported by forces F_d, F_s, F_i, F_b. Coordinate systems are shown: u (vertical), x_2 (horizontal), x_1 (horizontal), and η (vertical).</p>				



Figure 3.22: OrcaFlex model geometric view

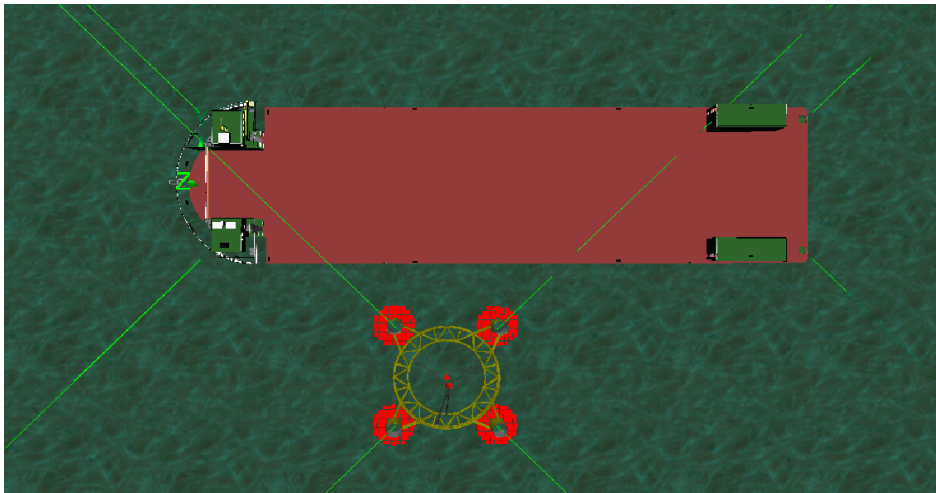


Figure 3.23: OrcaFlex model top view



Figure 3.24: OrcaFlex model side view

Effect of Slamming on the Hoisting Wire

The first step in the investigation is to understand the behavior of the slam force and the response on the hoisting wire. This will be explained in this Chapter. The behavior is analyzed by using a simple model. The model will increase in complexity to recreate the real life situation in Chapter 5 and 6.

First the simulation set-up will be discussed. Next the result and discussions are given. In the result section a discussion is performed on one time domain simulation. After this a comparison is given for all performed simulations for this set-up.

4.1 Simulation set-up I

The goal of the first test is to understand the effect of slamming on the dynamic tension and DAF of the hoisting wire. The test will focus on understanding the slam force characteristics and response of the template. This corresponding research questions are listed as follows.

- What is the behavior of slamming on the mud mats?
- What is the behavior of slamming on the template?
- How does this effect the motion of the template?
- How does the motion effect the DAF?
- How does Cs effect the tension in the Hoisting wire?

A schematic view of the test set-up is given in Figure 4.1. The hoisting wire will be fixed in space. No interaction of the vessel is taken into account. The template static position is where the bottom side of the mud-mat coincides with the mean water level. Since the

vertical wave speed is maximum at the mean water level it is assumed that the maximum slam force occurs at this point. A range of wave periods, $T_{wave} = 4.17 - 13.86$ is chosen for the incoming wave. The incoming wave induces a slam force on the template. Slam coefficient are evaluated in the range of $C_s = 2.5 - 13.04$. All other wave forces are discarded in this test.

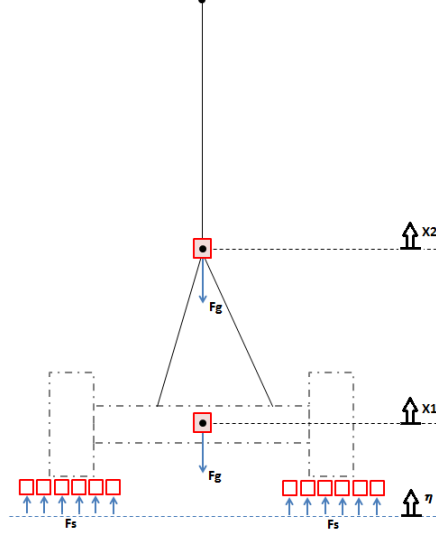


Figure 4.1: Simulation set-up I

The assumptions made simplify the equations of motion of the system. The vertical equations of motion are given in Equation 4.1 and Equation 4.2, Where $V_{rel} = \dot{X}_1 - \dot{\eta}$. The pitch equation of motion is given in Equation 4.3. For other degree of freedom the similar simplifications hold.

$$m_1 \ddot{X}_1 + k_2(X_1 - X_2) - m_1 g = F_s(V_{rel}, A(t), C_s) \quad (4.1)$$

$$m_2 \ddot{X}_2 + k_2(X_2 - X_1) + k_1 X_2 = 0 \quad (4.2)$$

$$I_{yy} \ddot{\theta} = F_s(V_{rel}, A(t), C_s) \cdot \frac{1}{2} L_{templ} \quad (4.3)$$

4.2 Results and discussions on the effect of slamming on the hoisting wire

This test will investigate the effect of slamming on the dynamic tension and DAF of the hoisting wire. Test 1 will not consider motion induced by the vessel and will only include slamming as a wave force. First, the behavior of slamming on the mud mats is investigated. Next the total slam effect on the template is investigated. The influence of the slam force on the motions of the template is checked afterwards. Lastly, the effect of the motions on the dynamic tension is discussed.

This section will focus on answering the listed questions. In this test 135 time simulations are performed. 5 slam coefficients are considered together with 27 wave periods. An investigation on 1 time simulation is performed first. A comparison is made for all simulations in section 5.1.2.

4.2.1 Time domain simulation

This section will explain the investigation on 1 simulation. The time simulation chosen has a wave period of 7.1 s and slam coefficient of 11.5. This is assumed to be a good representation for explaining the phenomena.

The first step in understanding the behavior of the wave slamming force is to check the incoming wave. The wave elevation as a function of time for 2 wave periods is given in Figure 4.2. The parameters of importance for the incoming wave are the wave period and the wave length. The wave length is calculated by Equation 4.4.

$$\lambda = \frac{g}{2\pi} \cdot T^2 \tag{4.4}$$

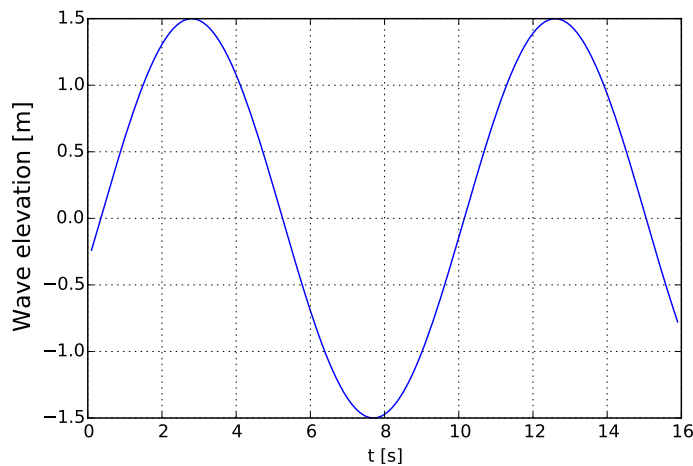


Figure 4.2: Wave elevation $T = 7.1$ s

The incoming wave induces slamming on the mud mats of the template. The slam force on each mud mat for 2 wave periods is given in Figure 4.3. What can be seen from the figure is that there is a clear difference in the behavior of mud mats 4 and 2 (front) compared to mud mats 1 and 3 (aft).

The values for the front mud mats are a factor 3 higher and have a different shape. The shape of the front mud mats are high peaks and have a short impact time. This is a indication for a high relative velocity.

The shape of the aft mud mats have longer impact time and are divided into 2 peaks. The longer impact time is caused by the lower relative velocity. The 2 peaks are caused by the presence of the hole in the mud mats. The hole changes the maximum slam area. The maximum slam area will not be at the maximum in the middle of the mud mat but in front and back of the hole. This causes a slamming behavior of 2 peaks.

The presence of the whole has less influence on the front mud mats. The short impact duration makes that the mud mat segments are affected at 1 instant.

The 2 types observed in the front and aft mud mat are mostly observed in all simulations. In general a high peak and short time duration are observed together. This means a large relative motion and slam area causing a large slam force. Similarly, a long impact time indicates a low relative motion and will result in a increasing influence of the hole. For increased impact time the size and shape of the observed 2 peaks will become the same.

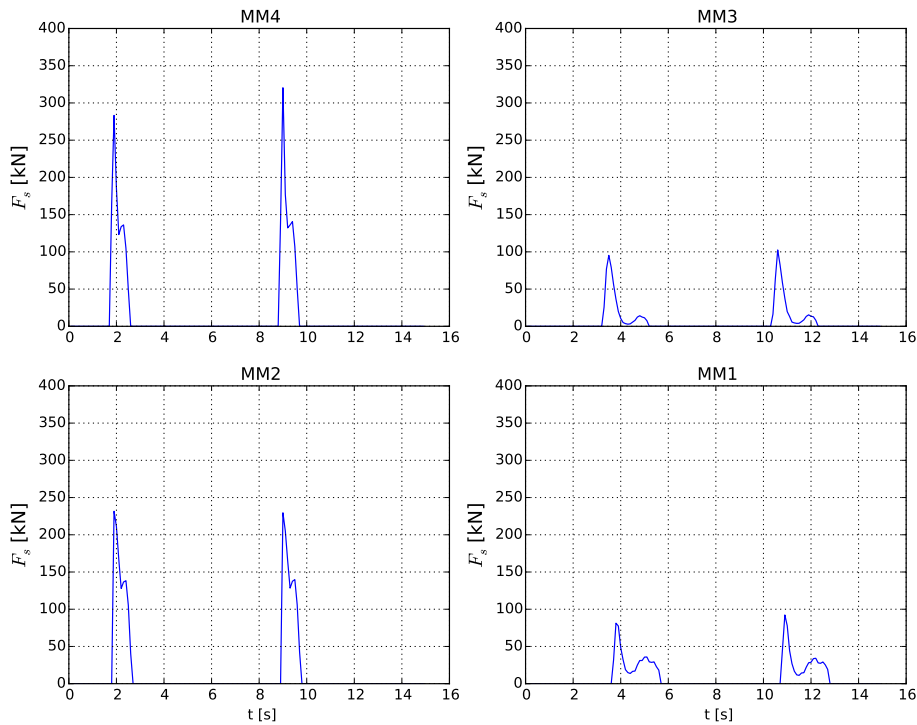


Figure 4.3: Slam force over time for each mud mat at $T=7.1s$

In order to characterize the slamming behavior of the complete simulation $F_{s,max}$, $F_{s,avg}$, $t_{s,max}$, $t_{s,avg}$ and number of occurrences are extracted from the simulation. The values for this simulation for each mud mat are given in Table 4.1.

As seen from the figure the maximum slam force is significantly higher for mud mats 2

4.2 Results and discussions on the effect of slamming on the hoisting wire 47

and 4 then for mud mats 1 and 3. The average slam force is an indication of the slam force in time. The average slam force is half of the maximum slam force for mud mat 3. The reason for this is the identification method of slamming. This will be elaborated in the following paragraph.

In order to understand this behavior, the identification of slamming needs to be explained. the total slam force on 1 mud mat is created by summing the 60 buoy components. This creates a vector in time. In order to identify each slam force, a high pass filter is applied. It was determined to apply a filter lower limit of 10 kN. This is 0.4 % of the template mass. This was chosen by an optimization of the data identification. For small slam phenomena like mud mat 3, the filter will cause the 2-peak slam behavior to identify as 2 separate slam forces. This causes the number of occurrences to double. This error will primarily occur for smaller wave periods. For small wave periods 2-peak slamming behavior occurs more often. In the case of an identification fault the average values cannot be used. This holds for the low $F_{s,avg}$ value of mud mat 3.

The maximum and average slam time indicate what shape can be expected and if the slam shape is consistent throughout the simulation. Mud mat 1 has a maximum slam time of 2 seconds. This slam time corresponds to a 2-peak shape. This is also shown in Figure 3.2. The average slam time is 1.98 s which means the shape can be assumed similar over time.

The number of slam occurrences is given in the last column. The number of slam occurrences is directly related to the wave period and is used to check the obtained values.

Table 4.1: Slam parameter summary for each mud mat

	$F_{s,max}$ [kN]	$F_{s,avg}$ [kN]	$t_{s,max}$ [s]	$t_{s,avg}$ [s]	n [-]
Mud Mat 1	92.3	80.4	2.1	1.98	133
Mud Mat 2	231.7	216.6	1.2	0.80	134
Mud Mat 3	103.7	56.1	0.8	0.60	261
Mud Mat 4	330.7	284.1	1.2	0.80	132

Overall it can be said that the behavior of the slam force is dependent on the relative velocity, slam area and inclination angle. The force can differ in shape and value for each mud mat. Two main behaviors can be observed. A short duration 1-peak shape and a long duration 2-peak shape. Dependent on the time duration the presence of the second peak will level out with the first peak. An overview on the slam parameter for each mud mat for all simulations are given in Appendix D.

The behavior of slamming on the mud mats is discussed. Next, the behavior of slamming on the template can be investigated. The total slam force on the template is found by a summation of the 4 mud mats. The total slam force together with the mud mat fractions for 2 wave periods are given in Figure 4.4.

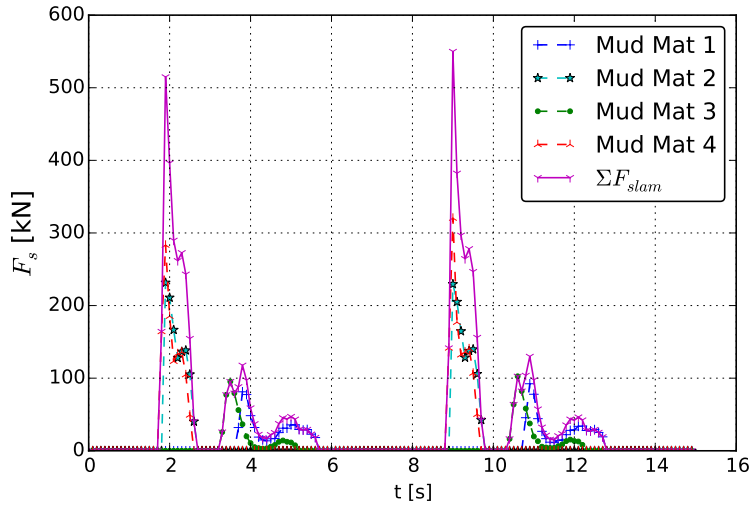


Figure 4.4: Slam force on each Mud mat at $T=7.1s$

What can be seen from the figure is that the largest peak is caused by the 2 front mud mats. The contribution of the aft mud mats are small. An overview on the slam force values of the simulation is given in Table 4.2. The slam parameters represent different properties for the total slam force compared to the local slam on the mud mats. What can be observed is a significant lower average slam force compared to the maximum slam force. This is due to the low contribution of the aft mud mats.

Table 4.2: Total slam force parameters

Parameter	Unit	Value
$F_{s,max}$	[kN]	526.6
$F_{s,avg}$	[kN]	305.5
$t_{slam,max}$	[s]	2.6
$t_{slam,avg}$	[s]	1.64
I_{max}	[kN · s]	226.6
I_{avg}	[kN · s]	163.3

The total slam force $F_{s,avg}$ gives an indication on the contributing behavior of the different mud mats. Due to the summation a more scattered slam field occurs. The average and maximum impulse of the slam force is given. This represents the energy of the force. This will give more insight in the effect of slamming on the template.

Table 4.2 shows a maximum slam force of 526.6 kN and a maximum slam time of 2.6 s. This would mean a high impact and large impact time. As mentioned before, this does not occur at the same time. Looking at the I_{max} it can be concluded that this is indeed not the case.

From the average values it can be determined that the 2 discussed slam behaviors occur in

4.2 Results and discussions on the effect of slamming on the hoisting wire 49

the total slam force of this simulations. Similar evaluation can be done for all simulation. An overview of the total slam force parameters is given in Appendix E.

The next step is to determine how this total slam force effects the motions of the template. An overview of the maximum deviations of the template during the installation for all degree of freedoms is given in Table 4.3. What can be observed is that the surge and sway motions are similar. Comparing the values with a wire length of 59m it can be concluded that the induced side leed angels are negligible. This is in coherence with the assumption made in the model.

Table 4.3: Maximum template motions

Parameter	Unit	Value
$Surge_{max}$	[cm]	19.6
$Sway_{max}$	[cm]	22
$Heave_{max}$	[cm]	4.2
$Roll_{max}$	[deg]	0.95
$Pitch_{max}$	[deg]	3.27
Yaw_{max}	[deg]	0.35

The heave motion is 4.2 cm which is very small compared to the wire length. However, it is known that small heave deviation has a significant effect on the tension in the wire. The roll and yaw motion are negligible. This was to be expected since a head wave is considered in this simulation. The pitch motion is expected to be influenced by the slamming force. The maximum pitch deviation is 3.27 degrees. From this it is concluded that the heave and pitch motions are the governing effected motions due to slamming.

In order to know how these motions are affected, a closer look will be taken on the 2 governing motions. The roll and pitch motion for 2 wave periods is given in Figure 4.5.

From the figure it can be seen that the pitch motion tends to follow the motion of the wave for this wave period. The first slam load occurs at 1.8 s. At this point the template is pitching down which means the template is rotating in the positive direction. During the first slam impact this rotation shifts from positive to negative. This means the first slam load forces the template to change direction. After the first impact the rotation is positive again. It can be concluded that the first slam force has a damping effect on the pitch motion.

At 3.2 s the second slam load strikes the template. This slam force is a 2-peak behavior slam load. What can be seen is that the first peak of this slam load is contributing to the excitation of the pitch motion. The contribution of peak 2 is small but has a damping effect on the motion.

It can be concluded that the slam force for this simulation is primarily damping the pitch motion. This is however not always the case for all the simulations. The slam force can

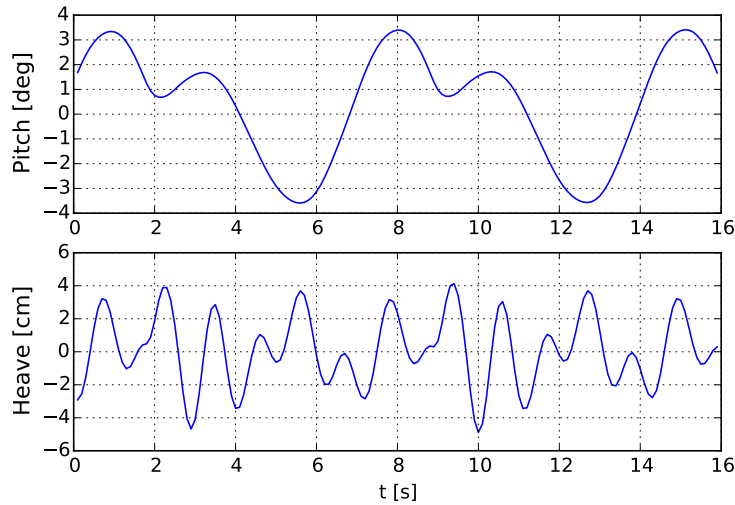


Figure 4.5: Roll and Pitch motion for 2 wave periods $T=7.1s$

damp or excite the pitch motion of the template depending on the wave period.

The heave motion of the template is strongly influenced by hoisting wire. The motion is governed by the eigenfrequencies of the rigging wires. The heave motion is a repetitive motion with a period equal to the wave period. The heave motion can be split up into 2 segments. The first segment occurs between 2 and 5 seconds. The template is excited by the first slam load and will oscillate in the heave eigenfrequency of the rigging wires afterwards. Segment 2 is initially excited due to the total impulse of the second slam force. Two combined signals can be observed. The continuation of the dampened eigenfrequencies and the template motion due to the impulse of the second slam force.

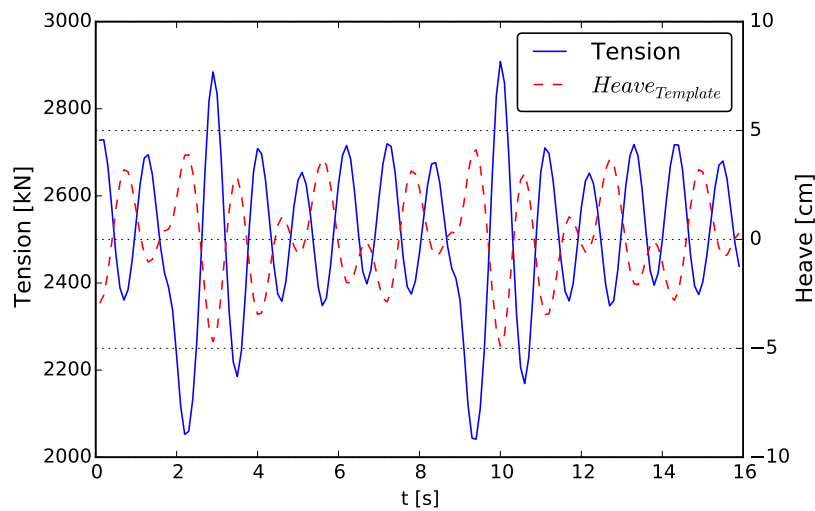


Figure 4.6: Wire tension heave motion comparison

4.2 Results and discussions on the effect of slamming on the hoisting wire 51

In conclusion 2 possible behaviors are found in the simulation. Behavior 1 is a slam force which is damping the roll motion and is effecting the heave motion. Behavior 2 is a slam force which is exciting the roll motion but has a small influence on the heave motion.

Table 4.4: *Tension and corresponding DAF*

Parameter	Unit	Value
$Tension_{dyn,max}$	[kN]	402.2
DAF	[-]	1.16

The last step in analyzing the time domain simulation is to check how these motions effect the tension and DAF in the hoisting wire. The wire tension for 2 wave periods is illustrated in Figure 4.6. The heave motion of the template is illustrated for comparison. What can be seen is that the tension is out of phase with the horizontal motion of the template. This was to be expected. The roll motion on the tension is small. From this a maximum dynamic tension can be obtained. The maximum dynamic tension is found by subtracting the maximum tension by the mean tension. From this the DAF on the hoisting wire can be found. The relation that was used is given in Equation 3.20. The $Tension_{dyn,max}$ and DAF of the simulation are given in Table 4.4.

4.2.2 Comparison for different slam coefficients and wave periods

The analysis for 1 slam coefficient and 1 wave period was performed. In order to understand the complete slamming behavior on the tension in the hoisting wire, different slam coefficients and wave periods are considered. This section will compare the performed simulations for all slam coefficients and wave periods.

First the total slam force is analyzed. The total slam force is a summation of slam forces occurring at the mud mats. A closer look will be taken at the contribution of the mud mats on the slam force for all wave periods. The total maximum slam force and contributing mud mat fractions for a range of wave periods are given in Figure 4.7.

What can be seen from the figure is a clear correlation between the front mud mats (2 and 4) and the aft Mud Mats (1 and 3). The total force of the slam load is set up in different manners for different wave periods. The individual mud mat forces are similar and approximately 200 kN for a wave period of 10 seconds. The total slam load is however 700 kN which is a peak in the slam loading. This peak is calculated by summing the contributions of all mud mats on the total slam load.

In the region of $T_w = 5.43$ and 7.00 s another peak occurs. This is not due to the contribution of all mud mats. The 2 front mud mat contributions govern the slam force. The contribution of the aft mud mats is small. This behavior was also observed in the simulation case discussed in section 4.1.1.

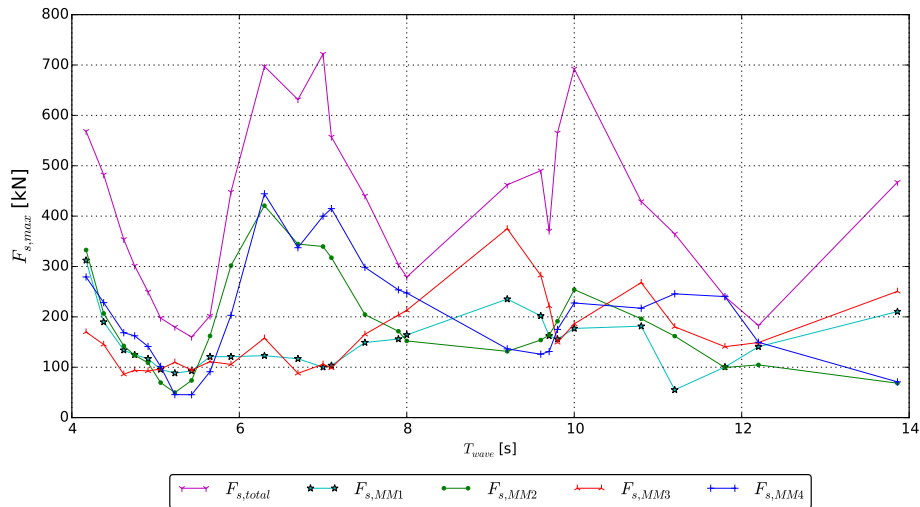


Figure 4.7: Total slam force and contributing Mud Mat fractions for Wave periods T , $Cs=13.04$

The difference in behavior can be explained by the angle and length of the wave. For large wave periods the wavelength is long and the incidence angle is small. This will cause the slam force of the mud mats to occur simultaneously. For shorter and sharper waves this is not the case. The front mud mats are however hit at the same time for a longitudinal waves.

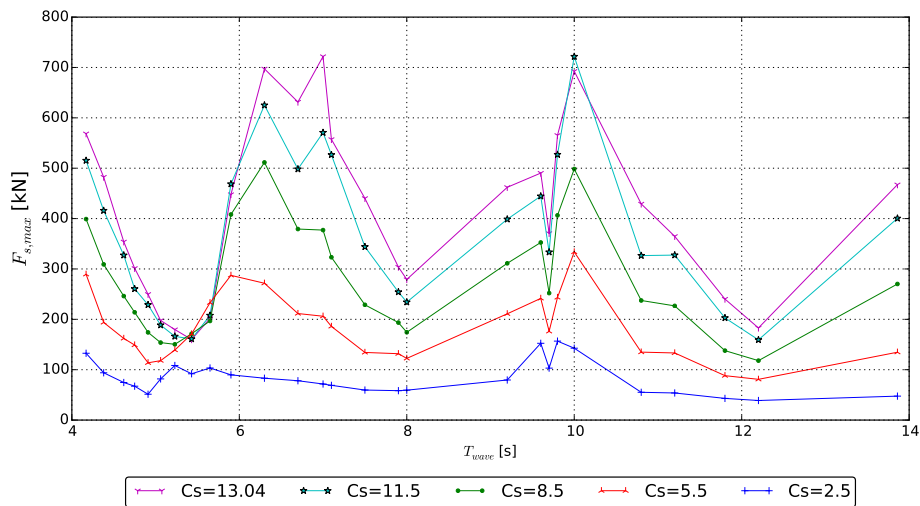


Figure 4.8: Total slam force versus Wave periods for different Cs values

Figure 4.8 illustrates the total slam force for a range of wave periods and different slam coefficients. Two clear peaks can be seen from the figure. The range of the first peak is between $T=5.43$ and 7.00 s. This corresponds to a wave length of 2 and 4 times the template length. Clear correlation can be seen between the pitch and heave motion at

these wave lengths. This means the template is affected by the shape of the wave. In these wave lengths the template tries to follow the motion of the waves causing high roll motions. For longer waves the template is not able to follow these motions, causing a high heave response. This creates a high slam force.

The 1st peak is dependent on the length of the template and the shape of the wave. The peak indicates a form of resonance in the system. The wave periods are however not close to any of the eigenfrequencies of the system. The reason for this peak is the distance between the templates. The wave will hit the front and back mud mats with a time delay. A schematic representation is given in Figure 4.9. This Δt can corresponds with the eigenfrequencies of the riggings. Different mud mat distances were investigated and it showed that the distance and corresponding Δt coincide with the riggings eigenfrequency. 2 peaks can be observed. This is due to the axial stiffness of the riggings and the pure horizontal stiffness. They are both induced by the incoming wave.

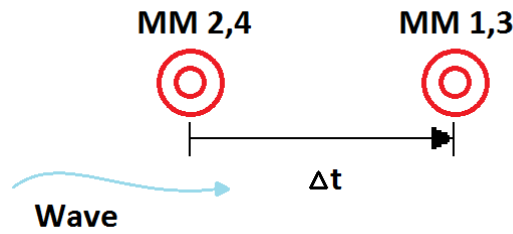


Figure 4.9: Schematic representation of δt for the wave impact on the template.

A second clear peak is observed near a wave period of 9.8 s. This is the pitch eigenfrequency of the system. The incoming wave cause the system to move in the eigenfrequency. The pitch motion will not follow the wave shape. This will have an intensifying effect on the slam force.

The considered values for C_s show similar behavior for different wave periods. Higher slam forces are obtained for higher slam coefficients. This was to be expected. The behavior of the slam force intensifies for higher values of C_s . Almost no peak is visible between $T= 5.43$ and $7.00s$ for $C_s=2.5$. For a slam coefficient of 13.04 however this is a critical region. It can be concluded that the slam force does not increase linearly with C_s . This means the choice of the slam coefficient influences other parameters like the slam area and relative velocity. This increases the error if wrong C_s values are chosen. The next step is to analyze how slamming effects the motions and tension of the template.

The pitch and heave motion of the template for different values of C_s and wave periods are illustrated in Figure 4.10. The pitch motion varies from 1 to 3 degrees for long waves and from 5.5 and 7 degrees for short waves. Large pitch motions are noticed close to the heave eigenfrequency of the system. It can be seen that the behavior for different C_s values differs. The peak pitch motion changes. The peak tends to shift left for small

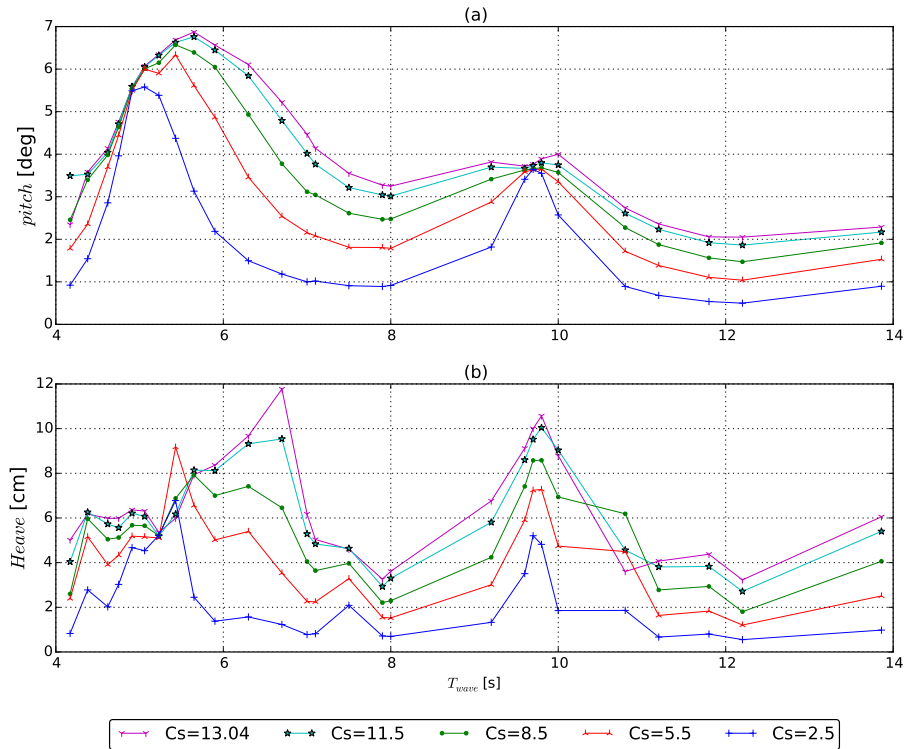


Figure 4.10: Pitch (a) & Heave motion (b) over Wave periods T for different C_s values

slam coefficients. A possible explanation is that the generated force is too small for the template to follow the wave. For smaller waves the force is large enough to get in a pitch motion pattern. It can be seen that for short waves the slam force primarily influences the pitch motions. The energy of the slam force will induce the pitch motion. This means less energy is spent on the heave motion causing the heave response to decrease. This has direct influence on the slam force. Comparing Figure 4.8 and Figure 4.10 a strong correlation can be seen in the region $T=4$ and $T=6$. It shows that high pitch motions result in low slam forces.

A shift in maximum heave height can also be observed in the short wave region. Again a peak is observed near the pitch eigenfrequency of the system. It can be concluded that a change in C_s value influences the response of the template and therefore the dynamic tension in the wire.

The last step in the analysis is to check how this motion affects the wire tension and DAF for different wave periods. What can be observed is that the 2 peaks observed in the slam force are not present in the dynamic tension in the region between wave periods of 6 and 8 seconds. Only the horizontal motion affects the tension. Therefore only 1 peak is observed. The transverse eigenfrequency is governed by the pitch motion of the template and will therefore not affect the dynamic tension.

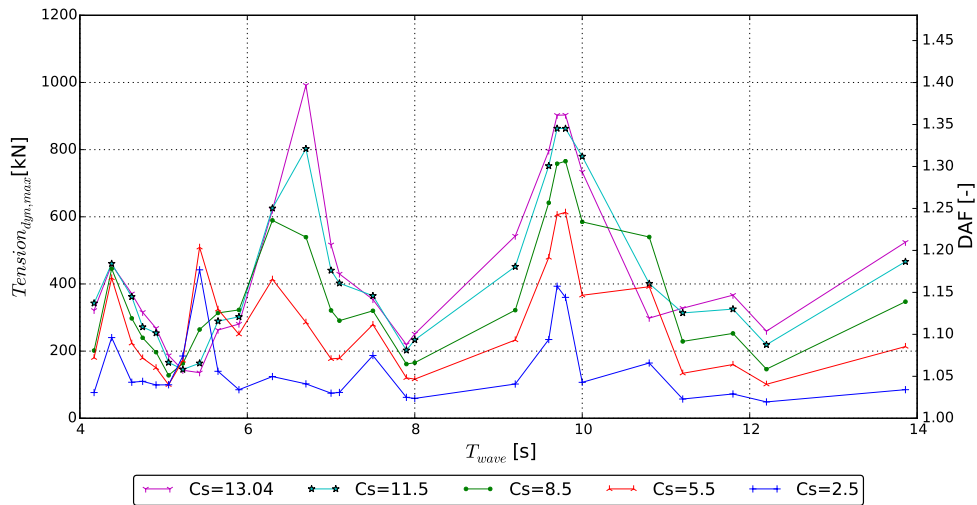


Figure 4.11: Dynamic tension and DAF of the hoisting wire

The maximum dynamic tension together with the corresponding amplification factor is given in Figure 4.11. A strong correlation can be observed between the heave motion and the tension in the hoisting wire. Two peaks are observed. This is in correspondence with the analysis made in section 4.2.1 simulation. A maximum dynamic tension of 992 kN is found at a wave period of 6.70 s. The corresponding amplification factor is 1.40. This is far more than a DAF of 1.2 described by DNV. In the following tests the differences will be analyzed further. DNV [12]

Furthermore it can be observed that a change in slam coefficients gives different behaviors. The response is not proportional to C_s . The bandwidth of the wave slamming force responses is large at the eigenfrequencies. The considered values for C_s can be compared with DNV guidelines. If a slam coefficient of 5 is chosen a possible error of 24 % is found. This error is made for the assumed conditions in this test. This is however not a realistic load case. The next tests will focus on whether this error will be made when considering vessel motions and other wave forces.

This concludes the analysis of test 1. The goal of this test was to analyze the effect of slamming on the dynamic tension in the wire for different values of C_s and T_w . An overview will be given on the obtained answers for the related questions of this test.

A time domain simulation for 1 slam coefficient and 1 wave period was analyzed. The first question to be answered was how the slam force behaved on the mud mats. It was concluded that 2 main types of slamming occur on the mud mats. A high peak short duration or a 2-peak long duration slam behavior. The next question was how slamming would effect the total template. It was found that the total slam forces of the mud mats resulted in a different behavior than the local slam behavior. After this it was questioned

how the total slam force would effect the motions of the template. It could be concluded that the heave and pitch were primarily effected. The last question was what the effect of the motions would have on the dynamic tension and the DAF on the hoisting wire. It was found that the heave motion is governing for the tension in the wire.

Once the elaboration on the time domain simulation was performed comparisons were done on all 135 time simulation for different C_s and T_w values. First the contribution of each mud mat for different wave periods was checked. It was concluded that the maximum slam force was set-up differently for different wave periods. For long waves all mud mats contributed. For shorter waves the front mud mats became of higher influence. Next the slam behavior was checked for different values of C_s . It was observed that C_s influences the behavior of slamming in a non-proportional manner. This was also observed from the pitch and heave motion of the template for different wave periods. Lastly the effect of slamming in the dynamic tension and DAF was discussed. It was concluded that C_s has a non-proportional effect on the dynamic tension and DAF. A maximum DAF of 1.4 was found. Comparing the obtained values with guidelines a total possible error of 24 % was found.

Influence of the Vessel Motions

The influence of the vessel motion on the slam behavior will be investigated in this Chapter. The Chapter will discuss the influence of the crane tip motion on the slam force, template motion and wire tension of the system. Similar to the Chapter 4 the simulation set-up will be discussed first. After this the results and discussion will be given.

5.1 Simulation set-up II

This section will give an overview of the simulation set-up with the implementation of the vessel motions. The following questions are considered in this test.

- What is the affect of the vessel motion on the total slam force?
- What is the affect of the vessel motion on the template motion and what is the contribution of the slam force on this motion?
- How does this effect the dynamic tension and DAF of the system?
- How does C_s effect the tension in the hoisting wire when the effect of vessel motions is included in the analysis?

A schematic view of this second test is given Figure 5.1. The motions of the vessel will be included in OrcaFlex via force RAOs. The template and hoisting wire are connected to the vessel at the crane tip. This creates a extra excitation point $u(t)$ in the vertical motion. No shielding of the vessel is taken into account. Only slamming is considered as wave force similar to test 1. Again a total of 135 simulation are performed. The simulation simulate 27 wave periods and 5 slam coefficients in the range of $T_{wave} = 4.17 - 13.86$ and $C_s = 2.5 - 13.04$ respectively.

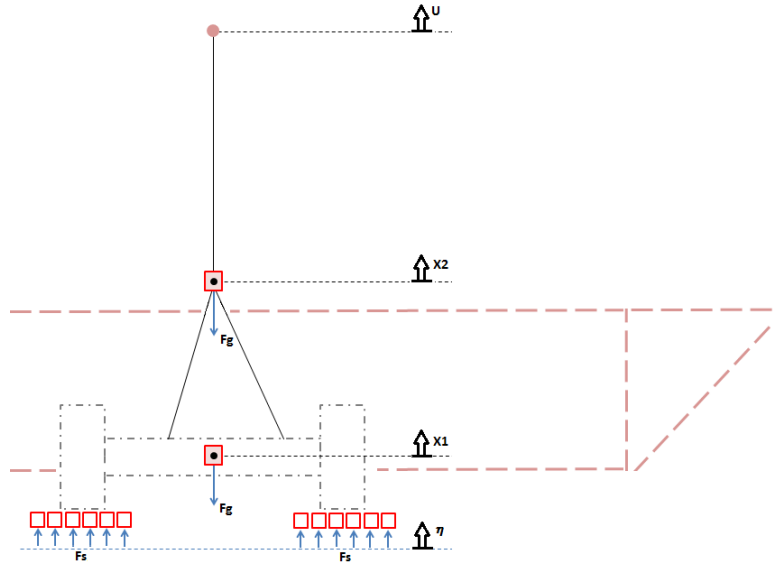


Figure 5.1: Simulation set-up II

The vessel motion will change the equations of motion of the system. The vertical equations of motion for this test are given in Equation 5.1 and Equation 5.2. The equation of motion for pitch is given in Equation 5.3.

$$m_1 \ddot{X}_1 + k_2(X_1 - X_2) - m_1 g = F_s(V_{rel}, A(t), C_s) \quad (5.1)$$

$$m_2 \ddot{X}_2 + k_2(X_2 - X_1) + k_1(u - X_2) = 0 \quad (5.2)$$

$$I_{yy} \ddot{\theta} = F_s(V_{rel}, A(t), C_s) \cdot \frac{1}{2} L_{templ} \quad (5.3)$$

5.2 Results and discussions on the influence of the vessel motions

The case discussed in Chapter 4 focused on understanding the slamming behavior and response of the template. The test did not include other wave forces than slamming and assumed the hosting wire was fixed in space. This is however not the case in reality. The hoisting wire is connected to a crane which is positioned on the vessel. This test will focus on the influence of this vessel motion. A time simulation will be investigated to discuss the changes from the crane tip motions. After this a comparison will be made for different wave periods.

5.2.1 Time domain simulation

In this section the behavior of the slam force and motions are discussed in the time domain. The main goal is to check the effect of the contribution of the vessel motions. Figure 5.2 illustrates the slam force for 2 wave periods on all mud mats. Compared to the test in Chapter 4 the differences between the front mud mats and aft mud mats have increased. The front mud mats have a slam force 5 times higher than the aft mud mats. The behavior of the slam force has changed as well. For the front mud mats it can be observed that the slam time has shortened which results in a sharper peak behavior of the slam force. It can be concluded that the effect of the vessel motion causes the local slamming behavior to intensify.

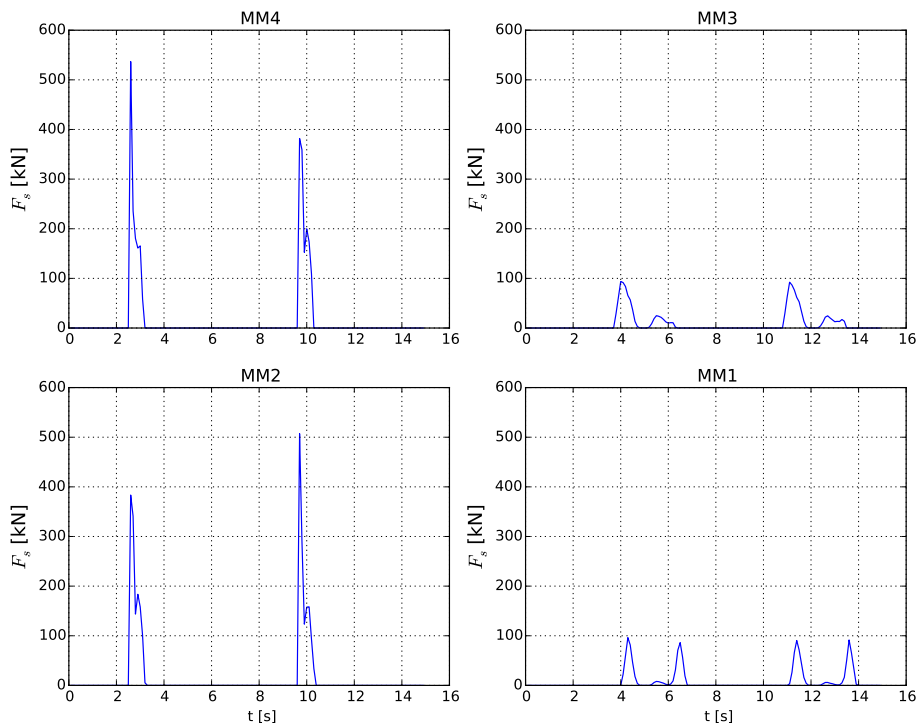


Figure 5.2: Slam force over time for each Mud mat [$C_s=11.5$, $T_w=7.1s$]

This intensifying effect of the vessel motion on the local slam force has a direct effect on the total slam force of the template. Figure 5.3 illustrates the total slam force for 2 wave periods. The intensifying effect of the slam forces is affecting the total slam force twice as much due to the summation. The contribution of the aft mud mats is almost negligible in this case.

A maximum slam force on the template of 981.1 kN was found including the vessel motion. The maximum slam force found in test 1 was equal to 526.6 kN. This means an increase of 86 % due to the vessel motion. The slam force found in test 2 is 39 % of the weight of the template. From this it can be concluded that the vessel motion can have a

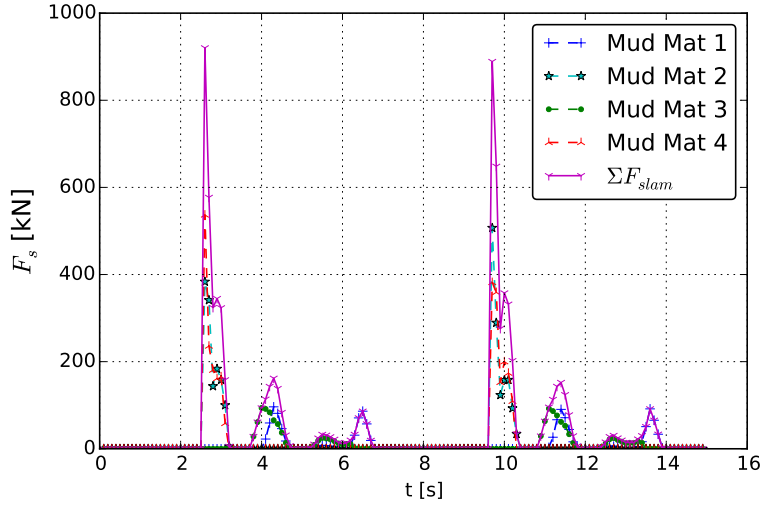


Figure 5.3: Slam force on each Mud mat $T_w=7.1s$

significant influence on the wave slamming force.

As mentioned, $t_{slam,max}$ has shortened. Compared to test 1 the slamming impact decreased by 0.9 seconds. Another point of attention is the average slam time. The maximum slam time increased but the average slam time remained constant. This is due to the changing behavior of the aft mud mats. Due to the small force and large impact time behavior the average slam time stays constant. The increasing force and decreased impact results in a higher impulse of 226.6 kNs . The impulse is increased by 5 % which is small compared to other changes. An overview of the obtained values is given in Table 5.1. It can be concluded that the motion of the vessel created a larger slam force. The motions influence the local impact speed and slam area causing the slam force to increase.

Table 5.1: Total slam force parameters

Parameter	Unit	Value
$F_{s,max}$	$[kN]$	981.1
$F_{s,avg}$	$[kN]$	347.3
$t_{slam,max}$	$[s]$	0.9
$t_{slam,avg}$	$[s]$	0.6
I_{max}	$[kN \cdot s]$	239.5
I_{avg}	$[kN \cdot s]$	116.1

Now the total slam force is discussed, it can be investigated how the motions of the template are influenced. An overview on the maximum elevation of all degrees of freedom for the template is given in Table 5.2.

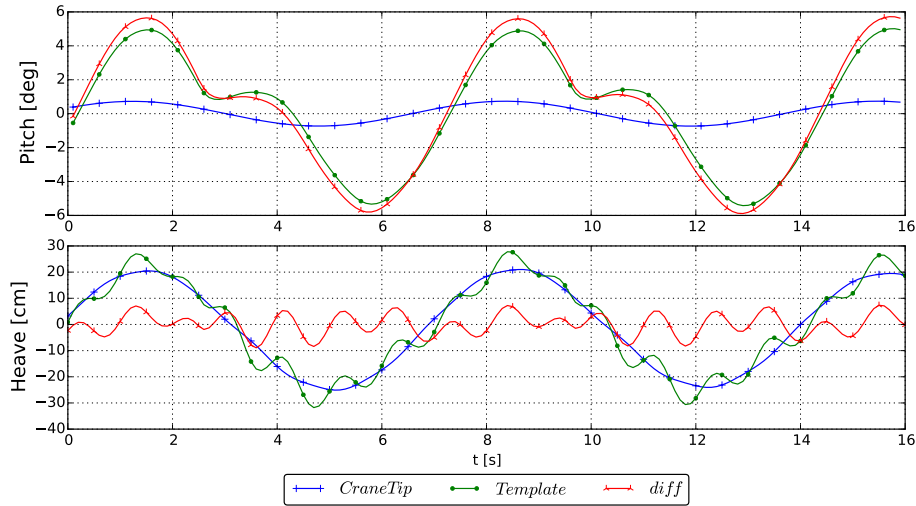
As expected the surge motion of the template will follow the motion of the vessel hence the large maximum surge elevation. The sway motion is not effected since head waves are

Table 5.2: Maximum template motions

Parameter	Unit	Value
X_{max}	[cm]	71.85
Y_{max}	[cm]	16.62
Z_{max}	[cm]	31.38
$Roll_{max}$	[deg]	0.83
$Pitch_{max}$	[deg]	5.52
Yaw_{max}	[deg]	0.39

used. The heave motion is strongly effected by the vessel motion. The heave response of the template is a combination of the vessel motion and the reaction of the slam force. The roll and yaw motion of the template are not effected and remain negligible. The pitch motion is increased. A possible explanation for this is the increased interaction with the waves due to the added heave motion. The higher slam force causes the template to increase the pitch motion.

Similar to test 1 in Chapter 4 the pitch and heave motion will be investigated further. It will be investigated whether the motion of the template is primarily effected by the vessel. The heave and pitch motion for 2 wave periods are given in Figure 5.4. In the figure the crane tip and template motion are considered. Both motions have a strong influence on the tension of the hoisting wire. The difference is given to check which motion is governing and to check what the effect is in the hoisting wire.

**Figure 5.4:** Roll and Pitch motion for 2 wave periods $T=7.1s$

First the pitch motion is considered. What can be seen is that the pitch motion of the vessel has small influence on the template motion. This was to be expected. The pitch behavior is the same as for test 1. It can be noted that the maximum pitch is higher. This is due to the increased slam force caused by the heave motion of the vessel.

The heave motion is of relevance in order to investigate the tension in the wire. An important parameter is the difference of the crane tip and template motion. The difference is related to the stretch of the wire and is therefore directly related to the behavior of the tension in the wire. What can be seen is that the template heave motion is primarily influenced by the vessel. It oscillates around the heave motion in the eigenfrequency of the riggings. The difference is governed by the eigenfrequency of the riggings similar to test 1. The maximum heave motion is 31.38 cm. This is significantly higher compared to test 1. From the difference graph in the figure it can be seen that the heave motion of the vessel has a small influence on the tension of the wire. It can therefore be concluded that the vessel motion affects the slamming force on the template but not the wire tension of the system directly. The tension is however influenced by the slam force. The vessel motion influences the tension of the hoisting wire indirectly.

The tension in the hoisting wire together with the heave difference or equivalent stretch is given in Figure 5.5. The heave difference in Figure 5.5 represents the elevation along the mean value of the initially stretched wire. A negative heave difference means a higher stretch from the mean. A positive heave difference means a lower stretch from the mean.

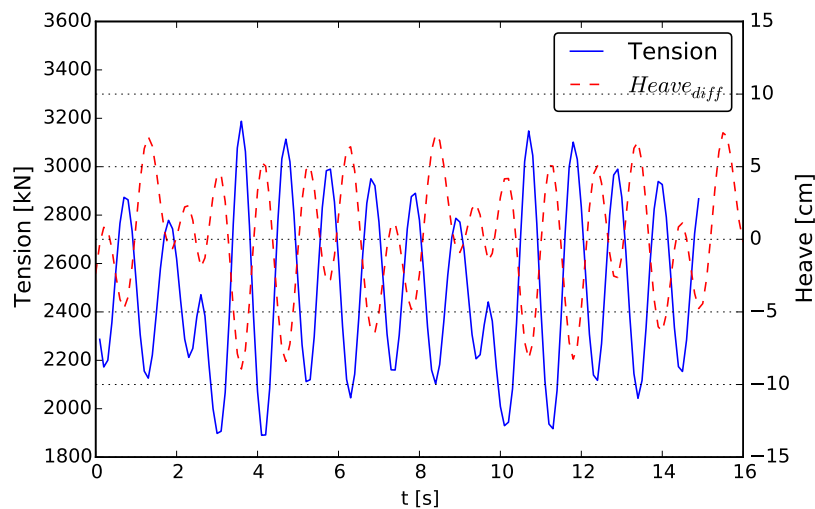


Figure 5.5: Wire tension heave motion comparison

Similar behavior can be seen as in Chapter 4. There are however differences. In test 1 the heave amplitude and tension were correlated. For test 2 this is not the case. The phase is directly correlated which was to be expected. However the amplitude is not related. Reason for this is that 2 effects are influencing the tension in the wire.

The first effect is the tension due to the stretch similar to test 1. The second effect is the presence of the slam force. The tension is directly effected by the slam force due to the high slam force for this wave period. The slam force hits the template at 2.7 and 11.4 s.

From the figure it can be seen that at these point the heave is elevated. From this point it starts to decay in the eigenfrequency. For this wave period slamming is governing. This is however not necessarily the case for all wave motions.

For this time simulation a maximum dynamic tension of 670.9 kN was found. This corresponds to a DAF of 1.27 as given in Table 5.3. The increase of the slam force is larger than the increase in DAF. This means the DAF and slam force are not proportionately correlated. The DAF is increased by 9.5 % compared to test 1.

Table 5.3: Tension and corresponding DAF

Parameter	Unit	Value
$Tension_{dyn,max}$	[kN]	670.9
DAF	[-]	1.27

This concludes the time domain comparison and analysis for this test. The next step is to check the effect of the vessel motion for different values of C_s and T_w .

5.2.2 Comparison for different slam coefficients and wave periods

This section will investigate the effect of the vessel motion on the wave slamming force and wire tension for different values of C_s and T_w . First the slam force will be discussed. Secondly the effect on the tension and DAF will be investigated.

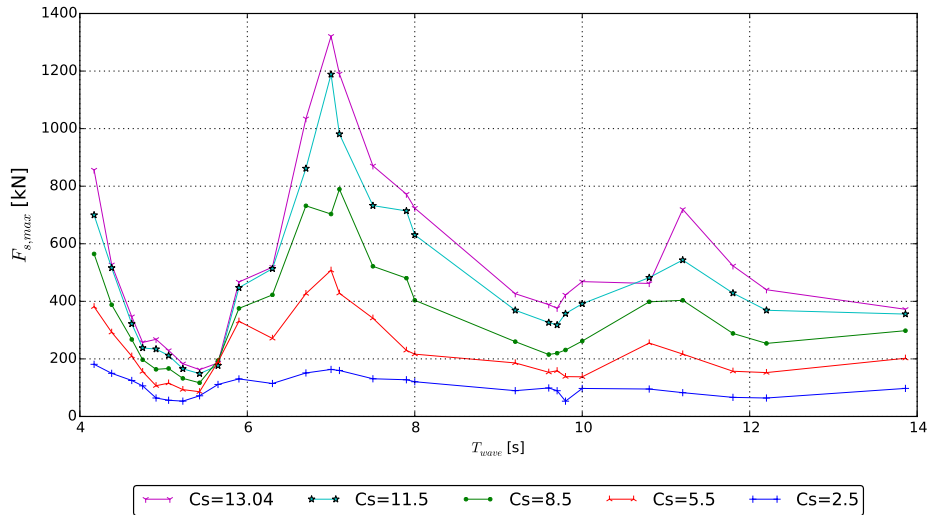


Figure 5.6: Slam force over wave period for different C_s values

Figure 5.6 illustrates the maximum slam for different values of C_s and T_w . A maximum slam force of 1312.1 kN is found at $T_w = 7s$. This is 52 % of the template weight. A clear peak can be observed. It was observed that the front mud mats are governing. The

incoming wave together with the vessel motion causes a beneficial orientation and velocity for the front mud mats. This behavior was also observed in Chapter 4.

In comparison with Chapter 4 only 1 peak is visible. The peak corresponds to the transverse eigenfrequency of the riggings. This is related to the pitch motion of the template. It can be concluded that the combined heave of the vessel and template pitch motion produce the maximum force. Furthermore no peak is observed at the pitch eigenfrequency. The heave motion of the vessel will damp this motion causing the template not to move in the eigenfrequency.

The behavior of the different values of C_s is similar. The influence of the slam coefficient on the system response has decreased. This is a direct effect of the vessel motion. The vessel motion restricts the freedom of the template and will therefore govern the influence of the slam behavior.

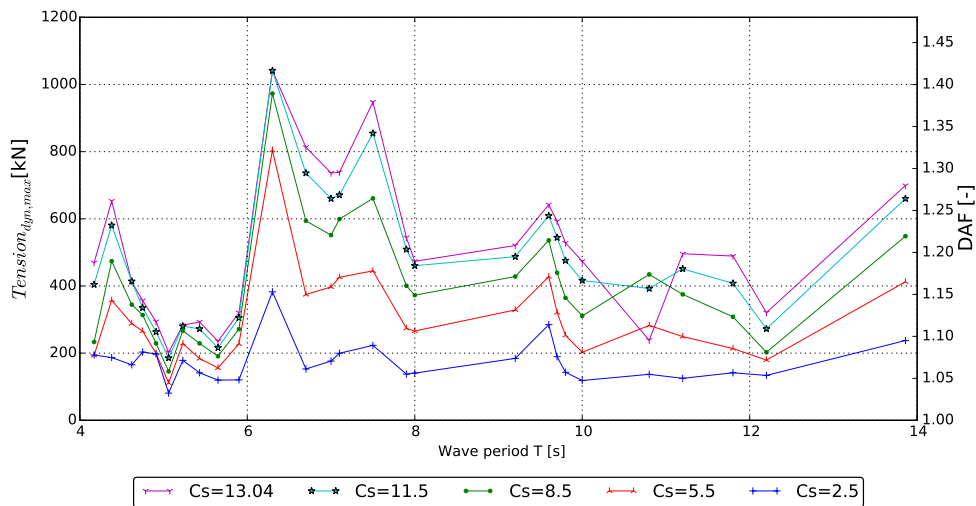


Figure 5.7: Dynamic tension and DAF of the hoisting wire

The last step in investigation the slam behavior on the system is to see how the wave slamming force effects the dynamic tension and DAF in the hoisting wire. The maximum dynamic tension and corresponding DAF is given in Figure 5.7. A maximum dynamic tension of 1041.2 kN is found with a corresponding DAF of 1.42. The maximum DAF is found at 6.7 seconds. This defers from the DAF found in Chapter 4. The wire tension and wave slamming force responds different to the template motions.

In the region between 6 and 8 seconds 2 peaks are observed. The excitation of 1 peak is caused by the impact time between the 2 templates Δt as explained in Chapter 4. At the peak close to 6 seconds Δt and the heave eigenfrequency of the rigging coincide. The peak close to 8 seconds is not caused by this phenomena. This excitation is caused by vessel and template being out of phase.

The maximum DAF of 1.42 is similar compared to the maximum DAF of 1.40 found in test 1. It can be concluded that the vessel motion influences the maximum slam force but not the maximum DAF. The vessel motions causes a decrease in the influence of the slam coefficient for all wave periods. Considering a slam coefficient of 5 as described by DNV a possible maximum error of 0.2 is found. This gives an error of 17 %. It can be concluded that by including the vessel motion the total possible error is decreased.

This concludes the analysis of the second test. The goal of this test was to check the effect of the vessel motions on the slam force and DAF in the hoisting wire. The questions and corresponding conclusions will be given in the following paragraphs.

A time domain simulation was analyzed to check the influence of the vessel motions. It was concluded that the vessel motions have an intensifying effect on the slam force. Next, the template motion was considered. From the obtained figures it could be seen that the pitch motion of the template was influenced primarily by the slam force. The influence of the vessel is governing for the heave motion. Next, it was questioned how the motions and forces would effect the tension and DAF of the system. It was found that the vessel motion has a small influence on the dynamic tension and DAF.

A comparison was made between a range of C_s and T_w values. It was found that the vessel motion increases the slam force. Furthermore, the behavior of different wave periods is changed. Main changes are no excitation at the pitch eigenfrequency and no influence on the pitch behavior at wave lengths between 0.25 and 0.5 times the length of the template. The maximum dynamic tension was found to be similar to values obtained in test 1. A different response to the slam force was found. The total possible error made from the design code is decreased when the vessel motions are included.

Other Wave Forces and Irregular Waves

So far the effect of slamming and the influence of the vessel motion have been discussed. This Chapter will discuss the influence of the other wave forces and the effect of irregular waves. Two tests will be performed. First, the influence of the buoyancy, drag and inertia are elaborated. Secondly, the effect of irregular waves on the behavior of the slam force is discussed. For both tests the same simulation set-up is used. This will be elaborated first.

6.1 Simulation set-up III

This simulation set-up will be used to perform 2 tests. First, the test on investigating the other wave forces is discussed. Next, the test on investigating the effect of irregular waves is elaborated. Finally, a overview of the simulation set-up will be given.

Influence of F_i , F_d and F_b

This test will focus on the contribution of the other wave forces on the system. The buoyancy, inertia and drag are taken into account. Investigation is done on how the other wave forces effect the behavior of the slam force. A comparison is made between the analysis performed in Chapter 5. A evaluation can be done on the influence and importance of the slam force in the installation of the template. The following questions are considered.

- What is the effect of the buoyancy, inertia and drag force on the total slam force?
- What is the effect of these waves forces on the template motion and what is the contribution of the slam force on this motion?
- How does this affect the dynamic tension and DAF of the system?

- How does C_s affect the tension in the hoisting wire including the vessel motions and all wave forces?

Similar to the previous tests 27 wave periods and 5 values of C_s are considered giving a total of 135 simulations .

Irregular waves

At this point only regular waves were considered. Test 4 will analyze the effect of irregular waves on the behavior of the template. The focus of the test is to analyze whether the effect of the slam coefficient changes. The considered questions are as follows.

- How do irregular waves influence the slam force?
- What is the scatter of the slam force?
- Is the influence of C_s on the maximum dynamic tension effected by irregular waves?

In this test 5 simulations are performed. All values of C_s are considered. A JONSWAP spectrum is used with a significant wave height and peak period of 3 m and 7 s respectively.

Simulation set-up

Figure 6.1 illustrates the schematic view of the simulation set-up. Simulation set-up III includes the vessel motions and all wave forces.

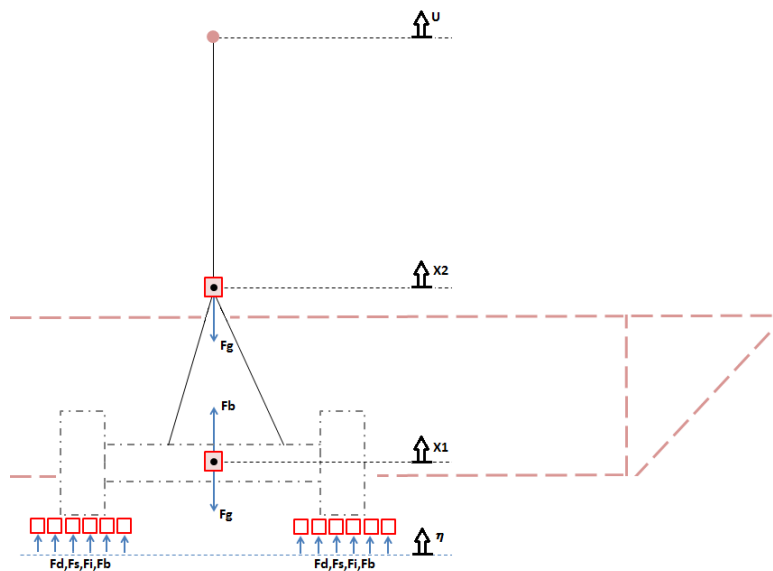


Figure 6.1: Simulation set-up III

The wave forces are included using characteristic area and force coefficients given in

Chapter 3. Including all wave forces gives the vertical and pitch equations of motion as given in Equation 6.1, Equation 6.2 and Equation 6.2 respectively.

$$(1 + C_a(t))m_1\ddot{X}_1 + \frac{1}{2}\rho C_d(t)A(t)V_{rel}|V_{rel}| + k_2(X_1 - X_2) - m_1g + \rho g \nabla(t) = F_s(V_{rel}, A(t), C_s) \quad (6.1)$$

$$m_2\ddot{X}_2 + k_2(X_2 - X_1) + k_1(u - X_2) = 0 \quad (6.2)$$

$$I_{yy}\ddot{\theta} + \frac{1}{2}\rho C_d(t)A(t)V_{rel}|V_{rel}| \cdot \frac{1}{2}L_{templ} = F_s(V_{rel}, A(t), C_s) \cdot \frac{1}{2}L_{templ} \quad (6.3)$$

6.2 Results and discussions on the influence of F_i , F_d and F_b

The tests performed so far focused on the behavior of the slam force and the contribution of the vessel motions. The next step is to include all wave forces. In this section the buoyancy, inertia and drag forces on the mud mats are taken into account. The goal of this test is to check the effect of these forces on the slam force, motion and tension in the hoisting wire. A time domain simulation will be discussed to understand the behavior of the considered forces. Afterwards the effect on the slam force and dynamic tension is discussed for a range of T_w values.

6.2.1 Time domain simulation

Figure 6.2 illustrates the wave forces for 2 wave periods. What can be seen from the figure is that the slam force is the governing wave force. The value of the slam force is lower and must be influenced by the other wave forces. This influence will be elaborated further. The maximum values for all considered wave forces are given in Table 6.1.

Table 6.1: Maximum wave forces

Parameter	Unit	Value
$F_{s,max}$	[kN]	793.7
$F_{i,max}$	[kN]	140.1
$F_{d,max}$	[kN]	104.1
$F_{b,max}$	[kN]	33.3

The obtained maximum inertia force is 140.1 kN. The behavior of the inertia force is governed by 2 peaks. These are caused by the front and back mud mats hitting the water. It can be seen that the inertia force acts an instant after the occurrence of the slam force. The inertia force damps the behavior of the template due to this delay.

The drag force is dependent on the velocity squared and contact area. Two peaks can be seen aft of the first slam force and aft of the second inertia force. This time span is

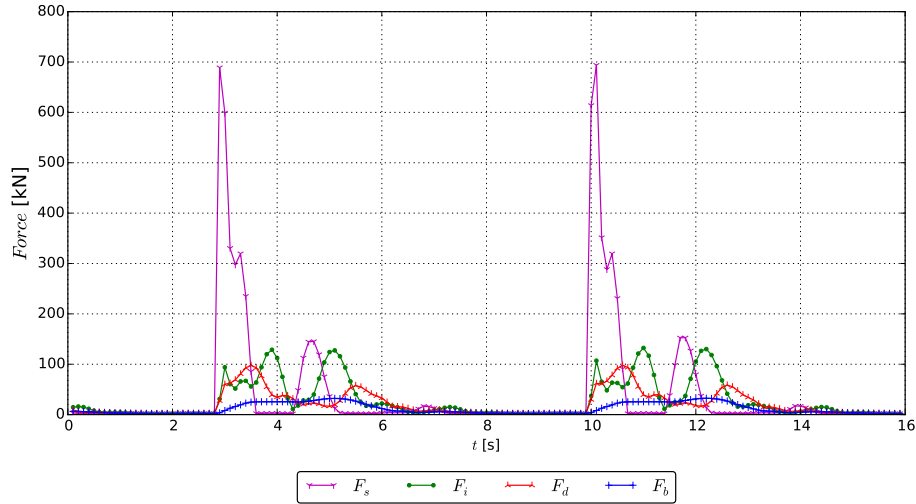


Figure 6.2: Wave force comparison

different compared to the slam and inertia force. This behavior indicates that drag forces damp the system.

The last considered wave force is the buoyancy force. The buoyancy force acts when the mud-mats are submerged. A maximum buoyancy force of 33.3 kN was found. The mud mats have limited buoyancy and therefore is of small influence.

The next step is to investigate the effect of the buoyancy, drag and inertia force on the slam force. A maximum slam force of 793.7 kN was found. Compared to the 981.1 kN of found in Chapter 5, this is significantly lower. The decrease in maximum slam force has 2 main causes.

First, the slam force is damped by the other wave forces. Secondly, the wave forces cause a different reaction in the motion of the template and therefore create a different force. This is further discussed in comparing the slam force for different wave periods.

Table 6.2: Total slam force parameters

Parameter	Unit	Value
$F_{s,max}$	[kN]	793.7
$F_{s,avg}$	[kN]	290.9
$t_{slam,max}$	[s]	1.3
$t_{slam,avg}$	[s]	1.0
I_{max}	[kN * s]	243.7
I_{avg}	[kN * s]	98.6

The behavior of the slam force is also changed compared to test 2. The slam force behav-

ior is directly related to the maximum force. From Figure 6.2 it can be seen that there is an influence of the second peak. However, the overall shape is governed by 1 peak. Furthermore, the slam time is increased compared to test 2. This behavior is in coherence with the observation done in Chapter 4. An overview of the slam force parameters is given in Table 6.2.

The next step is to investigate the effect of the wave forces on the motion of the template. An overview on the maximum elevation is given in Table 6.3. It is observed that the maxima of the motions are smaller compared tot test 2. The difference with test 2 is however small. This would indicate that the buoyancy, inertia and drag force have no influence on the motion of the template.

Table 6.3: Maximum template motions

Parameter	Unit	Value
X_{max}	[cm]	66.34
Y_{max}	[cm]	15.52
Z_{max}	[cm]	28.44
$Roll_{max}$	[deg]	1.27
$Pitch_{max}$	[deg]	5.03
Yaw_{max}	[deg]	0.67

In order to check this, the heave and pitch motion are given for 2 wave periods. These governing motions are illustrated in Figure 6.3. The figure shows the crane tip motion response of test 2 and the response of test 3. Comparing the pitch motion from test 3 with test 2 it can be seen that the motion is damped due to the contributing wave forces. This damping effect creates a delay in the pitch response of the system. This is in agreement with the drag and inertia forces investigated previously in this section. The maximum elevation of the pitch is effected slightly.

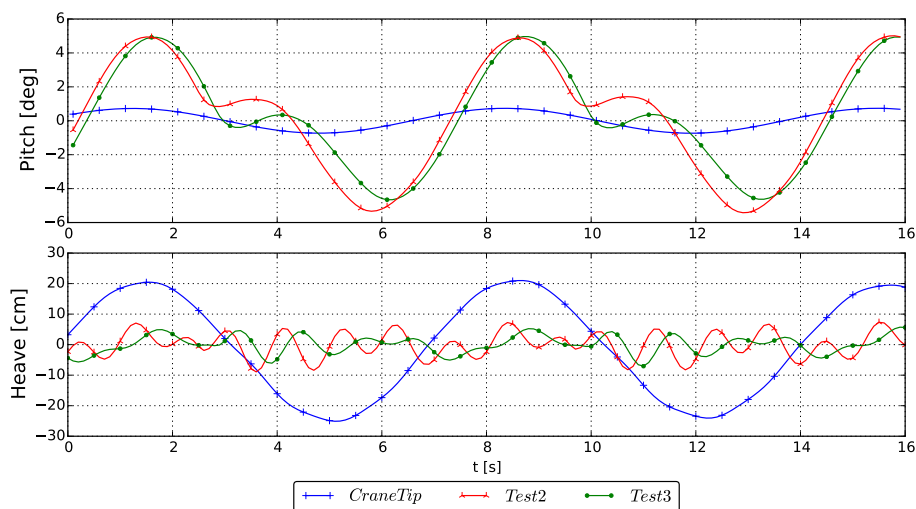


Figure 6.3: Roll and Pitch motion for 2 wave periods $T=7.1s$

Furthermore the heave motion is given in Figure 6.3. Similar to the pitch motion a delay is observed. A difference is observed in the height of the peaks in the signal. For test 3 this is lower in all cases. From this it is concluded that the considered wave forces do have an influence on the motion of the template. The inertia, drag and buoyancy force damp the response of template motions.

The last step in investigating the time domain simulation is to see how the induced motions of the template affect the tension in the wire. From previous tests it was observed that the heave motion is directly related to the tension. The heave motion and corresponding wire tension are given in Figure 6.4.

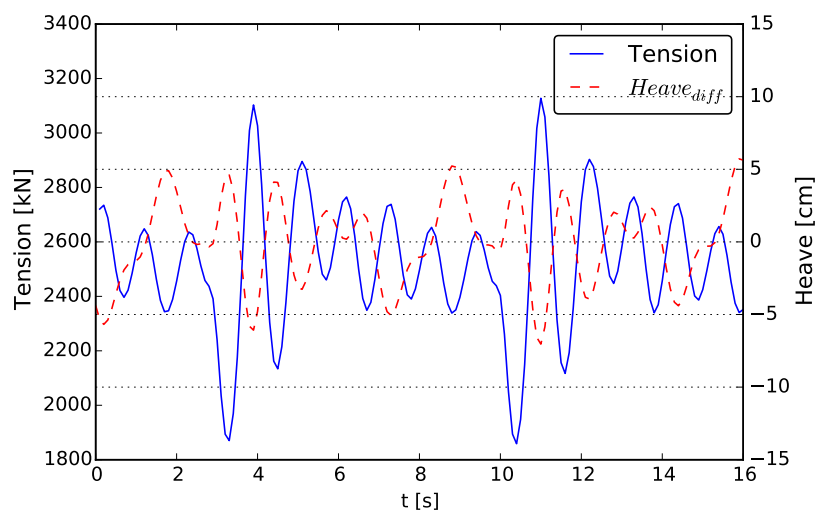


Figure 6.4: Wire tension heave motion comparison

As for previous tests the tension follows the heave motion behavior. Again, the tension force is governed by the eigenfrequency of the riggings. The tension is excited by the incoming wave force similar to test 2. The tension decays in the eigenfrequency after impact. For test 3 this decay is different then for test 1 and 2. This is due to the damping of the other wave forces. It can be concluded that the buoyancy, inertia and drag damp the tension in the wire.

From the calculated wire tension in the simulation a maximum dynamic tension of 613.8 kN was found. This is 8.5 % lower then the maximum tension found in test 2. The maximum tension together with the corresponding DAF is given in Table 6.4.

Table 6.4: Tension and corresponding DAF

Parameter	Unit	Value
$Tension_{dyn,max}$	[kN]	613.8
DAF	[-]	1.24

It must be noted that the time domain comparison between tests gives more insight into the behavior of the forces and motion but may be misleading due to the changing behavior

of the response for different wave periods. Therefore the behavior of the slam force and response on the wire tension for different wave periods is important to understand. This will be discussed in the following section.

6.2.2 Comparison for different C_s and wave periods

The effect of the buoyancy, inertia and drag force on the slam force and template motion is investigated in the time domain. The next step is to check this influence for a range of wave periods. This section will discuss the influence of the included wave forces and will investigate the effect of the slam coefficient on the slam force and dynamic tension in the wire. A comparison will be made from results obtained in Chapter 5.

Figure 6.5 illustrates the maximum slam force for a range of C_s and T_w values. A maximum slam force of 1079.3 kN was found occurring at a wave period of 7.00 seconds. This is 18 % lower compared to test 2. Similarities can be observed in the overall shape of the slam force compared to test 2. The peak in test 3 is flattened compared to test 2. This is due to damping of the included wave forces. Another point which can be noted is the difference between the slam coefficients. The damping effect causes a decrease in the range of the slam force. This means the influence of the slam coefficient decreases. This is beneficial when choosing a DNV approach for determining the slam force and motion response. The possible maximum error is decreased in this manner.

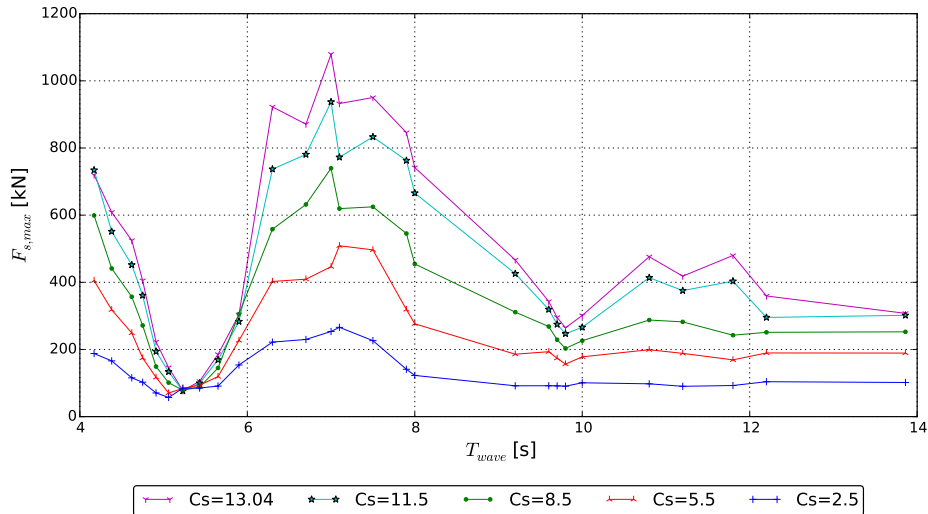


Figure 6.5: Slam force over wave period for different C_s values

The maximum dynamic tension and corresponding DAF are given in Figure 6.6. A maximum tension of 923.0 kN was found at $T_w = 6.7$ seconds. This corresponds to a maximum DAF of 1.37. The maximum slam force does not occur at the same wave period as the maximum dynamic tension similar to test 1 and 2. This is due to the response of the template. In the case of a wave period of 7 seconds a large slam force is present. The template reaction is an induced pitch motion. This motion behavior is less observed for

a wave period of 6.7 seconds causing a higher dynamic tension.

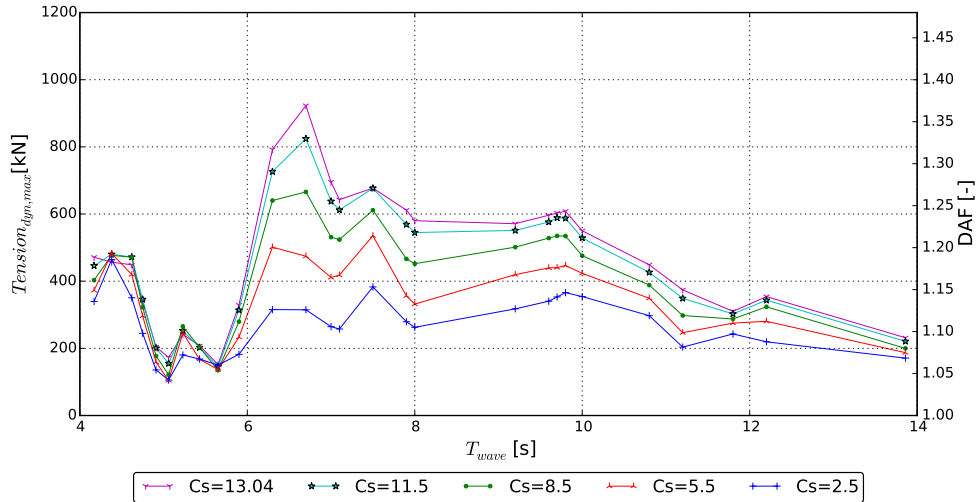


Figure 6.6: Dynamic Tensions and DAF of the hoisting wire

It also can be observed that the effect of the slam coefficient is decreased. This is beneficial for the possible maximum error. A possible maximum error was found to be 18 %. This is decreased compared to test 2. It can be concluded that the value of the slam coefficients has less influence on the slam force and dynamic tension of the wire if all wave forces are considered. Main reason is the damping behavior of the included wave forces on the system.

This concludes the third test of this investigation. The main goal of test 3 was to investigate the effect of the buoyancy, inertia and drag force on the slam force and motion of the template. First, the behavior of the buoyancy, inertia and drag was compared with the slam force. It was found that the slam force is governing. Furthermore, it was concluded that the drag and inertia could have an influence due to their shift in time. The buoyancy force was found to be small. It was found that the inertia and drag force damp the slam force. The included forces cause the slam force to decrease and change shape. Next, the effect of the wave forces on the template was investigated. It was found that the slam force is the governing force on the motion of the template. It was observed that the inertia and drag force damp the template motion. This resulted in a smaller dynamic tension and DAF.

After the time simulation analysis it was checked how the observed damping would effect the slam force and tension for a range of T_w and C_s values. It was found that the overall slam force decreased. Furthermore, it was concluded that the effect of C_s decreased. After the maximum slam force the dynamic tension and DAF were investigated. A maximum DAF of 1.37 was found. Similar to the slam force a decrease in the influence of the slam coefficients was found. This resulted in a reduction of the possible maximum error. A possible maximum error of 18 % was found comparing to DNV standards. Comparing

this with project safety margins it can be concluded that this possible maximum error will not effect the operations of the Wiking project.

6.3 Results and discussion on the influence of irregular waves

The wave slamming force, motions and wire tension was analyzed for a range of wave periods in regular waves. In reality the wave motions are irregular. It was observed that the motions and forces were inflicted due to the repetitive motion of the regular waves. This is not possible for real waves. This section will discuss the effect of irregular waves on the behavior of the slam force. The consequences on the dynamic tension and DAF will be discussed.

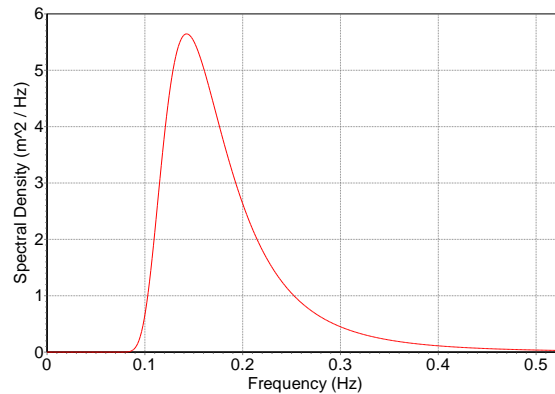


Figure 6.7: Jonswap spectrum [Hs=3, Tp=7]

The JONSWAP spectrum is illustrated in Figure 6.7. A significant wave height of 3 meter and peak period of 7 seconds is considered. This is the measured extreme case at the Wiking site. The total energy is divided over the spectrum with a maximum at 7 seconds. The spectrum influences the slam force. It must be noted that 1 seed is considered. This means the result can differ for other simulations. It is however assumed that the overall behavior can be compared. In this section a short elaboration will be given on the time simulation of $C_s = 11.5$. The elaboration will be followed by a comparison between the slam coefficients.

6.3.1 Time domain simulation

This section will discuss the behavior of the slam force for irregular waves assuming a slam coefficient of 11.5. The total slam force on the template for 1 minute is illustrated in Figure 6.8. The slam force is scattered compared to the regular wave tests. Short waves influence the forces causing more peaks in 1 slam instant. Furthermore increased scatter is observed in the height and slam time of the force. The 2 slam behaviors described in

Chapter 4 are present in the complete simulation. This was expected since the energy of the waves differs at each time step.

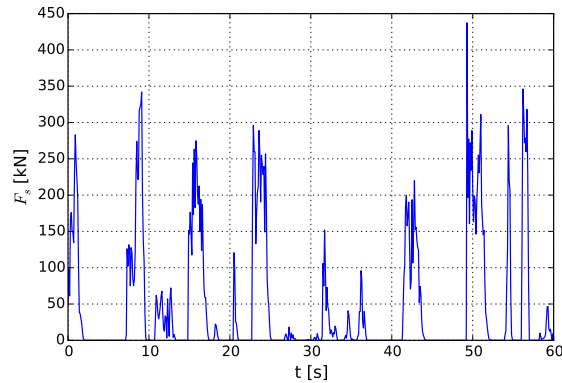


Figure 6.8: Total slam force over time in irregular waves

In order to identify the behavior of the wave slamming force a histogram can be made. The number of occurrences versus the maximum slam force is given in Figure 6.9. A histogram together with the trend line is illustrated. The slam forces were counted similar to test 1. A logarithmic behavior can be seen in Figure 6.9. This is caused by the scatter of the energy in the waves and the 2-peak behavior of the small waves. This causes small slam forces to govern the behavior.

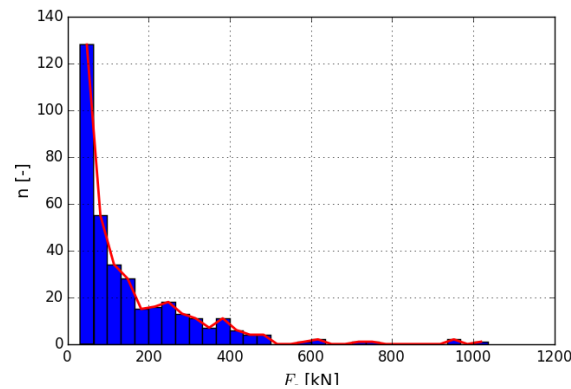


Figure 6.9: Slam force Histogram

6.3.2 Comparison for different C_s

The last step in analyzing the effect of irregular waves on the wave slamming force is to check the effect for C_s values between 2.5 – 13.04. The trend lines of the histogram for all slam coefficients is given in Figure 6.10. What can be observed is that the trend line shape changes. For C_s values of 2.5 and 5.5 the scatter becomes smaller. The small wave slamming forces become more dominant. Furthermore, it can be notified that there is

almost no difference between $C_s = 8.5, 11.5$ and 13.04 . This indicates that the effect of the slam coefficient decreases for higher values of C_s .

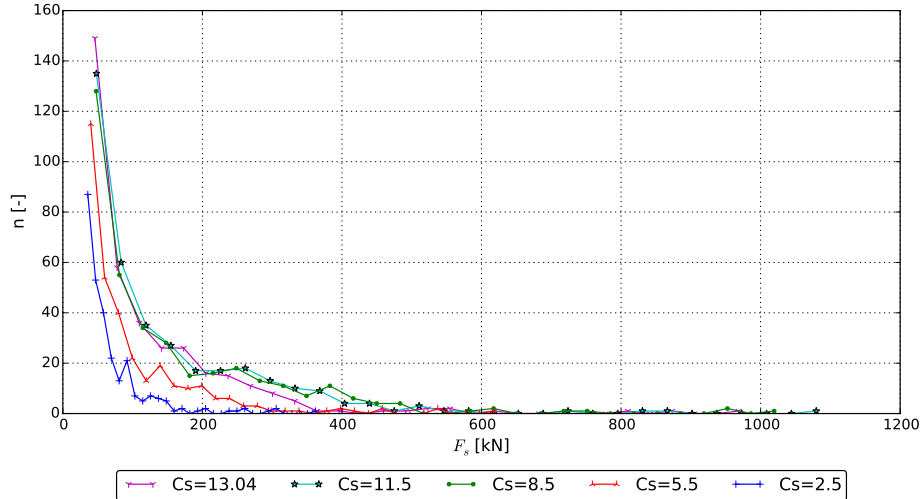


Figure 6.10: Histogram trend lines for different values of C_s

This concludes the discussion on the effect of irregular waves on the slam force of the template. First the influence of irregular waves on the slam force was discussed in a time simulation. The slam coefficient considered was 11.5 . An increase in scatter on the slam behavior was found. Furthermore a larger range in height and slam time was observed.

In order to investigate the scatter in the slam force a histogram was made. It was found that small slam forces govern the total behavior. The last question to be investigated was the effect of the slam coefficient on this scatter. It was concluded that the influence of the slam coefficient decreased on the total behavior of the slam force.

Conclusions and Recommendations

Conclusions and recommendations will be given for further work. The conclusions are focused on answering the thesis objective. Recommendations are given on improving the performed simulations. Lastly, issues are discussed for further research. The formulated thesis objective was written as follows.

Determine the effect of the slam force on the total motion and loading in the hoisting wire during lowering of the template through the wave zone.

Conclusions

The effect of the wave slamming force on the template motions and hoisting wire tension was investigated during lowering of the template through the wave zone. It was found that the slam force was the governing external force. Furthermore it was found that slamming is difficult to estimate. A range of C_s values was considered to cope with the uncertainties.

It was observed that the behavior of the wave slamming force was different on each mud mat. A clear difference was found in the behavior on the front and aft mud mats. Two types of wave slamming forces were observed. First a impulse behavior was observed. The slam force had a high peak force and short impact time. The second behavior which was a distributed slam force with a long impact time.

The effect of the slam force in the hoisting wire was dependent on the motions of the template. It was found that the heave motion and pitch motion where the main motions of influence. Increased excitations were observed near the pitch eigenfrequency of the template. Furthermore it was found that the time of impact Δt between the mud mats coincided with the riggings eigenfrequency in wave periods between 6 and 8 seconds.

The heave motion of the template was directly related to the tension in the hoisting wire. Furthermore it was concluded that large slam forces did not necessarily induce large tensions in the hoisting wire.

The effect of the vessel motion intensified the wave slamming force. This resulted in larger template motions. The effect on the DAF and tension in the hoisting wire was however small. The slam force was damped when drag, inertia and buoyancy were taken into account. The damping resulted in a delay in the motion response. The last effect that was checked was the influence of the irregular waves. The irregular waves induced a scatter in the wave slamming force.

The slam force hydrodynamic behavior was characterized by the slam coefficient. The influence of the C_s value was checked. Significant differences were found. The wave slamming force was not proportional with the chosen slam coefficient. It was concluded that the slam coefficient affects the contact area and relative velocity of the template. It was found that the effect of the slam coefficient decreases with the vessel motion contribution. A further decrease in influence of C_s was found when adding F_i , F_d and F_b .

A maximum dynamic amplification factor of 1.37 was found. The maximum DAF difference in the considered C_s range was 25 %. A comparison was made between the minimum C_s value according to guidelines. A possible maximum error of 18 % was found.

The performed tests were conducted for an extreme case with a wave height of 3 meter. Due to these extreme environmental conditions, the obtained possible maximum error was considered to be within commonly used safety margins. It was found that the wave slamming force did not exceed the crane load capacity. From this it was concluded that the wave slamming force will not limit the operational conditions for the Wiking project. Lastly, it was concluded that thorough local flow analysis like CFD will not improve the prediction of the tension in the hoisting wire. The reason for this is the reduced influence of the slam coefficient on the hoisting wire.

Recommendations

Recommendations are given on the improvement of the simulation. Suggestions are given for possible future research.

Simulation Improvements

- Simplifications are made in the model. An important assumption is the Froude-Krylov approach. This approach does not take into account viscous effects. This is of influence on the behavior of the force. In order to improve the accuracy of the model this should be taken into account.
- The model assumes a critical slam force behavior at the height of the mean water line. More heights can be considered to investigate the behavior of the slam force at different moments in the lowering phase. The model could include the lowering speed of the winch through the wave zone as well.
- In the model it is assumed that the characteristics of the incoming slamming force are the same. However, due to the entrapment of the water particles this slamming

behavior differs under the mud mat. For improving the estimation of the slam force a pattern in values of C_s could be chosen.

- OrcaFlex provides limited tools to validate the model. Validation checks must be performed by hand or with other software. This creates errors. This should be improved in the OrcaFlex Software.

Further Research

- One wave direction was considered in the performed simulations . The effect of other wave angles could be taken into account. The shielding effect of the vessel could be investigated to optimize the ship heading for the lowering operation.
- It was found that the mud mat distance affects the slam force and behavior of the template. An investigation can be performed to alter the distance between the mud mats and check the effect. The amount and location of mud mats could be altered to check the influence of the configuration of the mud mats.
- It was observed in the simulation that the hole in the mud mats affects the slam force by creating a 2-peak behavior. Different shapes and sizes could be used to investigate the influence of the mud mat geometry.
- Experimental tests can be performed to verify and investigate the slam force behavior. Several local phenomena have been verified by experimental tests. However, few experiments are performed on the effect of slamming on the operability of the system.
- More cases could be investigated like the lift-off from the deck and installation on the sea bed. A comparison could be made on the importance of the slam force compared to other critical phases in the installation.
- Using a passive heave compensator will lower the dynamic tension in the hoisting wire. It can be investigated for which sea conditions the heave compensator is economically beneficial.
- The template can be lowered through the wave zone under an angle. This will reduce the horizontal motion but will increase the side lead angles of the hoisting wire. An investigation can be done on the pros and cons of such an operation.
- Local structural effects due to slamming could be investigated. Since the slam force is an impulse force, local failure of the structure can occur. This could be critical for the design of the structure.

References

- [1] DNV. Modelling and Analysis of Marine Operations. Technical Report RP-H103, Det Norsk Veritas, April 2011.
- [2] D. Karunkaran K. Aarset, A. Sarkar. Lessons learnt from lifting operations and towing of heavy structures in north sea. *Offshore Technology Conference*, 2011.
- [3] Volker Bertram. *Practical Ship Hydrodynamics (2nd Edition)*. Elsevier, 2012.
- [4] O.M. Faltinsen. *Sea loads on ships and offshore structures*. Cambridge University Press, Cambridge, 1990. ISBN 0-521-52396-6.
- [5] W.M. Lin M. Greenhow. Non-linear free surface effects: experimetns and theory. Technical report, Department Ocean Engineering, Cambridge, 1983.
- [6] Shaojun Liu Hu. Numerical investigation of wave slamming of flat bottom body during water entry process. *Hindawi Publishing Corporation*, 2014.
- [7] J.R. Wright N.J. Smith, P.K. Stansby. The slam force on a flat plate in free flight due to impact on a wave crest. *Journal of fluid and structures* 12, 1992.
- [8] M. Gharib F.J. Huera-Huarte, d. Jeon. Experimental investigation of water slamming loads on panels. *Elsevier*, 2011.
- [9] ANSYS. Installations of subsea equipment. Technical report, ANSYS Inc., 2011.
- [10] G. Clauss. *Offshore Structures Vol. 1, conceptual design and hydromechanics*. Springer, 1992.
- [11] Turgut Sarpkaya. *Wave Forces on Offshore Structures*. Cambridge university press, 2010.
- [12] DNV. Environmental Conditions and Environtmental Loads. Technical Report RP-C205, DNV, April 2014.
- [13] W.W. Massie J.M.J. Journee. *Offshore Hydrodynamics* . TU Delft, 2001.

-
- [14] M. E. Weber R. Clift, J.R. Grace. *Bubbles, Drops and Particles*. Academic Press, 1978.
- [15] National Aeronautics NASA and Space Administration. Shape effect on drag. URL <http://www.grc.nasa.gov/WWW/k-12/airplane/shaped.html>.
- [16] *Aqwa-line manual 14.0*. ANSYS Inc., 2011.
- [17] R. Zhao & O. Faltinsen. Slamming loads on high-speed vessels. In *ONR conference Korea*, 1992.
- [18] C.A. Garrido-Mendoza. Numerical simulation of hydrodynamic of a circular disk oscillating near a seabed. *OMAE*, 2013.
- [19] K.P. Thiagarajan H. Wadhwa. B Krishnamoorthy. Variation of heave added mass and damping near seabed. *ASME*, 2010.
- [20] K. P. Thiagarajan K. Vu, B. Chenu. Hydrodynamic damping due to prous plates. *World Scientific Engineering ACAdemy and Society*, 2008.
- [21] D. Dray L. Tao. Hydrodynamic performance of solid and porous heave plates. *Ocean Engineering*, 2008.
- [22] Th. Von Karman. The impact on seaplane floats during landing. Technical report, Natioanal Advisory Committe for Aeronautics, 1929.
- [23] H. Wagner. The phenomena of impact and planning on water. *zeitschrift fur angewandte mathematic und mechanic* 12, 193-215, 1932.
- [24] S.Chuang. Experiments on flat-bottom slamming. *Journal of Ship Research* 10-17, 1966.
- [25] J. Verhagen. The impact of a flate plate on a water surface. *Journal of ship research* 211-223, 1967.
- [26] M. Greenhow. Wedge entry into initially calm water. *Applied Ocean Research*, 1987.
- [27] S.C. Kot C.O. Ng. Computations of water impact on a two-dimensional flat-bottom body with a volume-of-fluid method. *Ocean engineering*, 1992.
- [28] C.F. Kettleborough B. R. Koehler. Hydrodynamic impact of a falling body upon a viscous incompressible fluid. *J. Ship e.* 21 165-181, 1977.
- [29] P.M. Koola N. Suchithra. A study of wave impact on horizontal slabs. *Pergamon*, 1994.
- [30] M.C. Lin. Simultaneous measurements of water impact on a two-dimensional body. Technical report, fluid dynamics research 19(3), 1997.
- [31] J. STear R. Ramos G. Bea, T. Xu. Wave forces on decks of offshore platforms. *Journall of waterway,port,coastal and ocean engineering*, 1999.
- [32] M. Ohkusu E.V. Ermanyuk. Impact of a disk on shallow water. *Elsevier*, 2004.

-
- [33] S. Nallayarasu G. Sekhar. Wave slam/slap loads on structural members in the air-gap. *ASME International conference on ocean, offshore and arctic engineering*, 2011.
- [34] *IEC 61400-1*. Dansk standard, 2007.
- [35] *Lifting Analysis B2*. Boskalis, 2014. ISBN OE13TE009.
- [36] R. Nous. Wire tension analysis for offshore wind installation. Technical report, NTNU, 2014.
- [37] *Technical and operational description for Wikingen Pre-piling template*. NorWind installer, 2014. ISBN IBE.WIK.TE.MS.002.R04.
- [38] *Wikingen Offshore Wind Farm WTG Foundation installation*. Offshore Wind Force, 2014. ISBN WIK-INL-M-OWFJV-0011.
- [39] *Marine equipment handbook*. Balmoral, 2004.
- [40] Jorgen Fredsoe. *Hydrodynamics*. MEK-DTU, 2008.
- [41] I. G. Jonsson A. Svendsen. *Hydrodynamics of coastal regions*. Technical University Denmark DTU, DK-2800 Lyngby, 1982. ISBN 87-87245-57-4.
- [42] Leo H. Holthuijsen. *Waves In oceanic and coastal waters*. Cambridge University Press, Cambridge, 2007. ISBN 978-0-521-86028-4.

Linear Wave Kinematics

Table 2.1. Velocity potential, dispersion relation, wave profile, pressure, velocity and acceleration for regular sinusoidal propagating waves on finite and infinite water depth according to linear theory

	Finite water depth	Infinite water depth
Velocity potential	$\phi = \frac{g\zeta_a}{\omega} \frac{\cosh k(z+h)}{\cosh kh} \cos(\omega t - kx)$	$\phi = \frac{g\zeta_a}{\omega} e^{kz} \cos(\omega t - kx)$
Connection between wave number k and circular frequency ω	$\frac{\omega^2}{g} = k \tanh kh$	$\frac{\omega^2}{g} = k$
Connection between wavelength λ and wave period T	$\lambda = \frac{g}{2\pi} T^2 \tanh \frac{2\pi}{\lambda} h$	$\lambda = \frac{g}{2\pi} T^2$
Wave profile	$\zeta = \zeta_a \sin(\omega t - kx)$	$\zeta = \zeta_a \sin(\omega t - kx)$
Dynamic pressure	$p_D = \rho g \zeta_a \frac{\cosh k(z+h)}{\cosh kh} \sin(\omega t - kx)$	$p_D = \rho g \zeta_a e^{kz} \sin(\omega t - kx)$
x-component of velocity	$u = \omega \zeta_a \frac{\cosh k(z+h)}{\sinh kh} \sin(\omega t - kx)$	$u = \omega \zeta_a e^{kz} \sin(\omega t - kx)$
z-component of velocity	$w = \omega \zeta_a \frac{\sinh k(z+h)}{\sinh kh} \cos(\omega t - kx)$	$w = \omega \zeta_a e^{kz} \cos(\omega t - kx)$
x-component of acceleration	$a_1 = \omega^2 \zeta_a \frac{\cosh k(z+h)}{\sinh kh} \cos(\omega t - kx)$	$a_1 = \omega^2 \zeta_a e^{kz} \cos(\omega t - kx)$
z-component of acceleration	$a_3 = -\omega^2 \zeta_a \frac{\sinh k(z+h)}{\sinh kh} \sin(\omega t - kx)$	$a_3 = -\omega^2 \zeta_a e^{kz} \sin(\omega t - kx)$

$\omega = 2\pi/T$, $k = 2\pi/\lambda$, T = Wave period, λ = Wavelength, ζ_a = Wave amplitude, g = Acceleration of gravity, t = Time variable, x = direction of wave propagation, z = vertical coordinate, $z = 0$ mean waterlevel, h = average waterdepth. Total pressure in the fluid: $p_D + p_0$ (p_0 = atmospheric pressure).

Figure A.1: Linear theory relations for regular sinusoidal propagating waves on finite and infinite water depth. Faltinsen [4]

Appendix B

Verification Vessel RAOs

This Appendix will present the comparison between the RAOs of the of the coupled and uncoupled system. The uncoupled reference values from Boskalis are presented as well. The RAOs for 6 degree of freedom are given for 3 wave directions.

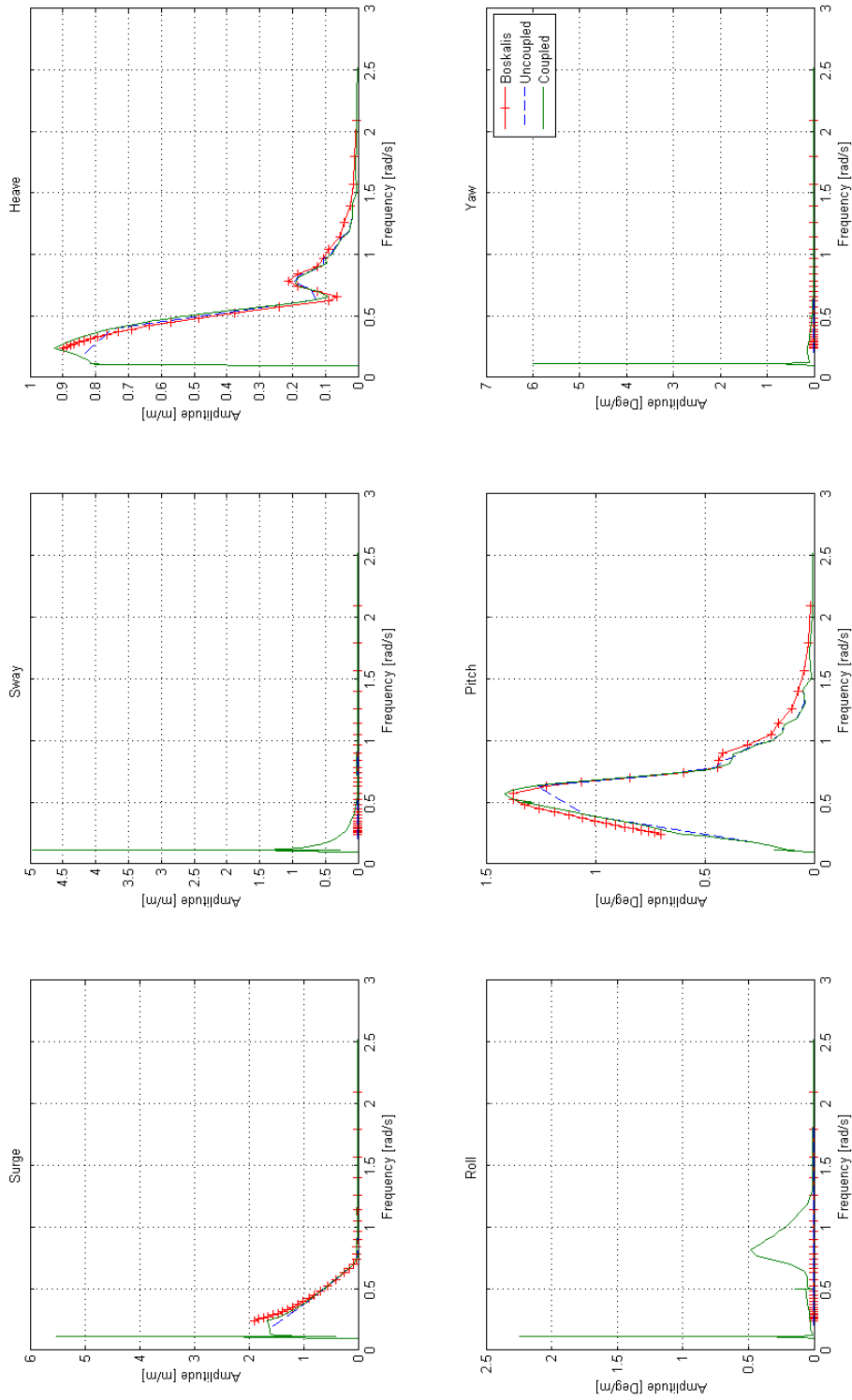


Figure B.1: Coupled/Uncoupled RAOs: 0deg

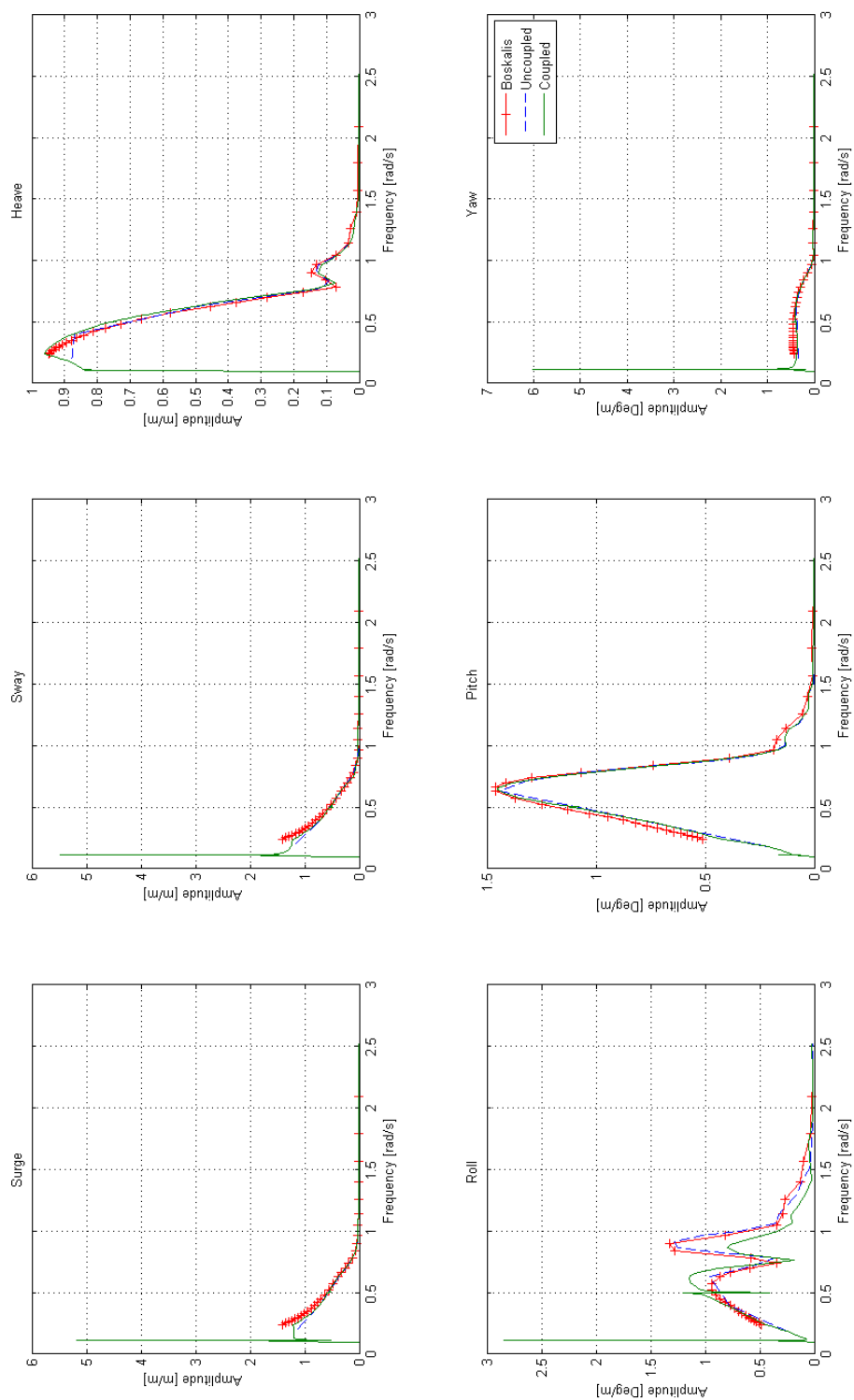


Figure B.2: Coupled/Uncoupled RAOs: 45deg

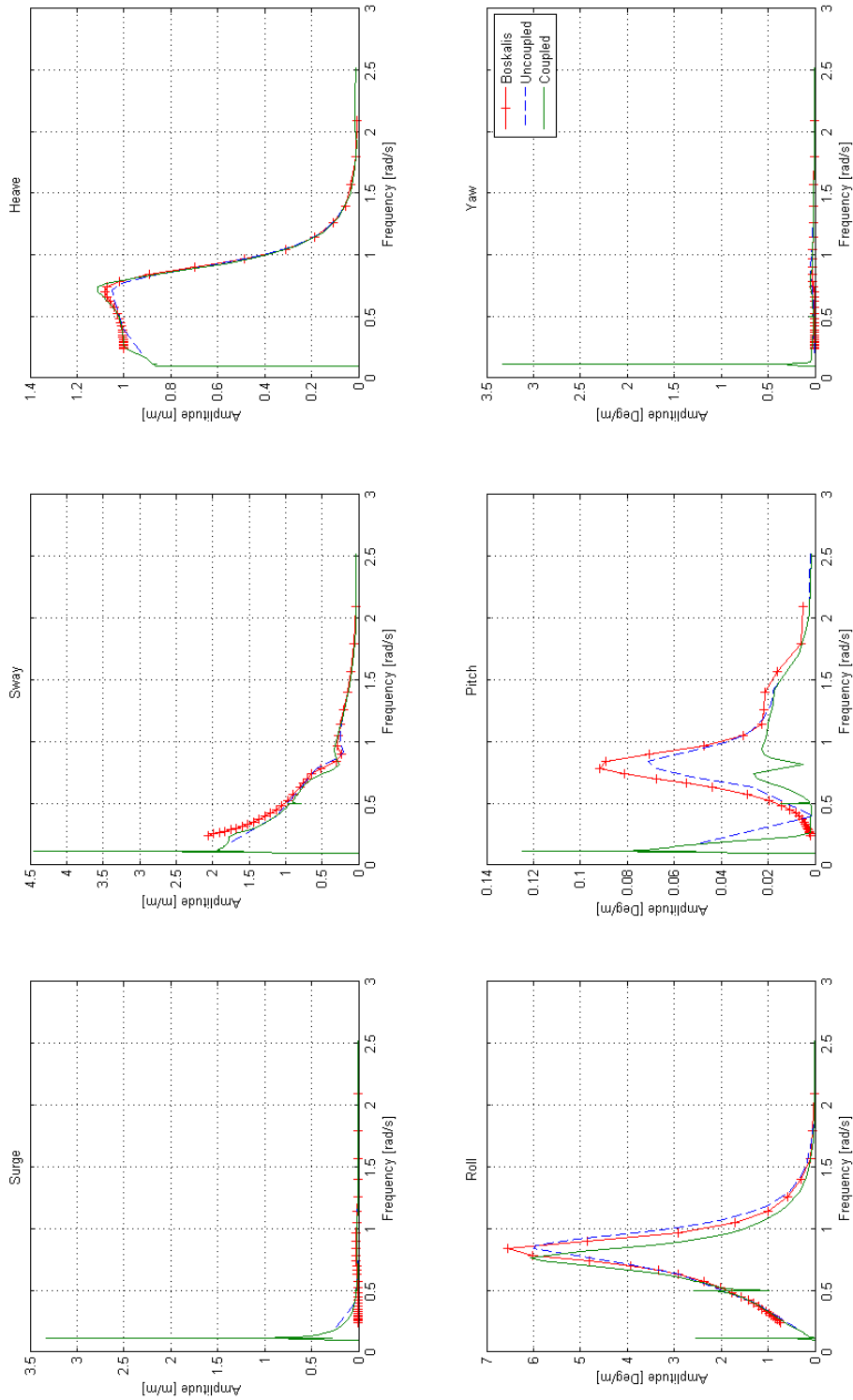


Figure B.3: Coupled/Uncoupled RAOs: 90deg

Summary Theoretical Background

This Appendix gives a summary of the literature study performed in the Pre-theis. Nous [36]

Hydrodynamic fundamentals

A short description will be given on the continuity equation, conservation of momentum, Navier Stokes and Euler equations. After this potential flow theory and airy waves will be discussed

Navier-Stokes, Euler and Bernoulli

In hydrodynamics the water is assumed continuous. This means that regardless of the volume of the considered water, the behaviour will be the same. Furthermore it is assumed that the water is homogeneous and of constant temperature so constant density. Conservation off mass is assumed which means that the net flux of the mass per unit width through the surface is zero. This can be noted as given in Equation C.1. This equation is known as the continuity equation. This relation is used extensively in wave theory.

$$\frac{\partial u}{\partial x} + \frac{\partial v}{\partial y} + \frac{\partial w}{\partial z} = 0 \quad (\text{C.1})$$

Next to continuity the fluid must satisfy conservation of momentum. This mean that Newton's second law holds for each particle in the fluid. The conservation of momentum is also referred to as the equation of motions in the fluid. This can be written as Equation C.2.

$$m \frac{d\mathbf{V}}{dt} = \sum \bar{K} \quad (\text{C.2})$$

This relation can be used to obtain relations for the accelerations for each specific particle. This is however not practical. The relations can be rewritten for the accelerations in a fixed point. Rewriting the equation gives the relations given in Equation C.3. The relations are known as the Navier Stokes equation. The Navier Stokes equation describe the complete fluid motions.

$$\frac{D\mathbf{V}}{Dt} = \mathbf{F} - \frac{\nabla p}{\rho} + \nu \nabla^2 \mathbf{V} \quad (\text{C.3})$$

In Equation C.3 \mathbf{V} is the velocity vector. \mathbf{F} is the Force vector which by default is the gravitational force. Nabla ∇ is the vector differential operator which are the partial derivatives in all degrees of freedom. The use of the Navier Stokes equation is however not practical since it takes a lot of time to find a solution. Therefore assumptions are made to simplify the problem. An assumptions often used is neglecting the viscous forces in the fluid. With this the Navier Stokes equations can be simplified in the form given in Equation C.4. These are known as the Euler equations.

$$\frac{D\mathbf{V}}{Dt} = \mathbf{F} - \frac{\nabla p}{\rho} \quad (\text{C.4})$$

Potential flow

In order to describe the wave behaviour at sea a more elegant method can be used to find the velocity field. The potential flow theory will be discussed in this section. Fredsoe [40]

Velocity potential

In order to consider the potential flow theory the assumption is made that the sea water is incompressible and inviscid. The velocity vector can be described with the use of the velocity potential. This is given in Equation C.5.

$$\mathbf{V} = \nabla \phi \equiv i \frac{\partial \phi}{\partial x} + j \frac{\partial \phi}{\partial y} + k \frac{\partial \phi}{\partial z} \quad (\text{C.5})$$

The velocity potential is used for analysing irrotational fluid motions. The fluid is irrotational when the vorticity vector is 0. The criteria for a irrotational fluid is given by Equation C.6. From this it can be found that the velocity potential needs to satisfy the Laplace equation. This is given in Equation C.7. The Laplace equation is the continuity equation expressed in terms of the velocity potential.

$$\boldsymbol{\omega} = \nabla \times \mathbf{V} \quad (\text{C.6})$$

$$i \frac{\partial^2 \phi}{\partial x^2} + j \frac{\partial^2 \phi}{\partial y^2} + k \frac{\partial^2 \phi}{\partial z^2} = 0 \quad (\text{C.7})$$

Next the equation of motions can be considered. The euler equation given in Equation C.4 can be rewritten for a inviscid and irrotational flow. This means the relation in Equation C.8 must hold. Similar relations can be written for the different 3D planes. From this the Euler equations can be rewritten in the following form given in Equation C.9. Here n is the velocity direction u, v and w .

$$\frac{\partial u}{\partial z} = \frac{\partial w}{\partial x} \quad (\text{C.8})$$

$$\left(\frac{\partial \Phi}{\partial t} + \frac{|\nabla \Phi|^2}{2} + \frac{p}{\rho} + gz \right) = C_n(n, t) \quad (\text{C.9})$$

Since the equation in the different velocity directions are identical the constant C_n can be considered equal for each velocity direction. This gives the following equation given in Equation C.10. This equation is known as the Bernoulli equation. This equation is non linear and true for unsteady irrotational and inviscid flow.

$$\left(\frac{\partial \Phi}{\partial t} + \frac{|\nabla \Phi|^2}{2} + \frac{p}{\rho} + gz \right) = C(t) \quad (\text{C.10})$$

The Bernoulli and Laplace equation are used for solving the flow problem. In order to fully define the problem boundary conditions need to be determined. This will be elaborated in the following section.

Boundary conditions

The first 2 boundary conditions are found by assuming that no fluid can go trough the body of the model. Similarly it is assumed that no flow can go through the sea bed. Since the body can have a velocity component the boundary condition can be described as Equation C.11. the parameter n describes the differentiation along the normal of the body. The boundary condition for the soil is given in Equation C.12.

$$\frac{\partial \phi}{\partial n} = \mathbf{U} \cdot \mathbf{n} \quad (\text{C.11})$$

$$\frac{\partial \phi}{\partial z} = 0; \quad z = -h \quad (\text{C.12})$$

In order to find the kinematic boundary condition at the free surface the assumptions is made that a fluid particle stays on the free surface. This follows the equation given in Equation C.13. Here F is the rate of change function in time of a fluid particle. From this the boundary condition can be obtained given in Equation C.14.

$$F(x, y, z, t) = z - \zeta(x, y, t) = 0 \quad (\text{C.13})$$

$$\frac{\partial \zeta}{\partial t} + \frac{\partial \phi}{\partial x} \frac{\partial \zeta}{\partial x} + \frac{\partial \phi}{\partial y} \frac{\partial \zeta}{\partial y} - \frac{\partial \phi}{\partial z} = 0 \quad (\text{C.14})$$

the last boundary condition considered is the dynamic free surface condition. This means that the water pressure is equal to the constant atmospheric pressure. This can be written as Equation C.15. This is performed in order to simplify the problem. Equation C.14 is a non linear boundary conditions. It is therefore not known were the free surface is before it is solved. The free surface can be linearised by assuming the velocity potential is proportional to the wave amplitude. This assumption is valid if the wave amplitude is small relative to the characteristic wavelength and body dimensions. Using Taylor expansion in Equation C.14 and Equation C.15 the boundary condition can be rewritten as given in Equation C.16. A more common form is given in Equation C.17 and Equation C.18 known as the kinematic condition and dynamic condition of the free surface respectively.

$$g\zeta + \frac{\partial\phi}{\partial t} + \frac{1}{2} \left(\left(\frac{\partial\phi}{\partial x} \right)^2 + \left(\frac{\partial\phi}{\partial y} \right)^2 + \left(\frac{\partial\phi}{\partial z} \right)^2 \right) = 0 \quad (\text{C.15})$$

$$\frac{\partial^2\phi}{\partial t^2} + g\frac{\partial\phi}{\partial z} = 0; \quad z = 0 \quad (\text{C.16})$$

$$\frac{\partial\zeta}{\partial t} = \frac{\partial\phi}{\partial z} \quad z = 0 \quad (\text{C.17})$$

$$g\zeta + \frac{\partial\phi}{\partial t} = 0 \quad z = 0 \quad (\text{C.18})$$

The boundary condition given in Equation C.16 can be rewritten assuming that the velocity potential is oscillating harmonically in time. This is given in Equation C.19.

$$-\omega^2\phi + g\frac{\partial\phi}{\partial z} = 0; \quad z = 0 \quad (\text{C.19})$$

Airy waves

From the potential flow linear wave theory or airy wave theory can be derived. Linear wave theory is based on the the Laplace and Bernoulli equations together with simplified boundary conditions as discussed in section C. An overview on the basic equation and boundary conditions for the linear wave theory is given in Figure A.1. A. Svendsen [41], Holthuijsen [42]

Reynolds and Keulegan-Carpenter

The wave forces can be characterized by there corresponding non-dimensional coefficients. extensive research has been done on the determination of the coefficients. In many cases the dependence of the coefficients may be written as a function of the Reynolds number and the Keulegan-Carpenter number. The relation for the Reynolds number is given in Equation C.20. The Reynolds number depends on the flow velocity, cylinder diameter and

the kinematic velocity. the Reynolds number describes the relation between the particle size and the object. This influences the behavior of the flow. J.M.J. Journee [13].

$$R_n = \frac{u_a \cdot D}{\nu} \quad (\text{C.20})$$

The relation for the Keulegan-Carpenter number is given by Equation C.21. The Keulegan-Carpenter number illustrates the effect of the oscillation flow period T , the diameter of the specimen and the flow velocity. With the Reynolds number and Keulegan-Carpenter number effects of the flow and body can be shown. The influence of the parameters will be elaborated further in this section.

$$KC = \frac{u_a \cdot T}{D} \quad (\text{C.21})$$

APPENDIX D : Slam Results for each Mud Mat

Cs	Tp	Mud Mat 1					Mud Mat 2					Mud Mat 3					Mud Mat 4				
		Fs,max	Fs,avg	ts,max	ts,avg	n	Fs,max	Fs,avg	ts,max	ts,avg	n	Fs,max	Fs,avg	ts,max	ts,avg	n	Fs,max	Fs,avg	ts,max	ts,avg	n
[-]	[s]	[kN]	[kN]	[s]	[s]	[-]	[kN]	[kN]	[s]	[s]	[-]	[kN]	[kN]	[s]	[s]	[-]	[kN]	[kN]	[s]	[s]	[-]
2.5	4.17	40.7	33.0	1.5	1.17	279	50.9	38.7	1.4	1.00	270	26.4	18.0	1.6	0.47	592	40.8	32.9	1.4	0.98	269
2.5	4.38	33.1	21.0	1.6	0.55	551	45.0	29.9	1.3	0.79	332	18.2	13.8	0.8	0.38	361	36.7	31.3	1.2	1.05	243
2.5	4.62	25.8	20.1	0.6	0.39	264	32.3	23.0	1.4	0.65	383	16.6	14.6	0.4	0.33	201	33.7	31.2	1.1	1.06	207
2.5	4.75	21.4	18.9	0.4	0.39	205	26.7	16.8	0.6	0.29	472	18.0	15.3	0.3	0.25	198	33.8	18.8	0.7	0.31	428
2.5	4.91	25.8	17.5	0.7	0.40	380	22.7	18.8	0.4	0.29	200	27.2	16.1	0.6	0.32	352	25.2	19.7	0.4	0.30	216
2.5	5.06	46.7	39.2	0.9	0.77	191	18.1	15.5	0.5	0.41	184	50.8	39.7	0.7	0.67	183	9.7	11.3	0.1	0.10	3
2.5	5.23	61.3	51.2	1.2	1.12	181	43.9	41.8	0.7	0.61	180	55.9	46.1	1.1	0.83	197	28.8	26.0	0.5	0.49	177
2.5	5.43	51.7	45.2	1.2	1.18	173	69.7	65.0	0.9	0.85	171	44.0	40.6	1.1	1.09	171	42.5	38.0	1.0	0.97	171
2.5	5.65	48.3	40.9	1.3	1.22	166	66.6	61.0	0.8	0.80	166	39.3	35.0	1.3	1.16	179	53.2	49.3	0.9	0.84	165
2.5	5.90	38.6	37.9	1.2	1.20	159	52.7	51.7	0.8	0.80	158	34.5	31.7	1.3	1.21	160	47.3	45.1	0.8	0.80	157
2.5	6.30	29.7	28.9	1.2	1.20	148	51.9	49.7	0.8	0.80	148	25.3	23.3	1.2	1.13	146	43.7	42.7	0.8	0.80	148
2.5	6.70	29.5	29.2	1.0	1.00	139	48.0	46.2	0.9	0.86	139	24.3	23.5	1.0	0.95	140	41.4	40.2	0.8	0.80	138
2.5	7.00	30.3	28.8	0.9	0.90	133	44.4	43.5	0.8	0.79	134	26.1	24.9	0.9	0.90	132	41.6	40.8	0.8	0.70	133
2.5	7.10	31.5	31.0	1.0	0.96	132	42.9	42.0	0.8	0.80	131	28.4	27.4	0.9	0.84	131	41.8	41.2	0.8	0.72	131
2.5	7.50	31.8	30.8	0.9	0.90	124	34.9	33.5	0.8	0.80	124	33.1	32.3	0.8	0.75	124	41.3	38.9	0.8	0.80	124
2.5	7.90	34.7	33.4	0.8	0.80	118	34.9	34.1	0.8	0.80	118	32.7	31.2	0.7	0.69	118	36.0	34.6	0.8	0.77	118
2.5	8.00	35.3	34.3	0.8	0.80	117	31.8	30.7	0.8	0.80	117	33.7	32.1	0.7	0.65	117	36.8	35.7	0.8	0.80	116
2.5	9.20	49.8	48.9	0.5	0.48	101	14.0	13.0	0.9	0.42	175	60.2	58.8	0.5	0.50	101	21.1	20.1	0.4	0.40	98
2.5	9.60	61.7	50.3	0.4	0.40	97	19.2	17.0	0.5	0.40	97	68.2	66.1	0.4	0.31	97	14.4	12.8	0.3	0.22	183
2.5	9.70	34.1	28.2	0.5	0.39	122	31.9	31.1	0.5	0.46	96	46.2	37.7	0.4	0.40	95	25.6	20.3	0.5	0.30	182
2.5	9.80	25.0	19.3	0.5	0.30	182	56.1	55.0	0.4	0.34	94	29.4	28.3	0.4	0.40	95	57.0	54.3	0.4	0.39	103
2.5	10.00	12.0	11.3	0.1	0.10	59	73.2	69.9	0.4	0.40	92	21.9	20.7	0.4	0.37	93	74.1	72.2	0.4	0.39	93
2.5	10.80	23.9	23.3	0.7	0.60	86	33.9	32.8	0.7	0.64	87	17.8	17.0	0.7	0.70	86	37.9	36.4	0.6	0.60	86
2.5	11.20	22.8	22.6	0.7	0.67	83	32.3	31.1	0.7	0.63	83	21.6	21.2	0.6	0.60	83	33.9	33.2	0.7	0.63	83
2.5	11.80	25.5	25.0	0.6	0.60	79	25.2	24.2	0.7	0.67	79	23.4	22.7	0.6	0.60	79	30.3	29.4	0.6	0.60	79
2.5	12.20	27.0	26.2	0.6	0.60	76	24.4	23.2	0.7	0.62	76	26.1	25.8	0.6	0.60	76	25.1	24.1	0.7	0.63	76
2.5	13.86	32.7	30.4	0.5	0.48	66	11.0	10.6	0.4	0.29	39	39.3	36.7	0.5	0.48	66	12.0	11.6	0.5	0.45	65
5.5	4.17	111.5	73.5	1.9	1.38	242	115.2	91.9	1.7	1.29	231	82.5	44.7	2.1	1.23	265	109.0	81.1	1.5	1.19	237
5.5	4.38	66.3	47.5	2.0	1.23	298	97.9	70.8	1.5	1.30	225	40.6	24.9	1.9	0.68	465	85.4	70.9	1.3	1.21	216
5.5	4.62	48.8	33.2	0.9	0.67	448	64.4	61.0	1.5	1.47	206	33.2	23.3	0.5	0.35	441	71.0	65.7	1.3	1.29	203
5.5	4.75	45.3	33.6	0.8	0.64	398	60.6	52.7	1.6	1.56	201	38.7	28.2	0.5	0.42	389	70.3	58.8	1.4	1.35	197
5.5	4.91	44.8	38.0	0.8	0.60	384	50.3	20.2	0.7	0.31	695	43.6	32.6	0.8	0.51	376	59.5	22.8	0.8	0.35	657
5.5	5.06	62.1	39.9	0.9	0.60	375	27.0	19.5	0.6	0.46	372	71.1	36.0	0.9	0.49	364	33.7	18.6	0.5	0.25	506
5.5	5.23	71.2	64.7	1.2	1.13	185	42.0	22.1	0.8	0.41	438	76.5	68.2	1.0	0.96	178	19.6	15.6	0.4	0.34	350
5.5	5.43	99.4	81.4	1.3	1.26	173	86.8	77.1	0.9	0.87	176	82.6	74.8	1.1	1.05	171	47.4	44.4	0.8	0.75	171
5.5	5.65	100.1	89.0	1.4	1.35	165	184.0	182.3	0.6	0.58	166	71.3	70.2	1.2	1.12	164	114.1	102.9	0.9	0.85	165
5.5	5.90	69.9	69.6	1.6	1.60	159	171.2	168.7	0.6	0.60	159	60.5	58.3	1.2	1.20	180	125.2	123.3	0.7	0.70	158

Cs	Tp	Mud Mat 1					Mud Mat 2					Mud Mat 3					Mud Mat 4				
		Fs,max	Fs,avg	ts,max	ts,avg	n	Fs,max	Fs,avg	ts,max	ts,avg	n	Fs,max	Fs,avg	ts,max	ts,avg	n	Fs,max	Fs,avg	ts,max	ts,avg	n
[-]	[s]	[kN]	[kN]	[s]	[s]	[-]	[kN]	[kN]	[s]	[s]	[-]	[kN]	[kN]	[s]	[s]	[-]	[kN]	[kN]	[s]	[s]	[-]
5.5	6.30	53.0	52.9	1.6	1.60	148	151.5	147.8	0.7	0.70	150	53.8	52.3	1.6	1.60	151	179.9	179.2	0.7	0.70	149
5.5	6.70	40.7	40.0	1.5	1.42	140	124.0	122.4	0.7	0.70	140	47.8	45.6	1.5	1.41	139	121.3	117.0	0.8	0.80	139
5.5	7.00	47.9	46.6	1.3	1.30	134	121.2	119.0	0.8	0.80	134	55.4	54.5	1.2	1.19	132	121.0	119.9	0.8	0.80	134
5.5	7.10	55.0	54.5	1.2	1.20	132	111.1	108.8	0.8	0.80	132	57.0	55.7	1.1	1.10	131	115.6	110.3	0.9	0.89	132
5.5	7.50	62.0	61.0	1.1	1.10	125	77.7	76.3	0.9	0.90	125	82.5	79.3	0.9	0.88	124	106.7	104.5	0.9	0.90	124
5.5	7.90	72.0	68.2	0.9	0.90	119	77.0	75.8	1.0	0.97	118	77.2	76.0	0.8	0.79	118	88.8	87.3	0.9	0.90	118
5.5	8.00	74.5	72.0	0.9	0.87	118	71.0	69.3	1.0	1.00	117	81.8	80.1	0.8	0.77	117	85.8	84.8	0.9	0.90	117
5.5	9.20	124.5	113.8	0.5	0.45	101	13.7	12.3	0.7	0.43	213	145.0	141.5	0.4	0.40	101	41.1	38.8	0.6	0.58	102
5.5	9.60	93.6	53.7	0.5	0.40	190	46.8	46.0	0.6	0.51	97	136.4	128.6	0.4	0.40	97	40.4	35.4	0.6	0.43	190
5.5	9.70	57.0	39.4	0.5	0.44	190	56.2	54.6	0.7	0.65	96	90.0	77.6	0.5	0.43	96	45.0	41.3	0.6	0.45	188
5.5	9.80	55.0	42.0	0.6	0.46	188	104.5	104.1	0.5	0.50	95	78.0	70.6	0.5	0.50	95	83.2	57.3	0.5	0.39	185
5.5	10.00	60.5	41.8	0.5	0.45	182	131.6	120.5	0.4	0.40	93	60.4	59.2	0.5	0.41	93	136.0	88.9	0.4	0.29	136
5.5	10.80	41.7	26.1	0.6	0.40	169	74.6	71.3	0.7	0.70	87	45.9	45.0	1.0	1.00	87	97.7	96.3	0.7	0.63	86
5.5	11.20	41.2	40.8	0.9	0.80	84	77.2	75.2	0.7	0.67	84	40.2	40.0	0.9	0.81	83	91.9	91.0	0.7	0.70	83
5.5	11.80	54.3	53.2	0.8	0.74	79	49.0	47.3	0.9	0.81	79	47.3	45.9	0.8	0.75	79	78.6	75.9	0.7	0.70	79
5.5	12.20	58.6	56.7	0.7	0.70	76	49.5	46.7	0.9	0.83	76	61.8	60.9	0.7	0.70	76	57.0	55.5	0.8	0.80	76
5.5	13.86	80.1	68.2	0.6	0.56	66	22.6	21.0	0.6	0.58	67	102.0	93.1	0.6	0.50	67	21.3	18.9	1.0	0.90	68
8.5	4.17	161.6	118.2	1.9	1.65	229	162.6	144.2	1.6	1.38	226	105.8	71.4	2.1	1.80	227	152.7	124.5	1.5	1.32	226
8.5	4.38	140.9	79.3	2.2	1.50	249	160.3	109.1	1.7	1.42	215	104.0	42.7	2.2	0.80	415	147.3	113.2	1.5	1.18	222
8.5	4.62	79.2	55.9	1.0	0.82	410	96.6	86.6	1.6	1.52	206	56.6	40.5	0.7	0.50	402	112.8	95.8	1.4	1.29	202
8.5	4.75	68.3	53.4	0.9	0.77	397	89.3	78.4	1.6	1.60	201	59.3	43.9	0.7	0.53	390	109.2	92.6	1.4	1.40	197
8.5	4.91	73.3	56.8	1.0	0.69	384	76.3	62.4	1.9	1.81	196	63.4	49.6	0.8	0.56	377	91.3	75.0	1.6	1.58	190
8.5	5.06	70.9	54.9	1.1	0.74	374	44.2	26.2	0.8	0.55	464	78.0	50.2	0.9	0.60	367	56.4	26.0	0.8	0.43	614
8.5	5.23	77.9	44.6	1.4	0.82	356	42.5	30.1	0.8	0.76	359	91.8	48.6	1.1	0.65	353	27.4	20.6	0.8	0.67	371
8.5	5.43	102.1	96.1	1.4	1.38	176	62.1	40.0	0.9	0.68	339	91.4	53.0	1.2	0.69	340	44.2	40.9	0.7	0.66	171
8.5	5.65	112.7	106.7	1.5	1.45	165	196.7	190.3	0.6	0.55	167	96.2	56.5	1.2	0.70	326	97.4	91.9	0.9	0.90	165
8.5	5.90	89.0	88.0	1.3	1.30	160	277.6	275.4	0.4	0.40	159	86.1	51.9	1.1	0.65	314	195.6	194.8	0.7	0.60	158
8.5	6.30	59.6	44.1	1.3	0.90	294	268.9	258.6	0.6	0.60	150	73.1	48.0	0.9	0.64	295	309.9	305.0	0.7	0.63	149
8.5	6.70	44.4	43.9	1.9	1.90	141	233.3	215.0	0.7	0.70	140	77.9	56.7	0.9	0.71	277	214.0	208.8	0.7	0.70	139
8.5	7.00	66.4	62.7	1.7	1.70	134	185.3	182.1	0.8	0.80	134	85.0	72.8	1.5	1.26	143	212.4	207.0	0.7	0.70	134
8.5	7.10	73.1	72.4	1.7	1.63	132	172.8	169.5	0.9	0.90	132	81.2	80.3	1.4	1.35	132	231.0	225.8	0.8	0.80	132
8.5	7.50	89.4	85.8	1.3	1.24	126	124.0	114.8	1.0	0.91	125	132.4	126.1	0.8	0.74	125	177.0	172.3	0.9	0.90	124
8.5	7.90	107.7	105.7	0.9	0.80	119	111.0	106.4	1.1	1.10	119	129.1	125.1	0.7	0.70	118	148.9	145.5	1.0	0.92	118
8.5	8.00	113.0	111.9	0.8	0.80	118	99.7	95.1	1.1	1.10	117	134.2	130.5	0.7	0.70	117	138.7	133.5	1.0	1.00	117
8.5	9.20	184.5	94.5	0.4	0.30	185	33.0	20.3	0.6	0.43	204	262.6	250.1	0.4	0.35	102	69.6	66.9	0.6	0.50	105
8.5	9.60	105.0	68.7	0.5	0.40	194	58.3	57.7	0.7	0.70	99	200.3	196.0	0.4	0.40	97	71.0	58.3	0.6	0.45	191
8.5	9.70	70.6	53.9	0.6	0.49	192	76.8	71.7	0.8	0.77	108	135.6	131.6	0.5	0.50	96	80.1	75.4	0.7	0.55	189
8.5	9.80	104.8	76.0	0.6	0.50	190	130.5	129.9	0.6	0.51	95	104.3	103.4	0.5	0.50	95	94.7	76.9	0.7	0.50	187

Cs	Tp	Mud Mat 1					Mud Mat 2					Mud Mat 3					Mud Mat 4				
		Fs,max	Fs,avg	ts,max	ts,avg	n	Fs,max	Fs,avg	ts,max	ts,avg	n	Fs,max	Fs,avg	ts,max	ts,avg	n	Fs,max	Fs,avg	ts,max	ts,avg	n
[-]	[s]	[kN]	[kN]	[s]	[s]	[-]	[kN]	[kN]	[s]	[s]	[-]	[kN]	[kN]	[s]	[s]	[-]	[kN]	[kN]	[s]	[s]	[-]
8.5	10.00	124.0	66.8	0.6	0.45	185	191.6	168.1	1.0	0.41	93	145.0	114.3	0.7	0.49	93	177.6	92.1	0.9	0.28	183
8.5	10.80	37.4	27.4	0.9	0.40	256	121.1	100.8	1.0	0.65	87	123.2	72.5	0.7	0.40	172	136.6	130.1	0.8	0.60	87
8.5	11.20	51.9	31.1	0.8	0.48	158	124.4	110.9	0.9	0.71	84	77.4	73.0	0.9	0.81	84	159.5	145.8	0.8	0.70	84
8.5	11.80	80.9	75.5	0.8	0.72	79	75.1	65.8	1.0	0.89	80	76.4	70.2	0.9	0.83	79	138.1	130.8	0.9	0.80	79
8.5	12.20	92.2	88.7	0.7	0.64	76	74.3	66.0	1.0	0.90	77	98.7	97.0	0.8	0.71	76	90.6	86.4	1.0	0.87	76
8.5	13.86	136.7	105.4	0.6	0.59	67	49.5	35.2	0.9	0.66	68	170.9	143.1	0.9	0.53	67	36.8	21.0	1.0	0.55	141
11.5	4.17	239.8	177.7	2.3	1.79	231	245.0	177.3	1.8	1.36	230	148.9	103.1	2.3	1.80	235	256.1	158.7	1.5	1.34	227
11.5	4.38	182.2	111.2	2.2	1.86	228	178.1	130.7	1.9	1.44	217	153.9	62.5	2.4	1.19	347	211.2	159.0	1.5	1.24	217
11.5	4.62	110.9	78.0	2.1	0.88	407	118.1	105.6	1.8	1.53	206	73.9	56.4	0.9	0.57	403	147.0	121.4	1.4	1.29	203
11.5	4.75	105.1	71.8	2.1	0.81	394	116.7	93.3	1.9	1.62	201	77.3	58.1	0.9	0.56	391	145.1	121.2	1.6	1.36	197
11.5	4.91	102.2	74.4	1.3	0.78	383	102.2	78.0	2.0	1.75	196	83.5	65.4	0.9	0.63	378	126.4	102.7	1.7	1.58	190
11.5	5.06	81.6	70.6	2.2	0.81	370	63.5	33.3	1.1	0.69	486	90.4	64.1	1.0	0.65	367	85.8	47.3	2.0	0.84	387
11.5	5.23	85.3	59.2	2.3	0.89	358	48.6	32.8	1.2	0.78	382	106.4	55.8	1.1	0.71	354	41.6	22.1	1.2	0.65	535
11.5	5.43	96.3	52.0	2.4	0.89	341	78.1	42.9	1.3	0.89	344	91.8	58.4	1.2	0.76	342	43.4	25.0	0.7	0.43	337
11.5	5.65	123.1	109.5	2.0	1.43	170	172.7	89.2	1.2	0.53	328	111.5	73.2	1.2	0.77	328	91.1	75.6	1.0	0.86	165
11.5	5.90	122.4	67.8	1.8	0.68	314	321.8	171.2	1.1	0.28	282	98.0	74.7	1.2	0.70	315	217.3	198.8	1.0	0.71	158
11.5	6.30	108.9	45.1	1.6	0.54	442	339.1	296.9	1.2	0.61	151	104.9	82.8	1.1	0.63	300	379.7	328.5	1.0	0.61	149
11.5	6.70	86.6	71.4	1.9	0.88	280	296.9	279.9	1.3	0.70	141	85.7	57.4	1.0	0.80	277	323.7	300.5	1.1	0.70	140
11.5	7.00	89.0	69.4	2.1	1.84	151	305.2	278.6	1.1	0.80	136	99.5	56.2	0.8	0.66	264	360.6	318.5	1.1	0.71	134
11.5	7.10	92.3	80.4	2.1	1.98	133	231.7	216.6	1.2	0.80	134	103.7	56.1	0.8	0.60	261	330.7	284.1	1.2	0.80	132
11.5	7.50	132.3	118.2	2.0	1.86	127	167.6	156.3	1.3	0.94	126	156.6	148.5	0.8	0.70	125	254.9	243.6	1.1	0.88	125
11.5	7.90	136.1	88.5	1.0	0.57	177	152.9	141.2	1.3	1.09	120	174.6	164.6	0.9	0.70	118	209.8	190.8	1.2	1.00	118
11.5	8.00	140.9	94.3	0.9	0.53	171	141.3	132.6	1.4	1.10	118	179.4	171.9	0.9	0.70	117	207.4	195.0	1.3	1.10	117
11.5	9.20	221.5	113.5	0.7	0.45	204	93.1	41.4	1.3	0.42	212	336.0	254.3	0.7	0.41	102	112.7	56.0	0.7	0.40	199
11.5	9.60	184.0	86.3	0.7	0.45	196	145.6	54.7	1.2	0.46	188	259.4	247.7	0.7	0.41	97	107.9	81.2	0.8	0.48	192
11.5	9.70	114.2	69.8	0.7	0.50	194	145.4	77.7	1.1	0.54	188	194.8	182.0	0.8	0.51	96	114.3	102.6	0.9	0.55	190
11.5	9.80	142.2	97.8	0.6	0.50	191	179.6	83.0	1.2	0.43	184	140.1	119.4	0.8	0.51	95	163.5	122.9	0.9	0.55	187
11.5	10.00	154.5	94.7	0.6	0.42	187	249.2	192.4	1.1	0.48	94	174.2	156.0	0.8	0.50	93	218.2	128.4	1.0	0.33	184
11.5	10.80	119.8	50.0	0.7	0.37	258	172.3	143.8	1.1	0.61	88	218.8	116.3	0.9	0.35	171	179.2	161.2	1.0	0.61	87
11.5	11.20	50.3	29.4	0.9	0.58	168	147.1	136.2	1.1	0.70	85	137.0	130.1	0.9	0.80	84	221.2	205.0	0.9	0.70	84
11.5	11.80	101.6	55.0	0.7	0.45	158	92.2	78.7	1.1	0.89	81	120.0	109.9	0.9	0.80	80	205.4	194.8	1.0	0.88	79
11.5	12.20	128.5	120.4	0.7	0.59	78	96.1	81.6	1.0	0.97	78	130.9	124.2	0.8	0.71	76	127.4	118.5	1.1	0.91	76
11.5	13.86	191.4	143.4	0.7	0.62	69	60.6	36.9	1.1	0.61	89	225.4	178.3	1.0	0.59	67	56.4	29.3	1.1	0.48	193
13.04	4.17	312.3	190.2	2.3	1.76	238	332.8	202.4	1.9	1.39	229	169.9	102.5	2.4	1.23	333	279.2	177.7	1.5	1.35	230
13.04	4.38	189.8	127.8	2.2	1.93	222	206.8	142.8	1.9	1.44	217	145.2	77.0	2.4	1.54	284	228.3	181.1	1.4	1.25	216
13.04	4.62	134.0	91.4	2.2	0.91	406	142.3	115.7	2.1	1.55	206	86.1	63.3	0.8	0.58	411	168.6	136.9	1.5	1.30	202
13.04	4.75	124.8	84.9	2.2	0.82	395	123.8	105.0	1.9	1.63	201	94.0	64.6	0.9	0.60	391	162.4	135.2	1.6	1.37	197
13.04	4.91	117.0	83.4	1.4	0.82	383	108.8	86.2	2.1	1.77	195	92.6	73.0	1.0	0.66	378	141.3	115.8	1.8	1.57	191

Cs	Tp	Mud Mat 1					Mud Mat 2					Mud Mat 3					Mud Mat 4				
		F _{s,max} [kN]	F _{s,avg} [kN]	t _{s,max} [s]	t _{s,avg} [s]	n [-]	F _{s,max} [kN]	F _{s,avg} [kN]	t _{s,max} [s]	t _{s,avg} [s]	n [-]	F _{s,max} [kN]	F _{s,avg} [kN]	t _{s,max} [s]	t _{s,avg} [s]	n [-]	F _{s,max} [kN]	F _{s,avg} [kN]	t _{s,max} [s]	t _{s,avg} [s]	n [-]
13.04	5.06	94.2	79.9	1.2	0.84	372	64.8	44.0	2.1	1.00	348	91.1	72.5	1.0	0.67	367	96.4	71.9	1.9	1.31	258
13.04	5.23	87.6	69.6	1.5	0.93	359	41.2	28.7	1.1	0.63	557	105.9	62.3	1.1	0.75	354	45.6	25.0	1.3	0.72	552
13.04	5.43	90.2	54.3	1.5	0.88	343	63.7	45.4	1.1	1.00	343	92.4	62.3	1.2	0.80	342	38.5	26.0	0.7	0.54	339
13.04	5.65	119.9	110.0	1.5	1.45	170	148.6	83.9	0.7	0.65	329	104.6	79.4	1.2	0.80	328	72.6	69.3	0.9	0.90	165
13.04	5.90	108.3	67.6	1.3	0.80	315	278.4	143.6	1.1	0.60	345	99.0	83.4	1.1	0.75	315	197.3	196.7	0.8	0.80	158
13.04	6.30	108.7	78.7	1.3	0.80	300	420.8	396.9	0.6	0.59	151	148.2	112.6	1.1	0.72	299	444.3	421.0	0.7	0.70	149
13.04	6.70	114.0	102.0	1.3	0.90	280	315.7	306.0	0.6	0.60	141	85.2	70.5	1.0	0.85	284	315.8	314.0	0.7	0.70	140
13.04	7.00	100.1	70.6	1.3	0.91	267	339.7	292.6	0.8	0.72	136	106.0	58.3	0.8	0.66	264	399.9	372.7	0.8	0.77	134
13.04	7.10	102.5	70.7	1.2	0.90	264	316.5	310.8	0.8	0.80	134	94.0	54.0	0.8	0.56	261	411.0	406.3	0.8	0.73	132
13.04	7.50	144.8	80.7	0.9	0.75	249	203.9	197.7	1.0	0.90	126	162.7	158.3	0.7	0.70	125	277.9	267.5	0.9	0.90	125
13.04	7.90	152.8	82.6	0.7	0.55	238	170.5	163.6	1.1	1.10	120	202.7	198.1	0.7	0.65	118	238.5	230.8	1.0	1.00	118
13.04	8.00	157.3	85.0	0.7	0.55	235	148.3	141.0	1.1	1.10	119	213.0	208.2	0.7	0.64	117	238.6	233.7	1.1	1.10	117
13.04	9.20	230.2	125.3	0.6	0.47	204	112.3	55.9	0.6	0.42	217	369.9	282.1	0.5	0.41	102	130.9	65.9	0.6	0.41	212
13.04	9.60	124.1	96.2	0.6	0.50	196	115.2	65.8	0.7	0.50	190	280.2	277.7	0.4	0.40	97	116.1	93.9	0.7	0.50	192
13.04	9.70	91.3	83.4	0.6	0.55	194	162.9	91.8	0.8	0.55	190	216.3	215.5	0.5	0.50	96	130.7	117.9	0.7	0.50	190
13.04	9.80	147.5	108.2	0.6	0.50	192	182.4	104.9	0.6	0.45	185	131.6	125.1	0.5	0.50	95	169.1	139.5	0.8	0.55	189
13.04	10.00	172.5	109.7	0.5	0.48	187	231.3	129.5	0.5	0.44	175	142.8	138.3	0.6	0.60	93	197.7	128.6	0.5	0.40	187
13.04	10.80	164.7	97.6	0.6	0.43	175	191.3	185.9	0.7	0.70	88	264.5	135.9	0.4	0.30	170	215.2	207.5	0.6	0.55	87
13.04	11.20	49.1	34.6	0.9	0.60	168	156.2	155.2	0.7	0.70	85	164.1	160.2	0.8	0.80	84	245.7	243.8	0.7	0.65	84
13.04	11.80	97.7	59.3	0.8	0.52	160	91.4	88.3	0.9	0.90	81	131.5	129.8	0.8	0.80	80	240.2	234.0	0.9	0.81	79
13.04	12.20	136.9	74.4	0.6	0.44	153	95.4	92.0	1.0	1.00	78	139.4	138.8	0.7	0.70	76	137.6	136.2	0.9	0.90	76
13.04	13.86	208.7	108.2	0.7	0.46	113	58.8	36.3	0.9	0.55	106	250.7	201.1	0.6	0.59	67	67.0	36.0	0.6	0.47	198

APPENDIX E : Template motion maxima

Cs	Tp	Surge _{max}	Sway _{max}	Heave _{max}	Roll _{max}	Pitch _{max}	Yaw _{max}	Cs	Tp	Surge _{max}	Sway _{max}	Heave _{max}	Roll _{max}	Pitch _{max}	Yaw _{max}
[-]	[s]		[cm]			[deg/m]		[-]	[s]		[cm]			[deg/m]	
2.5	4.17	13.6	57.7	0.8	1.02	0.92	0.50	5.5	4.17	34.7	292.4	2.4	4.57	1.78	2.04
2.5	4.38	12.0	13.5	2.8	0.51	1.54	0.19	5.5	4.38	23.8	108.5	5.2	1.81	2.36	0.83
2.5	4.62	18.7	13.5	2.0	0.47	2.86	0.41	5.5	4.62	29.6	12.5	3.9	0.65	3.70	0.53
2.5	4.75	22.4	12.3	3.0	0.43	3.96	0.17	5.5	4.75	24.7	6.5	4.3	0.53	4.45	0.11
2.5	4.91	29.0	12.2	4.7	0.55	5.49	0.17	5.5	4.91	28.3	7.7	5.2	0.63	5.50	0.27
2.5	5.06	33.9	11.1	4.5	0.66	5.58	0.16	5.5	5.06	38.7	17.5	5.2	0.80	6.00	0.26
2.5	5.23	38.6	6.5	5.2	0.40	5.38	0.12	5.5	5.23	30.5	6.4	5.1	0.57	5.90	0.11
2.5	5.43	28.4	6.8	6.8	0.26	4.37	0.19	5.5	5.43	39.1	9.2	9.2	0.37	6.33	0.21
2.5	5.65	21.1	14.2	2.4	0.25	3.13	0.43	5.5	5.65	25.5	4.2	6.6	0.36	5.61	0.10
2.5	5.90	15.2	7.2	1.4	0.21	2.19	0.04	5.5	5.90	20.8	3.8	5.0	0.32	4.87	0.08
2.5	6.30	10.8	8.3	1.6	0.19	1.50	0.04	5.5	6.30	16.7	3.8	5.4	0.38	3.46	0.06
2.5	6.70	10.1	11.7	1.2	0.24	1.18	0.05	5.5	6.70	14.6	6.6	3.5	0.33	2.54	0.17
2.5	7.00	5.4	11.9	0.8	0.24	1.00	0.06	5.5	7.00	13.0	9.9	2.3	0.35	2.16	0.07
2.5	7.10	9.3	10.1	0.8	0.20	1.02	0.04	5.5	7.10	12.9	8.1	2.2	0.31	2.08	0.08
2.5	7.50	7.7	15.3	2.1	0.27	0.91	0.12	5.5	7.50	12.1	10.3	3.3	0.31	1.81	0.05
2.5	7.90	5.8	11.0	0.7	0.20	0.89	0.03	5.5	7.90	13.1	11.9	1.5	0.26	1.81	0.05
2.5	8.00	8.2	10.4	0.7	0.17	0.91	0.03	5.5	8.00	12.2	12.7	1.5	0.27	1.79	0.05
2.5	9.20	14.5	12.8	1.3	0.29	1.82	0.02	5.5	9.20	22.3	11.7	3.0	0.48	2.88	0.04
2.5	9.60	28.3	12.4	3.5	0.67	3.41	0.06	5.5	9.60	23.8	10.8	5.9	0.72	3.58	0.14
2.5	9.70	24.7	14.5	5.2	0.75	3.64	0.12	5.5	9.70	21.7	8.1	7.2	0.71	3.63	0.11
2.5	9.80	23.7	13.2	4.8	0.80	3.55	0.07	5.5	9.80	23.5	9.0	7.3	0.81	3.65	0.09
2.5	10.00	15.9	13.9	1.9	0.69	2.57	0.06	5.5	10.00	19.9	9.3	4.7	0.97	3.35	0.06
2.5	10.80	7.1	11.6	1.9	0.26	0.89	0.06	5.5	10.80	11.9	8.1	4.5	0.46	1.72	0.12
2.5	11.20	5.4	11.6	0.7	0.19	0.68	0.05	5.5	11.20	9.7	7.6	1.6	0.33	1.38	0.10
2.5	11.80	5.2	13.2	0.8	0.23	0.54	0.04	5.5	11.80	9.2	10.2	1.8	0.34	1.11	0.14
2.5	12.20	5.3	14.1	0.6	0.23	0.50	0.04	5.5	12.20	11.5	12.3	1.2	0.32	1.04	0.09
2.5	13.86	9.9	19.4	1.0	0.43	0.90	0.02	5.5	13.86	19.9	21.9	2.5	0.68	1.53	0.03

Cs	Tp	Surge _{max}	Sway _{max}	Heave _{max}	Roll _{max}	Pitch _{max}	Yaw _{max}	Cs	Tp	Surge _{max}	Sway _{max}	Heave _{max}	Roll _{max}	Pitch _{max}	Yaw _{max}
[-]	[s]		[cm]			[deg/m]		[-]	[s]		[cm]			[deg/m]	
8.5	4.17	32.3	186.5	2.6	3.50	2.46	1.88	11.5	4.17	42.1	111.5	4.0	2.85	3.49	1.27
8.5	4.38	54.5	282.0	6.0	4.34	3.40	2.84	11.5	4.38	45.0	253.8	6.3	4.44	3.53	2.93
8.5	4.62	36.5	17.5	5.0	0.90	3.98	0.49	11.5	4.62	26.1	32.8	5.7	1.27	4.04	0.78
8.5	4.75	26.4	5.4	5.1	0.68	4.64	0.22	11.5	4.75	22.7	6.7	5.6	0.80	4.71	0.13
8.5	4.91	29.3	5.7	5.7	0.66	5.55	0.45	11.5	4.91	31.7	9.6	6.2	0.80	5.59	0.70
8.5	5.06	30.6	7.6	5.7	0.75	6.01	0.60	11.5	5.06	31.6	7.9	6.1	0.77	6.05	0.34
8.5	5.23	35.0	5.7	5.2	0.76	6.15	0.38	11.5	5.23	35.5	7.8	5.2	0.84	6.32	0.22
8.5	5.43	33.4	4.5	6.9	0.32	6.57	0.13	11.5	5.43	31.3	4.0	6.2	0.33	6.63	0.10
8.5	5.65	28.1	3.3	7.9	0.43	6.39	0.15	11.5	5.65	29.4	2.7	8.1	0.39	6.76	0.16
8.5	5.90	26.0	4.7	7.0	0.50	6.05	0.11	11.5	5.90	28.2	3.8	8.1	0.52	6.45	0.17
8.5	6.30	22.2	4.6	7.4	0.55	4.93	0.13	11.5	6.30	23.4	4.2	9.3	0.65	5.84	0.12
8.5	6.70	20.1	5.0	6.5	0.49	3.78	0.15	11.5	6.70	28.0	8.4	9.5	0.66	4.79	0.21
8.5	7.00	19.8	7.8	4.0	0.42	3.12	0.25	11.5	7.00	22.6	9.6	5.3	0.55	4.02	0.79
8.5	7.10	14.6	9.0	3.6	0.38	3.04	0.13	11.5	7.10	19.6	8.1	4.8	0.51	3.76	0.30
8.5	7.50	18.0	12.4	4.0	0.39	2.61	0.15	11.5	7.50	19.2	11.8	4.6	0.44	3.22	0.22
8.5	7.90	18.9	7.2	2.2	0.32	2.47	0.17	11.5	7.90	21.9	7.6	2.9	0.35	3.04	0.21
8.5	8.00	18.9	10.0	2.3	0.29	2.48	0.14	11.5	8.00	20.5	10.7	3.3	0.40	3.01	0.14
8.5	9.20	31.8	7.3	4.2	0.57	3.41	0.06	11.5	9.20	36.4	10.3	5.8	0.73	3.70	0.09
8.5	9.60	23.0	5.5	7.4	0.70	3.63	0.15	11.5	9.60	23.4	8.1	8.6	0.78	3.67	0.14
8.5	9.70	21.6	5.3	8.6	0.73	3.66	0.30	11.5	9.70	22.8	6.4	9.5	0.83	3.73	0.21
8.5	9.80	22.3	6.1	8.6	0.78	3.68	0.11	11.5	9.80	23.2	7.4	10.0	0.95	3.80	0.22
8.5	10.00	20.8	5.3	6.9	0.83	3.57	0.13	11.5	10.00	25.2	7.8	9.0	0.79	3.75	0.29
8.5	10.80	15.7	7.6	6.2	0.66	2.27	0.18	11.5	10.80	18.4	9.2	4.6	0.84	2.61	0.15
8.5	11.20	12.7	6.9	2.8	0.46	1.88	0.15	11.5	11.20	14.8	6.4	3.8	0.62	2.23	0.18
8.5	11.80	12.9	9.5	2.9	0.44	1.56	0.19	11.5	11.80	16.0	9.7	3.8	0.56	1.92	0.24
8.5	12.20	14.0	10.8	1.8	0.37	1.47	0.14	11.5	12.20	17.6	10.5	2.7	0.47	1.86	0.18
8.5	13.86	27.3	21.1	4.1	0.82	1.92	0.07	11.5	13.86	33.8	18.6	5.4	0.89	2.17	0.10

Cs	Tp	Surge _{max}	Sway _{max}	Heave _{max}	Roll _{max}	Pitch _{max}	Yaw _{max}
[-]	[s]	[cm]			[deg/m]		
13.04	4.17	38.7	39.5	5.0	3.96	2.35	3.04
13.04	4.38	41.7	204.4	6.2	3.54	3.58	2.22
13.04	4.62	32.5	35.5	6.0	1.44	4.14	0.91
13.04	4.75	31.1	17.5	6.0	1.02	4.76	0.42
13.04	4.91	30.3	8.9	6.4	0.80	5.57	0.32
13.04	5.06	30.5	6.6	6.3	0.77	6.07	0.25
13.04	5.23	33.9	6.8	5.4	0.85	6.34	0.22
13.04	5.43	32.1	4.4	6.0	0.39	6.69	0.08
13.04	5.65	30.3	3.0	7.9	0.39	6.87	0.19
13.04	5.90	28.4	3.2	8.4	0.50	6.56	0.25
13.04	6.30	30.3	6.1	9.7	0.67	6.11	0.25
13.04	6.70	22.1	3.8	11.8	0.70	5.22	0.15
13.04	7.00	29.7	12.1	6.2	0.72	4.47	1.23
13.04	7.10	22.5	7.1	5.0	0.57	4.14	0.21
13.04	7.50	21.8	4.6	4.6	0.53	3.55	0.41
13.04	7.90	23.8	6.5	3.3	0.42	3.27	0.21
13.04	8.00	21.3	11.2	3.6	0.51	3.25	0.22
13.04	9.20	44.8	11.4	6.8	0.83	3.82	0.11
13.04	9.60	25.6	8.1	9.1	0.79	3.72	0.15
13.04	9.70	23.6	7.1	10.0	0.86	3.76	0.12
13.04	9.80	23.4	8.6	10.6	1.05	3.89	0.18
13.04	10.00	22.3	8.3	8.8	1.46	4.00	0.36
13.04	10.80	19.6	8.6	3.6	0.91	2.74	0.13
13.04	11.20	14.8	6.0	4.1	0.68	2.36	0.16
13.04	11.80	16.4	10.3	4.4	0.66	2.06	0.30
13.04	12.20	19.5	10.4	3.2	0.55	2.05	0.21
13.04	13.86	37.0	20.1	6.1	0.95	2.29	0.16

APPENDIX F : Slam Results template

Cs	Tp	Fs,max	Fs,avg	t _{,max}	ts _{,avg}	lmax	lavg	Tension _{dyn,max}	DAF
[-]	[s]	[kN]	[kN]	[s]	[s]	[kN*s]	[kN*s]	[kN]	[-]
2.5	4.17	132.6	105.2	2.3	2.1	117.2	106.7	76.7	1.03
2.5	4.38	93.9	64.6	2.6	1.7	98.0	65.0	240.3	1.10
2.5	4.62	74.6	44.4	1.5	0.9	52.8	25.7	107.3	1.04
2.5	4.75	67.3	44.0	1.4	1.0	47.7	24.5	110.0	1.04
2.5	4.91	51.3	19.6	1.1	0.3	38.1	8.3	99.3	1.04
2.5	5.06	81.7	46.1	1.5	1.0	52.5	27.1	99.7	1.04
2.5	5.23	108.4	68.9	1.5	1.2	65.2	42.5	185.4	1.07
2.5	5.43	91.9	81.5	1.4	1.3	69.3	56.1	442.1	1.18
2.5	5.65	103.4	81.9	1.5	1.2	61.4	56.0	139.9	1.06
2.5	5.90	89.7	74.0	1.5	1.2	62.2	55.2	85.0	1.03
2.5	6.30	83.1	64.0	1.4	1.2	55.9	48.9	124.3	1.05
2.5	6.70	78.1	60.1	1.3	1.1	51.9	44.4	102.5	1.04
2.5	7.00	71.6	58.1	1.2	1.1	47.0	40.9	74.8	1.03
2.5	7.10	69.0	59.0	1.2	1.1	45.9	41.4	76.9	1.03
2.5	7.50	59.6	54.4	1.2	1.1	40.9	36.9	186.9	1.07
2.5	7.90	58.4	56.2	1.1	1.0	39.3	35.3	62.3	1.02
2.5	8.00	59.4	56.2	1.1	1.0	37.9	34.6	59.2	1.02
2.5	9.20	79.6	46.6	1.3	1.0	32.2	25.9	102.0	1.04
2.5	9.60	152.4	71.6	0.8	0.5	39.5	19.7	234.5	1.09
2.5	9.70	103.1	52.6	0.7	0.4	40.5	18.1	393.2	1.15
2.5	9.80	156.7	84.2	0.6	0.4	45.4	21.3	360.0	1.14
2.5	10.00	142.7	62.9	0.5	0.3	44.1	15.1	107.0	1.04
2.5	10.80	55.1	44.6	1.1	1.0	31.9	26.0	164.5	1.06
2.5	11.20	53.8	42.7	1.1	1.0	30.4	25.9	57.3	1.02
2.5	11.80	43.0	36.9	1.0	1.0	27.1	24.3	72.4	1.03
2.5	12.20	38.8	35.2	1.1	1.0	25.0	23.5	48.7	1.02
2.5	13.86	47.5	28.6	1.2	0.9	28.4	17.2	85.2	1.03
5.5	4.17	289.3	219.2	2.8	2.3	265.6	238.7	180.3	1.07
5.5	4.38	193.8	169.8	3.0	2.7	204.9	190.0	417.8	1.17
5.5	4.62	162.1	102.3	1.7	1.3	127.2	69.8	223.3	1.09
5.5	4.75	149.0	91.0	1.7	1.2	111.2	59.8	179.3	1.07
5.5	4.91	113.7	65.0	1.9	1.2	102.5	49.3	150.2	1.06
5.5	5.06	118.0	42.0	1.3	0.7	81.6	24.8	99.9	1.04
5.5	5.23	138.9	82.3	2.1	1.5	100.6	57.2	171.9	1.07
5.5	5.43	170.9	88.8	1.4	0.9	108.1	58.5	509.0	1.20
5.5	5.65	232.9	187.4	1.5	1.3	106.7	95.9	324.3	1.13
5.5	5.90	287.3	201.2	1.9	1.4	128.7	109.5	250.3	1.10
5.5	6.30	271.6	179.6	1.9	1.4	131.4	109.4	413.8	1.16
5.5	6.70	211.5	132.5	1.9	1.3	122.8	98.4	285.6	1.11
5.5	7.00	206.1	136.6	1.6	1.2	112.8	88.8	176.9	1.07
5.5	7.10	185.9	130.4	1.5	1.2	108.5	87.0	178.8	1.07
5.5	7.50	134.3	110.1	1.4	1.2	95.4	79.6	278.9	1.11
5.5	7.90	131.8	117.5	1.2	1.2	86.7	74.3	120.4	1.05
5.5	8.00	122.4	115.7	1.2	1.2	83.5	72.6	116.6	1.05

Cs	Tp	Fs,max	Fs,avg	t,max	ts,avg	lmax	lavg	Tensiondyn,max	DAF
[-]	[s]	[kN]	[kN]	[s]	[s]	[kN*s]	[kN*s]	[kN]	[-]
5.5	9.20	211.0	116.7	2.1	1.3	76.0	45.9	233.0	1.09
5.5	9.60	241.6	97.5	0.8	0.5	87.0	31.2	478.7	1.19
5.5	9.70	176.1	78.6	0.8	0.5	90.7	28.9	606.2	1.24
5.5	9.80	243.3	101.4	0.7	0.5	94.4	33.4	613.3	1.24
5.5	10.00	333.7	142.3	0.7	0.4	116.8	46.6	366.3	1.14
5.5	10.80	134.9	65.5	1.3	0.8	76.5	36.3	391.7	1.15
5.5	11.20	133.2	93.9	1.4	1.1	75.6	55.7	134.0	1.05
5.5	11.80	88.2	76.2	1.2	1.1	68.1	53.1	160.1	1.06
5.5	12.20	80.9	75.1	1.2	1.1	60.4	52.5	101.2	1.04
5.5	13.86	134.7	68.7	1.2	1.1	61.3	36.9	213.6	1.08
8.5	4.17	399.0	331.0	2.7	2.4	387.4	366.2	201.7	1.08
8.5	4.38	309.1	237.7	3.2	2.6	327.7	282.7	445.4	1.18
8.5	4.62	246.2	150.7	1.8	1.4	190.1	108.9	297.6	1.12
8.5	4.75	213.9	132.4	1.7	1.3	165.5	95.2	239.6	1.10
8.5	4.91	174.0	106.6	2.0	1.4	151.2	82.0	196.9	1.08
8.5	5.06	153.8	75.8	2.4	1.1	149.5	57.3	127.9	1.05
8.5	5.23	150.4	52.1	2.3	1.0	142.1	40.0	163.3	1.06
8.5	5.43	171.3	68.4	1.5	0.9	114.6	43.9	264.3	1.11
8.5	5.65	196.7	130.0	1.5	1.0	127.2	71.2	313.7	1.13
8.5	5.90	408.1	188.4	1.4	0.8	154.3	85.4	322.7	1.13
8.5	6.30	511.5	308.5	2.2	1.5	191.1	140.3	589.3	1.24
8.5	6.70	379.2	219.9	2.2	1.5	194.2	145.9	539.5	1.22
8.5	7.00	377.2	227.1	2.1	1.5	178.6	130.1	321.2	1.13
8.5	7.10	323.2	210.3	2.0	1.5	174.4	130.6	290.7	1.12
8.5	7.50	228.8	173.6	1.6	1.3	148.9	114.8	320.0	1.13
8.5	7.90	193.5	165.7	1.2	1.2	125.7	102.3	161.5	1.06
8.5	8.00	174.2	161.0	1.2	1.1	119.5	99.9	165.5	1.07
8.5	9.20	311.2	129.4	1.7	0.9	110.4	45.2	322.0	1.13
8.5	9.60	352.6	150.0	0.8	0.5	130.9	44.7	641.7	1.25
8.5	9.70	252.1	100.6	0.9	0.5	132.5	38.7	758.1	1.30
8.5	9.80	406.4	169.4	0.8	0.5	139.2	47.7	765.6	1.30
8.5	10.00	498.4	189.3	0.6	0.4	173.5	59.1	584.9	1.23
8.5	10.80	237.4	110.4	0.7	0.5	111.0	37.9	539.8	1.21
8.5	11.20	226.7	100.3	1.2	0.7	108.6	56.3	228.9	1.09
8.5	11.80	137.8	115.5	1.2	1.1	98.8	78.2	252.7	1.10
8.5	12.20	118.0	113.7	1.2	1.1	90.4	76.9	146.4	1.06
8.5	13.86	270.2	126.5	1.2	1.1	92.6	50.1	347.2	1.14
11.5	4.17	515.3	436.1	2.7	2.5	535.4	494.3	342.7	1.14
11.5	4.38	415.9	318.4	3.5	2.6	435.4	378.2	460.6	1.19
11.5	4.62	327.3	196.1	1.8	1.4	290.4	149.4	362.0	1.15
11.5	4.75	260.5	173.2	1.8	1.4	227.1	129.8	271.8	1.11
11.5	4.91	228.9	142.2	2.0	1.4	203.7	112.4	253.9	1.10
11.5	5.06	188.5	107.5	2.3	1.3	181.4	85.1	166.2	1.07
11.5	5.23	166.2	76.5	3.7	1.5	211.5	72.9	145.4	1.06
11.5	5.43	160.9	84.1	2.8	1.4	155.5	69.5	163.9	1.07

Cs	Tp	Fs,max	Fs,avg	t,max	ts,avg	lmax	lavg	Tensiondyn,max	DAF
[-]	[s]	[kN]	[kN]	[s]	[s]	[kN*s]	[kN*s]	[kN]	[-]
11.5	5.65	207.7	126.9	1.6	1.3	138.8	82.8	289.2	1.12
11.5	5.90	468.6	318.6	1.5	1.4	188.5	149.9	302.2	1.12
11.5	6.30	625.1	213.0	1.3	0.7	219.0	84.1	625.5	1.25
11.5	6.70	498.3	230.4	1.4	1.0	256.1	124.2	802.6	1.32
11.5	7.00	570.7	319.4	2.5	1.6	242.8	164.5	440.4	1.18
11.5	7.10	526.6	314.8	2.4	1.6	226.6	163.3	402.2	1.16
11.5	7.50	344.0	247.4	2.2	1.6	199.2	150.1	364.9	1.15
11.5	7.90	254.3	177.0	1.2	1.0	161.8	103.8	202.5	1.08
11.5	8.00	234.1	167.3	1.3	1.0	161.4	105.8	233.3	1.09
11.5	9.20	398.7	159.6	1.7	0.9	142.7	58.8	451.8	1.18
11.5	9.60	444.5	150.9	0.9	0.5	171.7	46.7	751.5	1.30
11.5	9.70	333.4	130.5	1.0	0.5	170.3	48.7	863.1	1.34
11.5	9.80	527.0	178.0	0.9	0.5	182.3	48.0	862.8	1.34
11.5	10.00	721.7	268.9	0.6	0.4	224.0	76.6	779.8	1.31
11.5	10.80	326.5	172.5	0.6	0.5	206.6	49.5	401.1	1.16
11.5	11.20	327.5	157.5	1.1	0.7	140.2	68.2	313.7	1.12
11.5	11.80	202.9	109.8	1.1	0.8	127.9	66.5	325.1	1.13
11.5	12.20	159.3	150.1	1.2	1.1	116.3	99.0	218.9	1.09
11.5	13.86	400.5	135.7	1.2	0.7	122.5	46.6	466.5	1.18
13.04	4.17	568.6	485.7	2.9	2.5	608.6	561.7	321.6	1.13
13.04	4.38	482.4	399.5	3.2	2.8	487.0	454.7	457.6	1.19
13.04	4.62	354.0	217.9	1.9	1.5	329.0	170.0	370.9	1.15
13.04	4.75	301.3	195.4	1.8	1.4	260.6	147.5	315.7	1.13
13.04	4.91	249.8	161.0	2.0	1.4	229.8	128.3	268.1	1.11
13.04	5.06	197.7	122.2	2.3	1.3	203.6	97.0	187.0	1.07
13.04	5.23	179.7	86.8	3.6	1.5	228.6	81.6	143.1	1.06
13.04	5.43	159.9	90.1	2.9	1.7	169.6	83.2	135.8	1.05
13.04	5.65	201.9	126.3	1.6	1.3	142.2	89.1	262.7	1.11
13.04	5.90	447.9	312.5	1.8	1.6	201.7	162.1	280.6	1.11
13.04	6.30	697.3	247.0	1.4	0.7	231.5	95.4	620.1	1.25
13.04	6.70	631.5	295.6	1.3	0.9	266.8	131.5	991.7	1.40
13.04	7.00	721.9	283.7	1.4	1.0	265.4	124.9	516.8	1.21
13.04	7.10	557.3	244.1	1.3	1.0	265.3	117.5	429.8	1.17
13.04	7.50	440.2	213.9	2.3	1.0	219.2	114.3	353.8	1.14
13.04	7.90	303.8	167.2	1.2	0.9	180.4	94.6	219.3	1.09
13.04	8.00	279.2	164.1	1.3	0.9	180.1	95.5	251.2	1.10
13.04	9.20	462.1	182.0	1.8	0.9	158.9	66.4	542.7	1.22
13.04	9.60	490.3	171.6	1.0	0.5	188.5	52.6	796.3	1.32
13.04	9.70	370.7	150.1	1.0	0.5	190.0	54.6	902.4	1.36
13.04	9.80	565.4	195.1	0.9	0.5	200.9	53.5	903.1	1.36
13.04	10.00	692.6	205.4	0.8	0.5	250.2	68.6	733.5	1.29
13.04	10.80	429.2	156.7	1.2	0.7	225.1	78.9	298.2	1.12
13.04	11.20	364.8	183.8	1.0	0.7	229.9	72.2	327.8	1.13
13.04	11.80	240.2	128.8	1.1	0.8	227.5	73.4	366.7	1.15
13.04	12.20	182.9	118.5	1.2	0.8	196.2	75.4	259.5	1.10

Cs	Tp	F _{s,max}	F _{s,avg}	t _{,max}	t _{s,avg}	l _{max}	l _{avg}	Tension _{dyn,max}	DAF
[-]	[s]	[kN]	[kN]	[s]	[s]	[kN*s]	[kN*s]	[kN]	[-]
13.04	13.86	467.4	132.0	1.2	0.6	140.2	42.1	524.2	1.21

APPENDIX F : Slam Results template TEST 2

Cs	Tp	Fs,max	Fs,avg	t,max	ts,avg	lmax	lavg	lSiOdyn,max	DAF
[-]	[s]	[kN]	[kN]	[s]	[s]	[kN*s]	[kN*s]	[kN]	[-]
2.5	4.17	181.2	160.4	2.3	2.2	183.2	169.5	194.5	1.08
2.5	4.38	149.9	137.5	2.7	2.6	156.5	147.6	186.9	1.07
2.5	4.62	125.0	112.4	3.2	3.1	123.7	112.6	165.2	1.07
2.5	4.75	106.3	83.1	1.7	1.4	85.2	43.7	203.2	1.08
2.5	4.91	64.2	44.8	2.3	1.5	69.9	23.8	197.6	1.08
2.5	5.06	56.3	53.3	4.4	4.4	62.6	50.5	81.0	1.03
2.5	5.23	53.2	46.7	4.6	4.5	67.6	61.5	178.5	1.07
2.5	5.43	71.8	56.6	2.2	1.9	49.3	37.3	141.4	1.06
2.5	5.65	111.2	74.1	2.1	1.5	51.4	43.8	119.7	1.05
2.5	5.90	130.5	81.7	1.9	1.3	53.5	49.2	120.4	1.05
2.5	6.30	114.5	79.1	1.9	1.3	57.5	49.5	382.6	1.15
2.5	6.70	151.2	93.1	1.9	1.3	64.2	51.4	152.9	1.06
2.5	7.00	163.4	100.0	1.8	1.3	67.8	53.5	176.4	1.07
2.5	7.10	159.8	102.2	1.7	1.2	67.5	53.6	199.6	1.08
2.5	7.50	131.0	88.5	1.6	1.2	66.4	52.3	223.2	1.09
2.5	7.90	127.5	96.4	1.5	1.2	63.1	51.3	137.6	1.05
2.5	8.00	120.7	96.3	1.5	1.2	62.6	50.3	140.5	1.06
2.5	9.20	89.6	78.2	1.2	1.1	51.0	42.5	184.3	1.07
2.5	9.60	99.0	51.2	1.9	1.1	34.9	25.0	284.8	1.11
2.5	9.70	89.5	59.4	2.8	1.8	51.9	33.0	189.3	1.07
2.5	9.80	53.1	48.7	2.8	1.9	41.4	29.8	143.0	1.06
2.5	10.00	97.3	53.3	1.7	1.0	42.5	23.5	118.5	1.05
2.5	10.80	95.3	66.2	1.5	1.2	49.9	40.2	136.9	1.05
2.5	11.20	82.7	62.8	1.4	1.2	48.0	41.2	125.0	1.05
2.5	11.80	66.3	59.4	1.3	1.2	43.2	38.9	141.5	1.06
2.5	12.20	64.1	59.4	1.3	1.2	40.0	36.7	133.7	1.05
2.5	13.86	97.5	53.1	2.0	1.4	39.1	30.7	237.5	1.09
5.5	4.17	381.2	333.8	2.3	2.3	390.7	362.2	193.4	1.08
5.5	4.38	292.4	263.4	2.8	2.7	320.0	296.6	357.5	1.14
5.5	4.62	209.3	186.4	3.3	3.2	208.1	188.9	287.8	1.11
5.5	4.75	155.9	100.6	2.0	1.5	159.9	69.8	265.6	1.11
5.5	4.91	106.8	61.6	2.5	1.8	128.7	53.7	199.4	1.08
5.5	5.06	115.9	106.7	4.5	4.4	110.7	94.7	111.1	1.04
5.5	5.23	93.3	88.3	5.0	4.9	101.9	94.2	228.5	1.09
5.5	5.43	85.9	81.5	5.0	5.0	118.8	110.7	183.9	1.07
5.5	5.65	190.1	118.9	2.4	1.7	84.2	69.6	156.1	1.06
5.5	5.90	330.8	186.4	2.4	1.6	93.9	83.4	227.7	1.09
5.5	6.30	271.2	181.4	2.4	1.5	107.4	92.7	804.1	1.32
5.5	6.70	426.8	238.1	2.4	1.5	141.1	100.6	374.7	1.15
5.5	7.00	507.9	268.3	2.4	1.5	147.1	106.2	397.1	1.16
5.5	7.10	428.0	248.5	2.3	1.5	144.8	102.8	426.0	1.17
5.5	7.50	341.4	206.3	2.2	1.5	143.0	104.7	445.0	1.18
5.5	7.90	229.6	177.8	2.2	1.5	129.6	102.5	273.8	1.11
5.5	8.00	216.5	176.8	2.2	1.5	126.0	101.5	265.9	1.11

Cs	Tp	Fs,max	Fs,avg	t,max	ts,avg	lmax	lavg	lSiOdyn,max	DAF
[-]	[s]	[kN]	[kN]	[s]	[s]	[kN*s]	[kN*s]	[kN]	[-]
5.5	9.20	186.0	103.5	1.5	1.1	87.9	58.0	328.7	1.13
5.5	9.60	153.5	113.3	2.8	1.9	126.2	78.4	427.6	1.17
5.5	9.70	158.8	117.7	2.8	1.9	109.2	73.8	320.8	1.13
5.5	9.80	138.4	110.5	2.8	1.9	92.7	68.5	252.9	1.10
5.5	10.00	137.8	113.2	2.9	2.0	88.6	68.0	202.7	1.08
5.5	10.80	255.1	154.8	2.1	1.4	107.8	81.5	282.7	1.11
5.5	11.20	216.8	133.1	1.7	1.3	105.8	82.4	249.3	1.10
5.5	11.80	157.1	117.8	1.6	1.3	97.1	80.4	213.6	1.08
5.5	12.20	152.5	120.9	1.4	1.3	92.6	78.5	179.5	1.07
5.5	13.86	202.2	103.0	3.6	1.8	132.9	64.5	412.3	1.16
8.5	4.17	564.7	490.1	2.4	2.3	594.3	549.2	233.3	1.10
8.5	4.38	388.0	359.4	2.8	2.7	461.9	424.3	474.0	1.19
8.5	4.62	267.5	230.0	3.4	3.0	294.4	253.6	344.6	1.14
8.5	4.75	197.1	121.9	2.1	1.7	233.6	107.0	313.5	1.13
8.5	4.91	163.8	98.6	2.6	1.8	184.4	83.9	229.0	1.09
8.5	5.06	166.7	155.3	4.5	4.5	153.0	137.3	145.7	1.06
8.5	5.23	132.4	123.8	5.1	5.1	135.0	122.8	266.7	1.11
8.5	5.43	117.0	110.6	5.2	5.2	146.6	136.2	229.0	1.09
8.5	5.65	194.4	123.7	2.7	1.9	105.4	86.3	190.8	1.08
8.5	5.90	375.5	205.6	2.7	1.8	118.1	103.4	271.5	1.11
8.5	6.30	422.4	266.3	2.9	1.8	147.0	122.6	972.9	1.39
8.5	6.70	731.9	398.6	2.9	1.7	197.0	138.0	593.8	1.24
8.5	7.00	703.2	381.2	2.8	1.7	208.3	138.1	551.4	1.22
8.5	7.10	789.5	438.8	2.8	1.7	210.6	146.1	599.1	1.24
8.5	7.50	521.7	311.8	2.6	1.7	206.6	147.9	660.8	1.26
8.5	7.90	480.6	300.8	2.8	1.9	195.2	145.3	400.5	1.16
8.5	8.00	403.7	250.2	2.8	1.7	181.7	127.4	372.6	1.15
8.5	9.20	259.9	161.5	2.8	1.3	238.2	87.8	428.1	1.17
8.5	9.60	215.2	162.6	2.8	1.9	178.7	120.3	535.8	1.21
8.5	9.70	220.0	169.7	2.8	2.0	163.2	113.9	439.2	1.17
8.5	9.80	231.0	177.0	2.9	2.0	145.0	107.6	364.6	1.14
8.5	10.00	261.9	193.3	2.9	2.0	129.5	102.9	310.8	1.12
8.5	10.80	398.3	167.5	1.4	1.1	147.4	73.3	434.4	1.17
8.5	11.20	403.6	226.6	2.2	1.5	155.6	114.3	375.0	1.15
8.5	11.80	288.5	183.8	1.9	1.4	152.9	116.6	308.3	1.12
8.5	12.20	253.8	177.0	1.9	1.5	142.5	111.4	202.6	1.08
8.5	13.86	298.0	126.2	3.4	1.7	186.7	74.3	548.2	1.22
11.5	4.17	699.8	638.7	2.4	2.3	786.9	714.5	404.3	1.17
11.5	4.38	516.2	439.2	2.8	2.7	574.5	527.7	580.7	1.24
11.5	4.62	321.9	258.8	3.4	2.7	384.0	288.3	414.0	1.17
11.5	4.75	238.1	151.3	2.1	1.7	311.6	144.4	335.1	1.13
11.5	4.91	234.0	134.5	2.6	1.8	241.8	112.4	263.4	1.11
11.5	5.06	211.9	131.8	3.1	2.0	199.8	93.0	185.6	1.07
11.5	5.23	165.7	156.6	5.2	5.1	165.2	150.9	280.3	1.11
11.5	5.43	148.8	138.6	5.3	5.2	173.8	159.5	272.3	1.11

Cs	Tp	Fs,max	Fs,avg	t,max	ts,avg	lmax	lavg	lSiOdyn,max	DAF
[-]	[s]	[kN]	[kN]	[s]	[s]	[kN*s]	[kN*s]	[kN]	[-]
11.5	5.65	176.8	133.9	2.9	2.0	126.0	100.4	215.9	1.09
11.5	5.90	447.4	429.5	4.0	4.0	256.5	232.8	305.2	1.12
11.5	6.30	513.4	228.9	1.7	1.2	177.3	94.4	1041.3	1.42
11.5	6.70	861.7	335.7	1.7	1.1	244.5	108.4	736.3	1.30
11.5	7.00	1188.6	439.3	1.8	1.1	268.8	122.1	660.4	1.26
11.5	7.10	981.1	347.3	1.7	1.1	239.5	116.1	670.9	1.27
11.5	7.50	732.6	311.0	3.0	1.2	262.6	134.4	854.7	1.34
11.5	7.90	714.1	309.8	3.1	1.2	258.8	132.6	509.0	1.20
11.5	8.00	630.8	280.4	1.5	1.2	244.2	126.2	460.3	1.18
11.5	9.20	368.9	217.3	2.7	1.9	287.5	169.1	487.3	1.19
11.5	9.60	326.4	227.7	2.8	2.0	228.3	156.5	609.2	1.24
11.5	9.70	317.8	229.1	2.8	2.0	214.5	152.7	544.3	1.22
11.5	9.80	357.4	256.5	2.9	2.0	197.2	147.2	475.8	1.19
11.5	10.00	391.5	276.4	2.9	2.1	176.9	138.2	416.3	1.17
11.5	10.80	482.4	268.6	1.4	1.0	169.2	94.9	392.4	1.16
11.5	11.20	543.4	304.1	2.7	1.7	197.0	141.0	450.9	1.18
11.5	11.80	428.6	266.1	2.1	1.5	204.6	144.1	407.9	1.16
11.5	12.20	368.9	245.9	2.1	1.6	197.7	142.2	272.4	1.11
11.5	13.86	355.7	174.9	1.9	1.4	244.6	85.0	660.2	1.26
13.04	4.17	856.4	714.3	2.4	2.3	886.5	787.9	469.3	1.20
13.04	4.38	527.3	474.5	2.9	2.7	625.2	574.4	653.0	1.27
13.04	4.62	346.9	276.9	3.5	2.7	427.2	318.0	412.6	1.17
13.04	4.75	257.1	167.4	2.1	1.7	348.2	163.2	356.6	1.14
13.04	4.91	268.1	152.7	2.6	1.8	270.9	126.6	293.8	1.12
13.04	5.06	229.3	145.8	3.0	2.0	217.5	102.8	202.4	1.08
13.04	5.23	183.3	172.6	5.2	5.1	180.2	165.4	283.0	1.11
13.04	5.43	162.6	149.5	10.8	5.2	371.2	162.9	292.8	1.12
13.04	5.65	185.9	140.9	2.9	2.0	223.0	108.1	235.4	1.09
13.04	5.90	467.2	448.3	4.0	4.0	276.9	253.2	320.5	1.13
13.04	6.30	518.7	237.0	1.7	1.3	186.2	100.1	1041.2	1.42
13.04	6.70	1034.6	388.0	1.8	1.1	265.5	117.6	813.0	1.33
13.04	7.00	1321.1	471.7	1.8	1.1	286.5	122.7	736.4	1.30
13.04	7.10	1190.4	403.9	1.8	1.1	278.0	130.3	738.4	1.30
13.04	7.50	870.8	362.0	1.9	1.1	289.8	147.2	947.6	1.38
13.04	7.90	772.3	344.8	1.6	1.2	292.1	146.3	544.0	1.22
13.04	8.00	723.8	332.7	1.6	1.2	276.1	142.3	473.4	1.19
13.04	9.20	426.5	248.5	2.7	2.0	315.3	189.3	520.5	1.21
13.04	9.60	388.4	260.7	2.9	2.0	255.9	174.7	642.0	1.26
13.04	9.70	376.0	264.2	2.9	2.0	242.6	172.1	592.4	1.24
13.04	9.80	422.2	295.5	2.9	2.1	225.4	166.2	527.9	1.21
13.04	10.00	468.4	326.8	3.0	2.1	205.7	160.5	473.8	1.19
13.04	10.80	462.1	317.7	1.6	0.9	239.9	114.6	238.4	1.09
13.04	11.20	719.5	277.5	1.4	1.1	208.5	101.6	496.1	1.20
13.04	11.80	523.3	314.6	2.3	1.6	229.2	162.0	489.1	1.19
13.04	12.20	440.3	299.6	2.2	1.6	222.3	153.5	320.7	1.13

Cs	Tp	Fs,max	Fs,avg	t,max	ts,avg	lmax	lavg	lSiOdyn,max	DAF
[-]	[s]	[kN]	[kN]	[s]	[s]	[kN*s]	[kN*s]	[kN]	[-]
13.04	13.86	372.3	199.1	1.8	1.4	269.0	95.1	699.3	1.28

APPENDIX F : Slam Results template TEST 3

Cs	Tp	Fs,max	Fs,avg	t _{,max}	ts _{,avg}	lmax	lavg	lSiO _{dyn,max}	DAF
[-]	[s]	[kN]	[kN]	[s]	[s]	[kN*s]	[kN*s]	[kN]	[-]
2.5	4.17	187.9	162.0	2.2	2.1	180.2	172.2	339.7	1.13
2.5	4.38	166.1	146.2	2.7	2.6	152.8	144.2	464.6	1.18
2.5	4.62	115.5	105.0	3.2	3.2	108.7	102.7	350.6	1.14
2.5	4.75	102.5	89.2	3.4	3.4	82.7	76.7	244.8	1.10
2.5	4.91	70.6	63.6	3.7	3.6	51.5	46.6	135.7	1.05
2.5	5.06	57.1	23.1	2.6	1.1	30.6	7.9	105.6	1.04
2.5	5.23	84.7	34.9	1.5	0.8	32.2	12.6	180.3	1.07
2.5	5.43	85.2	61.4	1.3	1.1	40.2	26.9	168.1	1.07
2.5	5.65	91.0	78.5	1.3	1.0	41.4	35.3	149.8	1.06
2.5	5.90	153.7	101.1	1.5	1.1	49.8	41.3	182.2	1.07
2.5	6.30	221.9	91.5	2.0	0.9	60.9	30.6	315.5	1.12
2.5	6.70	229.8	123.6	1.8	1.2	64.4	38.5	314.8	1.12
2.5	7.00	253.6	135.9	1.9	1.3	72.6	42.9	264.6	1.10
2.5	7.10	265.9	141.5	1.9	1.3	69.6	43.1	257.6	1.10
2.5	7.50	226.3	124.4	1.5	1.2	70.0	45.8	382.8	1.15
2.5	7.90	141.0	91.4	1.4	1.2	61.1	47.0	279.2	1.11
2.5	8.00	122.7	86.3	1.4	1.2	61.3	47.9	262.7	1.10
2.5	9.20	91.8	54.9	1.4	0.9	57.5	32.2	317.6	1.12
2.5	9.60	92.0	55.4	1.7	1.0	48.8	28.7	340.4	1.13
2.5	9.70	91.7	52.6	1.7	1.0	45.9	27.3	353.1	1.14
2.5	9.80	90.7	42.4	1.9	0.9	42.5	22.2	365.9	1.14
2.5	10.00	100.8	39.4	2.1	0.9	39.8	18.9	354.1	1.14
2.5	10.80	97.7	40.2	1.7	1.2	52.4	18.1	297.3	1.12
2.5	11.20	90.3	32.6	1.7	1.0	51.9	18.1	203.7	1.08
2.5	11.80	92.7	67.4	1.3	1.1	38.8	29.5	242.9	1.10
2.5	12.20	104.0	69.9	1.3	1.0	44.0	34.0	219.4	1.09
2.5	13.86	101.7	86.6	1.2	1.0	45.7	39.7	170.8	1.07
5.5	4.17	405.0	344.9	2.2	2.1	386.9	362.2	372.6	1.15
5.5	4.38	318.2	286.3	2.6	2.5	319.5	301.6	482.4	1.19
5.5	4.62	249.1	230.4	3.2	3.2	223.7	212.0	419.7	1.16
5.5	4.75	174.6	163.7	3.5	3.4	169.7	157.3	296.4	1.12
5.5	4.91	117.0	105.5	3.7	3.7	104.5	94.0	158.8	1.06
5.5	5.06	70.3	61.4	3.9	3.7	71.8	44.3	104.2	1.04
5.5	5.23	84.1	33.8	2.0	0.9	44.4	15.6	245.4	1.10
5.5	5.43	93.7	72.5	1.7	1.3	57.7	38.4	167.7	1.07
5.5	5.65	119.2	95.4	1.7	1.2	62.4	51.8	136.7	1.05
5.5	5.90	226.6	139.3	1.9	1.3	78.5	64.2	233.3	1.09
5.5	6.30	402.5	217.7	1.8	1.1	102.5	67.3	501.4	1.20
5.5	6.70	409.3	226.3	2.2	1.4	118.0	74.1	474.3	1.19
5.5	7.00	446.5	237.8	2.3	1.5	130.8	79.9	411.1	1.16
5.5	7.10	508.9	271.2	2.4	1.5	147.0	87.8	418.0	1.16
5.5	7.50	496.6	184.9	1.7	1.0	143.0	61.8	535.3	1.21
5.5	7.90	318.9	209.5	1.4	1.2	129.7	93.0	356.3	1.14
5.5	8.00	276.5	192.7	1.4	1.2	126.9	94.0	331.7	1.13

Cs	Tp	Fs,max	Fs,avg	t,max	ts,avg	Imax	Iavg	ISiOdyn,max	DAF
[-]	[s]	[kN]	[kN]	[s]	[s]	[kN*s]	[kN*s]	[kN]	[-]
5.5	9.20	185.9	96.2	1.6	1.1	116.2	57.8	419.6	1.17
5.5	9.60	193.4	86.2	2.0	1.1	103.7	45.2	439.6	1.17
5.5	9.70	173.8	90.2	2.1	1.2	97.4	48.9	440.5	1.17
5.5	9.80	156.6	96.2	2.2	1.4	89.7	52.0	446.7	1.18
5.5	10.00	178.1	94.3	2.3	1.5	148.2	49.1	423.4	1.17
5.5	10.80	199.3	61.8	1.8	1.1	109.8	29.5	349.2	1.14
5.5	11.20	188.4	68.5	1.9	1.2	110.3	38.7	246.5	1.10
5.5	11.80	169.1	99.9	1.3	0.9	75.4	41.9	275.2	1.11
5.5	12.20	189.6	134.8	1.3	1.1	87.1	67.9	280.6	1.11
5.5	13.86	189.3	159.6	1.2	1.0	116.5	79.4	187.1	1.07
8.5	4.17	599.1	519.2	2.2	2.1	568.4	531.0	403.1	1.16
8.5	4.38	441.3	389.2	2.6	2.5	469.9	440.3	477.0	1.19
8.5	4.62	357.0	318.3	3.3	3.2	320.7	298.1	471.5	1.19
8.5	4.75	271.6	250.5	3.5	3.4	228.3	213.2	322.6	1.13
8.5	4.91	149.1	140.0	3.8	3.8	133.6	117.4	177.2	1.07
8.5	5.06	101.2	46.0	4.0	1.3	80.1	22.9	121.5	1.05
8.5	5.23	78.5	36.0	2.7	1.1	53.6	19.9	265.3	1.10
8.5	5.43	87.9	73.7	2.0	1.4	64.0	42.3	202.8	1.08
8.5	5.65	145.0	101.7	1.9	1.4	69.9	59.1	134.6	1.05
8.5	5.90	305.4	173.5	2.0	1.3	94.7	75.9	279.4	1.11
8.5	6.30	558.1	303.1	2.1	1.3	134.9	89.2	640.1	1.25
8.5	6.70	631.8	292.3	2.5	1.3	171.1	91.6	665.8	1.26
8.5	7.00	739.6	262.5	1.5	1.0	192.5	80.0	531.3	1.21
8.5	7.10	619.5	232.1	1.4	1.0	202.5	76.6	523.8	1.21
8.5	7.50	624.8	234.9	1.6	0.9	200.6	84.1	611.6	1.24
8.5	7.90	545.2	217.7	1.3	0.9	193.0	89.7	466.4	1.18
8.5	8.00	454.7	201.8	1.3	0.9	188.7	89.9	452.1	1.18
8.5	9.20	311.2	139.7	1.9	1.2	158.9	81.6	501.4	1.20
8.5	9.60	268.4	141.6	3.3	1.6	239.8	91.7	528.4	1.21
8.5	9.70	229.0	129.2	3.4	1.8	230.1	94.6	534.8	1.21
8.5	9.80	203.0	112.2	3.4	2.0	221.7	102.0	534.4	1.21
8.5	10.00	226.1	116.1	3.4	2.4	207.2	105.9	475.9	1.19
8.5	10.80	287.7	120.0	1.9	1.5	143.1	53.7	388.4	1.15
8.5	11.20	282.2	102.2	1.9	1.2	162.3	57.7	297.8	1.12
8.5	11.80	242.5	122.5	2.2	1.4	191.1	90.7	287.4	1.11
8.5	12.20	251.1	199.1	1.2	1.1	123.0	93.7	323.7	1.13
8.5	13.86	252.6	213.9	1.3	1.1	163.1	110.5	199.9	1.08
11.5	4.17	734.2	624.7	2.3	2.2	705.3	649.1	446.1	1.18
11.5	4.38	551.4	499.4	2.6	2.5	610.4	568.0	480.1	1.19
11.5	4.62	452.0	396.8	3.3	3.2	408.1	368.0	471.9	1.19
11.5	4.75	361.0	332.5	3.5	3.5	275.4	254.2	346.0	1.14
11.5	4.91	194.3	104.2	2.4	1.8	128.0	69.9	200.6	1.08
11.5	5.06	133.7	57.2	1.5	1.0	72.2	23.8	155.0	1.06
11.5	5.23	76.3	42.6	2.7	1.3	54.4	25.2	252.6	1.10
11.5	5.43	99.7	76.0	2.1	1.5	63.7	44.0	202.5	1.08

Cs	Tp	Fs,max	Fs,avg	t,max	ts,avg	lmax	lavg	lSiOdyn,max	DAF
[-]	[s]	[kN]	[kN]	[s]	[s]	[kN*s]	[kN*s]	[kN]	[-]
11.5	5.65	168.9	109.3	2.0	1.4	72.8	63.3	145.1	1.06
11.5	5.90	283.3	163.2	2.1	1.4	106.7	84.2	313.9	1.12
11.5	6.30	736.9	335.2	2.4	1.4	145.4	99.6	726.3	1.29
11.5	6.70	780.7	288.9	1.4	1.0	220.0	88.2	824.3	1.33
11.5	7.00	937.2	323.3	1.3	0.9	254.4	99.0	638.0	1.25
11.5	7.10	772.5	252.1	1.3	0.8	241.2	88.5	612.0	1.24
11.5	7.50	833.0	297.7	1.0	0.9	264.9	112.2	676.8	1.27
11.5	7.90	762.9	283.7	1.2	1.0	246.1	113.2	569.0	1.23
11.5	8.00	665.8	267.9	1.3	1.0	237.4	113.4	544.8	1.22
11.5	9.20	425.8	199.2	3.2	1.8	337.3	141.7	551.2	1.22
11.5	9.60	319.2	153.2	3.3	2.2	292.0	144.0	576.2	1.23
11.5	9.70	274.8	138.1	3.4	2.2	281.7	142.7	588.7	1.23
11.5	9.80	246.8	127.2	3.4	2.3	269.8	139.0	587.5	1.23
11.5	10.00	266.0	141.8	3.4	2.4	255.5	133.1	528.7	1.21
11.5	10.80	413.8	166.8	1.9	1.5	183.1	73.3	426.5	1.17
11.5	11.20	375.4	135.0	1.9	1.2	210.2	74.5	348.9	1.14
11.5	11.80	403.4	199.2	2.1	1.4	248.0	122.2	302.5	1.12
11.5	12.20	295.4	189.2	1.2	0.8	247.2	82.5	343.4	1.14
11.5	13.86	301.8	256.8	1.4	1.2	203.0	136.9	221.0	1.09
13.04	4.17	719.7	645.1	2.8	2.5	764.6	695.0	471.1	1.19
13.04	4.38	608.8	552.6	2.6	2.5	681.3	627.3	456.5	1.18
13.04	4.62	524.7	458.7	3.3	3.2	437.1	398.5	448.9	1.18
13.04	4.75	405.2	373.1	3.6	3.5	297.0	272.2	338.1	1.13
13.04	4.91	222.8	115.3	2.4	1.8	134.4	72.5	204.3	1.08
13.04	5.06	146.3	63.3	1.3	0.9	57.7	25.2	172.9	1.07
13.04	5.23	77.7	48.0	2.8	1.4	57.1	28.0	241.9	1.10
13.04	5.43	105.2	78.2	2.1	1.5	65.0	44.8	207.8	1.08
13.04	5.65	185.4	114.5	2.1	1.4	74.2	64.8	152.2	1.06
13.04	5.90	303.4	178.6	2.1	1.4	109.7	85.2	328.9	1.13
13.04	6.30	922.4	400.1	2.4	1.4	159.9	107.7	792.0	1.31
13.04	6.70	870.9	260.2	1.4	0.8	240.4	80.9	923.0	1.37
13.04	7.00	1079.3	355.5	1.2	0.8	283.0	110.7	695.1	1.28
13.04	7.10	932.3	317.6	1.0	0.8	269.6	107.5	642.8	1.26
13.04	7.50	950.3	326.7	1.1	0.9	296.0	124.2	677.3	1.27
13.04	7.90	845.9	315.8	1.3	1.0	266.5	123.1	611.6	1.24
13.04	8.00	741.8	297.3	1.3	1.0	258.9	122.7	580.1	1.23
13.04	9.20	466.6	214.6	3.2	2.0	368.7	172.3	571.2	1.23
13.04	9.60	343.0	165.3	3.3	2.2	314.8	158.8	596.5	1.24
13.04	9.70	295.5	148.7	3.4	2.2	302.9	155.0	603.0	1.24
13.04	9.80	264.6	139.4	3.4	2.3	293.0	151.4	608.2	1.24
13.04	10.00	301.3	159.3	3.4	2.4	280.4	146.9	550.1	1.22
13.04	10.80	476.2	190.2	2.0	1.5	204.7	82.0	448.7	1.18
13.04	11.20	418.3	155.1	1.9	1.2	234.3	82.2	374.1	1.15
13.04	11.80	479.9	236.1	2.1	1.4	274.0	135.1	310.1	1.12
13.04	12.20	359.4	216.9	1.1	0.8	275.8	89.1	354.1	1.14

Cs	Tp	F _{s,max}	F _{s,avg}	t _{,max}	t _{s,avg}	I _{max}	I _{avg}	I _{SiO}	I _{dyn,max}	DAF
[-]	[s]	[kN]	[kN]	[s]	[s]	[kN*s]	[kN*s]	[kN]	[kN]	[-]
13.04	13.86	307.6	272.1	1.5	1.2	285.2	149.3	231.6	1.09	